# The Mechanism of Cu,Zn Superoxide Dismutase Oligomerization in Familial Amyotrophic Lateral Sclerosis

Kyle C. Wilcox

A thesis submitted to the faculty of the University of North Carolina at Chapel Hill in partial fulfillment of the requirements for the degree of Doctor of Philosophy in the School of Medicine (Department of Biochemistry and Biophysics).

Chapel Hill

2009

Approved by:

Michael Caplow

Mohanish Deshmukh

Nikolay Dokholyan

Brian Kuhlman

Gary Pielak

# ABSTRACT

Kyle Wilcox - The Mechanism of Cu,Zn Superoxide Dismutase Oligomerization in Familial Amyotrophic Lateral Sclerosis

(Under the direction of Nikolay V. Dokholyan)

Amyotrophic lateral sclerosis (ALS) is a degenerative disease of the motor neurons characterized by the progressive loss of muscle strength and eventual death due to selective killing of motor neurons in the brain stem and spinal cord. ALS consists of both sporadic and familial subtypes that share the same clinical progression of symptoms. Of the 10% of ALS cases considered familial ALS (FALS), 1 in 5 is the result of a mutation in the enzyme Cu,Zn superoxide dismutase (SOD1). Over 100 mutations have been identified, and though they are distributed evenly throughout the homodimeric structure of SOD1, the mutations have the general property of inducing SOD1 aggregation and toxicity in motor neurons and surrounding glial cells. In recent years, a shift has occurred in ALS research and the broader field of protein aggregation diseases toward the hypothesis that soluble oligomers, rather than the end products of aggregation, are the species responsible for the patterns of toxicity observed in these diseases.

Previous studies of SOD1 oligomerization have thus far focused on large-scale oligomers and ignored the earliest stages of oligomerization during which the transition from the native state of SOD1 occurs. Knowledge of structural transformations that initiate SOD1

aggregation, as well as the structure of early oligomeric intermediates, is essential for the design of strategies to prevent the aggregation of SOD1 in FALS.

The following chapters contain a multifaceted description of the initiation of SOD1 oligomerization including “first-principles” computational approaches for modeling the formation of aberrant SOD1 dimers, *in vitro* mechanistic studies of SOD1 oligomerization, as well as the characterization of the *in vivo* modification state of SOD1. By calling attention to the fact that SOD1 is highly post-translationally modified in-vivo and showing that mutations allow SOD1 to access altogether different oligomeric intermediates than wild type, we lay the groundwork for significant advances in understanding the structural basis of SOD1 oligomerization in ALS.

# Table of Contents

# List of Tables

Table

# List of Figures

Figure

# List of Abbreviations

| | |
|---|---|
| 6-OHDA | 6-hydroxydopamine |
| ALS | amyotrophic lateral sclerosis |
| C-CAD | collision-cell-activated dissociation |
| CID | collision-induced dissociation |
| CSF | cerebrospinal fluid |
| ECD | electron-capture dissociation |
| FALS | familial amyotrophic lateral sclerosis |
| FTD | frontotemporal dementia |
| LC | liquid chromatography |
| LMN | lower motor neuron |
| MALDI-TOF | matrix-assisted laser desorption ionization – time of flight |
| MD | molecular dynamics |
| μ-ESI-FTICR-MS | microelectrospray ionization Fourier transform ion cyclotron resonance mass spectroscopy |
| PLS | primary lateral sclerosis |
| PMA | progressive muscular atrophy |
| SOD1 | Cu,Zn superoxide dismutase |
| TDP-43 | trans-activated response DNA-binding protein – 43 kDa |
| UMN | upper motor neuron |

# CHAPTER 1

# INTRODUCTION

## ALS and other Motor neuron diseases

Amyotrophic lateral sclerosis (ALS) is one member of a larger spectrum of neurodegenerative diseases affecting motor neurons – including progressive muscular atrophy, primary lateral sclerosis, the spinal muscular atrophies, and frontotemporal dementia [1]. Having an incidence in the United States of about 2 cases per 100,000 individuals and a median survival time of 3 years after the appearance of symptoms, roughly 18,000 Americans are currently afflicted with ALS [2-4].

### Amyotrophic lateral sclerosis

ALS typically first appears in one limb and manifests itself through muscle weakness, cramps, or fasciculation [5-9]. These symptoms typically spread first within the spinal cord segment exhibiting the initial symptoms, then to other regions [5,10]. 25% of ALS presents with bulbar onset (characterized by impaired speech and difficulty swallowing), [5-9] followed by the typical progression to other regions of the body. ALS may also present with non-motor components such as Parkinsonism or dementia [11-14]. A recent study screening for signs of dementia in ALS reported that up to 50% of individuals from a group of 100 patients with ALS showed deficits in executive function [15].

Due to heterogeneity in the presentation of symptoms, several designations are used to classify affected individuals depending upon specific criteria: “definite ALS” is characterized by symptoms in 3 or more regions including both upper motor neuron (UMN) and lower motor neuron (LMN) signs; “probable ALS” is characterized by both UMN and LMN symptoms in 2 regions; and “possible ALS” must exhibit both UMN and LMN symptoms in only 1 region or LMN symptoms in 2 regions rostral to UMN signs [16].

ALS is likely a multivariate disease, initiated by a number of causes. Ninety percent of the incidence of ALS is sporadic while the remaining ten percent is associated with genetic mutations, primarily in the gene encoding Cu,Zn superoxide dismutase (SOD1). A third form of ALS was found in Guam in the 1950’s, and later in parts of New Guinea and Japan, that is marked by an incidence rate that is 50-100 times that of the rest of the world likely represent a combination of genetic susceptibility and environmental factors, as evidenced by a steady decline in the incidence over the last 40 years [17,18]. Whatever the cause of the disease, however, there is no clinical evidence showing that that the progression of the disease differs between familial and sporadic ALS.

**Primary lateral sclerosis**

In contrast to ALS, primary lateral sclerosis (PLS) is typically restricted to UMN symptoms and UMN pool pathology. PLS patients show an earlier age of onset than that of sporadic ALS, but with a much more favorable prognosis. The age of onset in PLS is 50 years [19,20], while the median survival time has been reported to be from 8.5-19 years [21].

## Progressive muscular atrophy

Progressive muscular atrophy (PMA) is restricted to lower motor neurons. As with PLS, this disease is characterized by an earlier age of onset, yet longer survival times than is ALS [21,22]. While there are no UMN symptoms in PMA, autopsies reveal typical ALS pathology in the motor cortex and corticospinal tracts [23,24].

### Frontotemporal dementia

Some degree of frontotemporal dementia (FTD) occurs in up to 50% of ALS cases [15]. Dementia can develop before or after motor neuron signs [25]. Interestingly, whether or not FTD symptoms develop before or after motor neurons signs has a profound effect on the prognosis in ALS with FTD. If FTD develops prior to the motor neuron symptoms associated with ALS, the median survival time drops to 2 year, relative to 3 years for typical ALS [26].

## Origin of Cytotoxicity

The origin of cytotoxicity in ALS is unclear, but several hypotheses exist based on available evidence:

### Apoptosis in ALS

Despite initial evidence against apoptosis as a mechanism of motor neuron death in ALS – primarily, the lack of clear morphological evidence in *post mortem* tissues – there are many lines of evidence that suggest a role of apoptosis in ALS pathogenesis. Autopsies of human ALS patients reveal chromatin condensation and $Le^{(Y)}$ immunostaining [27], DNA fragmentation in areas near the motor cortex the brain [28], and increased levels of apoptotic

initiator caspases 1 and 9 in cerebrospinal fluid [29]. The finding that XIAP, a caspase 3, 7, and 9 inhibitor, attenuates ALS progression when co-expressed in spinal cord motor neurons of mutant SOD1 transgenic mice [30] supports earlier data indicating the activation of caspases in ALS.

Increased expression levels of the pro-apoptotic protein Bax [31] and increased protein levels of Bax [32] and Harikari [33] is observed in spinal cord tissues. A decrease in levels of the anti-apoptotic protein Bcl-2 has also been noted [31]. The anti-apoptotic protein Bcl-2 is now known to bind to mutant SOD1 aggregates and localize to mitochondria in the spinal cords of $SOD1^{G93A}$ transgenic mice [34]. These findings are consistent with prior evidence for a protective effect of Bcl-2 expression in cell culture models of SOD1-mediated ALS [35].

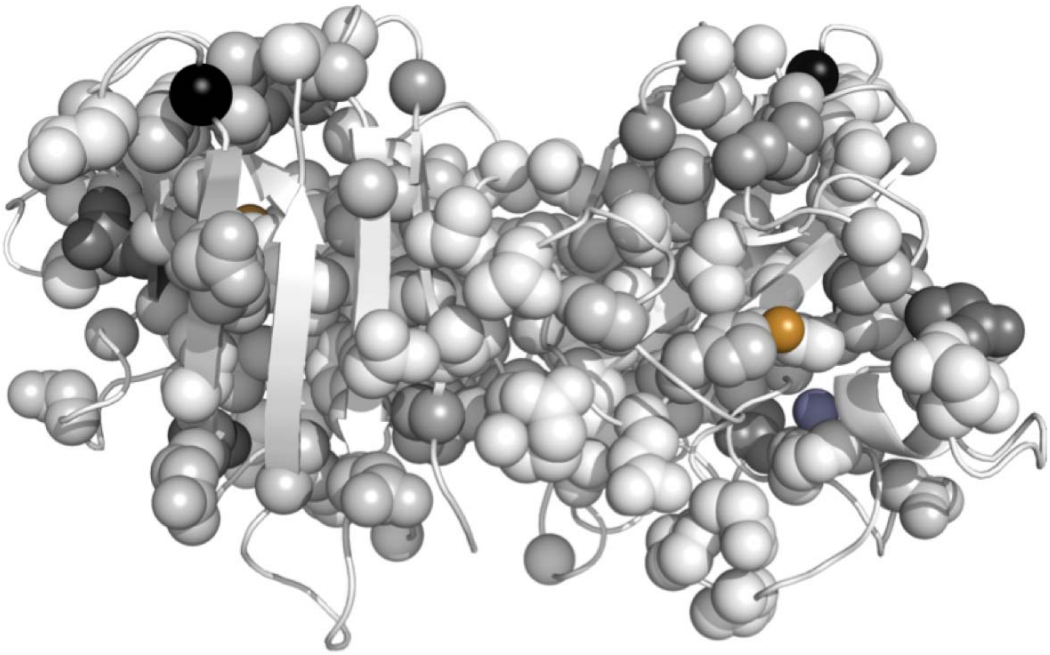

**Figure 1.1. Mutation sites in SOD1** The SOD1 dimer structure (PDB code 2v0a) with the sites found to be mutated in ALS patients represented by spheres. Darker shading denotes more mutations associated with a given position.

Taken together, the available lines of evidence point to the probable involvement of apoptotic pathways in ALS – more specifically, the mitochondrial pathway [36] rather than

extrinsic, receptor-mediated pathways [37]. Therapies that target apoptosis represent one avenue for treating ALS, but it is likely that the apoptotic phase of ALS is a response to an underlying toxic mechanism and therefore would not address the true cause of the disease.

**Excitotoxicity in ALS**

The killing of neurons by excessive activation of post-synaptic glutamate receptors is known as excitotoxicity [38]. The only drug approved for the treatment of ALS, Riluzole, was shown to inhibit excitotoxicity [39,40], yet clinical trials using other inhibitors of excitotoxicity, namely lamotrigine [41], topirimate [42], and gabapentin [43], have shown no effect on ALS. Still, multiple lines of evidence indicate that excitotoxicity plays a role in ALS pathogenesis.

First, statistically-significant increases in glutamate levels have been measured in blood plasma, both fasting [44] and following glutamate supplementation [44,45], in ALS patients relative to controls and similar increases were found in cerebrospinal fluid (CSF) [46,47]. In addition, multiple reports have been made outlining the reduction of glutamate in selective brain regions upon *post mortem* analysis [48,49]. Interestingly, as early as 1973 it was known that CSF from ALS patients has cytotoxic effects on cultured neurons [50-52], though the toxicity has not been directly linked to glutamate itself. The toxicity of ALS patient CSF to healthy neurons is mitigated by the application of both NMDA- and AMPA-receptor antagonists, as shown in a study that treated embryonic rat spinal cord tissue with CSF from patients homozygous for the D90A mutation in SOD1 [53]. Finally, in addition to differential regulation of glutamate or other excitotoxic factors in ALS, altered expression patterns of ionotropic glutamate receptors of the NMDA [54,55] and non-NMDA [56-58] subtypes, as well as the metabotropic glutamate receptors [59], has been reported in spinal cord tissues of ALS patients.

**Mitochondrial involvement in ALS**

Abnormal mitochondrial morphology was first reported in muscle tissue from ALS patients in 1966 [60]. Other evidence of mitochondrial pathology in ALS includes findings of vacuolated mitochondria near neurofilaments in sporadic and familial ALS [61], as well as observation of abnormal mitochondria in both upper and lower motor neuron pools [62-64]. However, such *post mortem* findings are limited by the inability to observe mitochondrial morphology in the early stages of ALS. The consequences of mitochondrial dysfunction in ALS might include an increased susceptibility of affected motor neurons to excitotoxicity, because mitochondrial dysfunction sensitizes motor neurons to glutamate toxicity [65,66]. The reverse scenario is that the abnormal mitochondrial morphology is a result of excitotoxicity, as suggested by studies showing that excitotoxicity-related $Ca^{2+}$ influx can overload mitochondria [65,66]. Mitochondrial dysfunction could also account for the increased levels of reactive oxygen species (ROS) observed in ALS [67,68]. Finally, cytochrome C release from damaged mitochondria initiates apoptosis, which plays a role in ALS as previously discussed.

**Protein aggregation**

Many diseases are now associated with protein aggregation and particularly with a form of ordered aggregate called the amyloid fibrils, which, regardless of the native sequence and structure of the precursor proteins, share distinct structural characteristics. From a protein-folding standpoint, the inherent properties of the polypeptide chain that allow proteins with little or no sequence or structural similarity to misfold and assemble into similar high-order structures are of vital interest. Studies of aggregate structure reveal defined characteristics such as extensive hydrogen bond networks perpendicular to the fiber axis, called a cross-β

conformation [69], and an α to β transition known to occur during the oligomerization of amyloid-forming proteins with significant helical content. Evidence for domain swapping as an early step in the aggregation process has been reported for several proteins [70-72]. In several aggregation-associated diseases including familial Amyotrophic Lateral Sclerosis and the transthyretin amyloidoses, the dissociation of a protein from its multimeric native state is known to be the rate limiting step for aggregation [73,74], suggesting a method for preventing aggregation by stabilizing the native interfaces of these assemblies [74,75].

Protein aggregates have alternately been deemed responsible for the pathologies of their various associated diseases and, more recently, credited with delaying or counteracting the observed pathologies by acting as a sink for highly cytotoxic soluble oligomers [76]. The viewpoint that soluble oligomers act as cytotoxic species has garnered widespread attention since at least 1999 when it was noted that the abundance of soluble Aβ 1-42 oligomers is a predictor of neuronal degeneration in Alzheimer's disease whereas amyloid levels do not correlate [77,78]. In 2003, Glabe and co-workers discovered that soluble oligomeric species from several disease-related proteins shared a common structural epitope to which an antibody was developed [79]. Later studies showed that soluble oligomers are able to disrupt the polarity of cellular membranes [80-82], one possible basis for disease-associated toxicity.

Various cellular protective mechanisms have evolved to ensure the proper folding of proteins. Molecular chaperones, for example, recognize misfolded proteins and provide an environment conducive to the formation of the appropriate native contacts [83]. Proteasomal machinery clears proteinaceous debris from the cell, employing ubiquitin ligases to tag misfolded proteins for degradation and removal [84,85]. One hypothesis formulated to explain the prevalence of protein aggregation in neurodegenerative diseases is that the ubiquitin

proteasome loses efficiency over time causing a buildup of protein aggregates and debris in post-mitotic cells such as neurons [86]. In support of this reasoning, parkin, an E3 ubiquitin ligase was found to be mutated in at least half of autosomal recessive juvenile parkinsonism patients, suggesting that a deficit in the clearance of its target protein leads to an early onset of symptoms [87].

**TDP-43 aggregation in sporadic ALS**

Recently, the association of a protein with sporadic ALS has caused a shift in the traditional thinking about the disease – providing a link between ALS and diverse ALS-related disorders. TDP-43, or the 43 kDa TAR DNA binding protein, was found to aggregate in both sporadic ALS and the related FLTD-U [88]. TDP-43 is a ubiquitously expressed protein that contains two RNA recognition motifs and a glycine-rich domain thought to be involved in protein-protein interactions. Hypothesized roles for the protein include transcriptional regulation and RNA processing [89,90]. In ALS, native TDP-43 is diminished in the nucleus, instead forming hyperphosphorylated nuclear and cytosolic aggregates [88,91], suggesting that the elimination of its normal nuclear function may be involved in the pathology of the disease. TDP-43 aggregation has been observed in a wider array of neurodegenerative diseases, though with a weaker association than in ALS. Two studies showed TDP-43 pathology in 30% of AD patients [92,93], while occurring in 75% of patients suffering from AD with hippocampal sclerosis [93].

The identification of several FALS families with mutations in TDP-43 [91,94-103] and the accumulation of TDP-43 aggregates in brain tissue [91,103] support the notion that the TDP-43 pathologies observed in sporadic ALS are capable of causing the disease rather than appearing as a consequence of a disease-related process. In the overwhelming majority of

cases, TDP-43 mutations occur in the glycine-rich of the C-terminal domain, which is thought to mediate protein-protein interactions [104].

TDP-43 inclusions, both neuronal and microglial are now held to be hallmarks of sporadic ALS and most familial forms of the disease. In the recently revamped understanding of ALS, SOD1-mediated FALS stands out as an obvious outlier. FALS resulting from mutations in SOD1 shows very little evidence for TDP-43 involvement [105-107]. The clinical aspects of the two diseases are similar, but the underlying mechanism is clearly different – *i.e.* no TDP-43 pathology is observed in SOD1-mediated ALS or in several mutant SOD1 mouse models [108]. Given the similarity in clinical progression, however, finding a common link in the pathological mechanisms of these two types of ALS may be a useful way to learn about the disease as a whole.

## Cu,Zn superoxide dismutase

### The properties of SOD1

The superoxide radical is a highly oxidizing species produced primarily as a byproduct in electron transport during oxidative phosphorylation at the mitochondrial membrane. SOD1 is the primary cytosolic enzyme that catalyzes the reduction of $O_2^{\bullet-}$, converting two molecules of $O_2^{\bullet-}$ to one molecule of $O_2$ and one molecule of $H_2O_2$, which is further converted to $H_2O$ and $O_2$ by the enzyme, catalase. In addition to the cytosolic SOD1, a mitochondrial isoform SOD2 exists, which uses a manganese atom, rather than a copper atom, in catalysis. A third, extracellular, superoxide dismutase, shares little structural similarity or sequence homology to SOD1.

Human SOD1 is a homodimeric metaloenzyme featuring one Cu and one Zn atom per 16 kDa monomer. Upon synthesis of SOD1, the N-terminal methionine is removed and the N-terminus of the remaining 153-residue polypeptide is acetylated. The Cu atom is the catalytic center of SOD1, while the Zn is responsible, in large part, for the extraordinary stability of SOD1. Wild type SOD1 has a $T_m$ of approximately 90 ºC, a $\Delta G_{fold}$ of 11.7 kcal/mol, and is active in 8 M urea. The structure of the SOD1 monomer is a β-barrel consisting of 8 anti-parallel β-strands in a Greek key arrangement in which strands 5 and 6 are inserted between strands 3 and 4. The active site of the enzyme is formed by two loops. The Zn-loop, which bridges strands 4-5 supplies many of the interactions that coordinate the Zn near the active site. The electrostatic loop coordinates the active site Cu, as well as forming contacts across the dimeric interface. Disulfide bonds in cytosolic proteins are exceedingly rare, yet the electrostatic loop is pinned to the β-barrel by a disulfide bond between Cys-57 and Cys-146. In addition to Cys-57 and Cys-146, two additional cysteines are also present in SOD1: Cys-6 and Cys-111. While Cys-6 is buried within the core of SOD1, Cys-111 is exposed to the environment and located in a pocket at the dimer interface. It has become a common practice in the field to mutate Cys-6 and Cys-111 to serine residues in order to prevent the formation of aberrant disulfide bonds in various experimental situations [109-113].

**SOD1 mutations in ALS**

Following the identification, in 1993, of 11 missense SOD1 mutations in 13 families with familial ALS, further studies have identified more than 115 missense mutations to date[1]. In addition to missense mutations, various other amino acid deletions and SOD1 truncation

[1] A complete list of FALS mutations in SOD1 is maintained online at http://alsod.iop.kcl.ac.uk/index.aspx

mutants have been identified in ALS families – including five synonymous single nucleotide polymorphisms at positions 10 [114], 59 [115], 139 [116], 140 [115,116], and 153 [116]. The ALS-associated mutations are distributed quite evenly across the primary and tertiary structure of SOD1 with the exception of residues 22-36 comprising β-strand 3 and the preceding loop, which has only been associated with FALS through mutations at position 29. Figure 1.1 shows the structure of the SOD1 dimer with the residues mutated in ALS represented by spheres. Mutations in SOD1 are, for the most part, destabilizing in the context of the monomer, the dimer, or both [113,117] and disease progression was shown to correlate with mutant instability [118]. It should be noted, however, that the degree to which a given mutation destabilizes SOD1 does not correlate with the severity of the ALS resulting from that mutation.

## Hypotheses for how SOD1 mutations result in ALS

### Glial effects

Non cell-autonomous mechanisms have been proposed to account for neuronal cytotoxicity in ALS based on data showing that expressing SOD1 mutants in astrocytes [119] are capable of inducing death of neighboring motor neurons through the release of a soluble cytotoxic species. To the same end, reducing the amount of SOD1 mutants in microglia increases motor neuron survival during later stages of ALS progression in transgenic mice [120]. Intriguingly, a complimentary scenario is also true, wherein non-neuronal cells expressing wild type SOD1 were found to extend the lifespan of neighboring motor neurons expressing SOD1 mutants [121].

Because of the central role of astrocytes in recycling glutamate at the synapse of motor neurons, these findings support the excitotoxic hypothesis of ALS discussed above – especially in light of studies showing the downregulation of astrocytic glutamate transporters in mice [122], rats [123], and humans [124] expressing mutant SOD1.

**Mitochondrial effects of SOD1 mutants**

Transgenic mice expressing mutants of SOD1 have proved valuable in examining mitochondrial pathology in ALS. SOD1G93A mice, in particular, show a disease progression similar to humans carrying SOD1 mutations consisting of a preclinical phase with no apparent muscle weakness, a period of rapid decline in muscle strength followed by a period of slower degeneration, and paralysis [125,126]. Mice in the preclinical phase prior to the onset of muscle weakness were found to feature axonal and dentritic mitochondrial vacuolization prior to motor neuron death [126-128].

Mechanistic studies of the mitochondrial defects uncovered an initial swelling of the mitochondrial intermembrane space [129] followed by the disintegration of inner membrane structures as measured by the dilution or disappearance of labeled cytochrome C – an inhabitant of the inner mitochondrial space [129,130]. These events might occur as a result of SOD1 mutants interfering with the function of molecular chaperones, which are necessary for protein import to mitochondria and subsequent refolding and the formation of functional mitochondrial protein complexes [131]. Alternatively, the interaction of SOD1 aggregates with Bcl-2 at the mitochondrial membrane [34] and/or preferential entry of SOD1 mutants into the mitochondrial intermembrane space [132] may induce the abnormal mitochondrial morphology observed in ALS.

**SOD1 Aggregation**

Neuronal and astrocytic aggregates containing SOD1 form in sporadic and familial ALS patients [133-137], as well as transgenic mice carrying mutations in SOD1 [138]. In-vitro aggregation studies of SOD1 mutants show the formation of annular structures [139,140] reminiscent of those formed by β-amyloid and α-synuclein [141,142]. Wild type bovine SOD1 is similarly capable of aggregation under destabilizing conditions [143]. Dimer dissociation has been established as a necessary event preceding aggregation [74,144], and is enhanced by the breakage of the C57-C146 disulfide bond [145]. The engineering of an inter-subunit disulfide, on the other hand, has the effect of restricting dimer dissociation and prohibiting subsequent SOD1 aggregation [140]. As a result of this finding, dimer stabilization using small molecules was proposed and tested as a therapeutic strategy to prevent SOD1 aggregation in SOD1-mediated FALS [146,147] with some encouraging results. Metal-deficient wild type and mutant SOD1 shows enhanced aggregation propensity [74,139], and both wild type and mutant apoSOD1 were shown to form soluble oligomers at physiological pH [148,149]. Because of recent evidence (discussed above) that oligomers are the cytotoxic species in a variety of neurodegenerative diseases characterized by the formation of proteinaceous aggregates [79,81], oligomeric SOD1 represents a valuable target for structural and mechanistic studies. The formation of stable early oligomers of both wild type SOD1 and a variety of SOD1 mutants is described in Chapter IV.

**Simulations of SOD1 folding and aggregation**

Simulations of SOD1 have contributed to the study of ALS in several ways. Atomic-resolution traditional molecular dynamics studies have probed the near-native dynamics of SOD1 dimers [150,151], suggesting that fluctuations in the loops enclosing the metals at the

active site can lead to SOD1 unfolding. Communication between SOD1 monomers was shown to be disrupted in a series of simulations of SOD1 mutants [150], illustrating how amino acid substitutions even distant from the dimer interface can result in enhanced monomer formation. The active site of SOD1 has also been studied using simulations [152-154], revealing that mutations result in overexposure of the Cu catalytic center, leaving it available for aberrant catalysis. The relative roles of the metal ions and the disulfide was studied in the context of both monomers and dimers of SOD1, revealing that although both metallation and disulfide formation stabilizes the dimer interface, metal binding contributes more toward monomer stability [155].

Because the size and timescale of aggregating systems of SOD1 are not amenable to study by all-atom molecular dynamics, simplified interaction potentials and coarse-grained protein models have been used to model the non-native association of misfolded SOD1 monomers *in silico* [156]. The results of that study are described at length in Chapter 2.

# CHAPTER 2

# SEQUENCE AND STRUCTURAL DETERMINANTS OF CU,ZN SUPEROXIDE DISMUTASE AGGREGATION


**Abstract**

Diverse point mutations in the enzyme Cu, Zn superoxide dismutase (SOD1) are linked to its aggregation in the familial form of the disease Amyotrophic Lateral Sclerosis. The disease-associated mutations are known to destabilize the protein, but the structural basis of the aggregation of the destabilized protein and the structure of aggregates are not well understood. Here, we investigate *in silico* the sequence and structural determinants of SOD1 aggregation: (a) we identify sequence fragments in SOD1 that have a high aggregation propensity, using only the sequence of SOD1, and (b) we perform molecular dynamics simulations of the SOD1 dimer folding and misfolding. In both cases, we identify identical regions of the protein as having high propensity to form intermolecular interactions. These regions correspond to the N- and C-termini, and two crossover loops and two β-strands in the Greek-key native fold of SOD1. Our results suggest that the high aggregation propensity of mutant SOD1 may result from a synergy of two factors: the presence of highly amyloidogenic sequence fragments (“hot-spots”), and the presence of these fragments in regions of the protein that are structurally most likely to form inter-molecular contacts under destabilizing conditions. Therefore, we postulate that the balance between the self-

association of aggregation-prone sequences and the specific structural context of these sequences in the native state determines the aggregation propensity of proteins.

## Introduction

The formation of protein aggregates is associated with cytotoxicity in more than 20 diverse human pathologies including amyotrophic lateral sclerosis, Alzheimer's, Parkinson's and prion diseases [157-159]. Experimental evidence suggests that specific, contiguous sequence fragments in proteins may be responsible for nucleating the conversion of native proteins to amyloids [160,161]. Peptides corresponding to sequence fragments of amyloid-forming polypeptides, such as the amyloid β peptide, yeast and human prion proteins, calcitonin, insulin, transthyretin, β2 microglobulin, and tau protein, have been shown to form amyloid fibrils *in vitro* (Ref. [162] and references therein). The contribution, if any, of the identified peptides to the aggregation of the whole protein, is determined by their context in the intact protein, but local structural propensities may also be important. For example, mutations found to diminish (or enhance) the aggregation of isolated helical peptide fragments of human procarboxypeptidase by enhancing helix-propensities (comprised of local interactions) also diminish (or enhance) the aggregation of the entire polypeptide chain [163]. Interestingly, the procarboxypeptidase mutations that diminish aggregation do not affect the overall stability of the protein under the conditions of aggregation, showing that aggregation propensity of the intact protein was modulated by controlling the local structural propensities of sequence without perturbing its overall stability. Furthermore, the insertion of fragments (that aggregate in isolation) of human β2-microglobulin and the PI-SH3 domain into their respective non-aggregating homologs, mouse β2-microglobulin and the α-

spectrin-SH3 domain, causes the engineered homologs to readily aggregate. Although the effect of the insertion of aggregating fragments on the overall stability of the protein was not determined, these results suggest that identification and engineering of sequence fragments that aggregate in isolation may be a strategy to modulate the aggregation of the intact protein [164,165].

In the aggregated state, amyloidogenic proteins have been found to be arranged as β-strands in sheets [162,166]. In aggregates formed by a fragment of the Aβ-peptide, the amino acid sequence is stacked in parallel β-strands and is on average in exact register [167]. Similarly, for a 12-mer peptide designed to form amyloid fibrils, in-register parallel β-strand topologies were observed in crystal structures [168]. Anti-parallel β-strand topologies have also been observed for peptide aggregates, and changes in amphiphilicity of the aggregating peptide were found to lead to a change from anti-parallel to parallel topology for peptides derived from Aβ-peptide [169]. Therefore, both parallel and anti-parallel topologies can be adopted by peptides depending on their sequence and environmental conditions. Thus, in a previous study, aggregation-prone short peptide sequences were successfully designed by estimating the fitness of the sequence in anti-parallel β-sheet conformations [170]. However, for larger intact proteins, considerable heterogeneity may exist in the alignment of amino acids from different polypeptide chains.

It is widely believed that protein aggregation requires partial or complete unfolding of the native state[162,171]. Unfolding may result in the exposure of amyloidogenic sequence fragments, which in turn may lead to oligomerization. It has been argued that natural selection has led to amyloidogenic sequence fragments being protected in the native states of protein structures found in nature [157,172]. Therefore, the ability of amyloidogenic sequences

to induce aggregation is modulated by the global stability and the structure of proteins. Protein aggregation propensity is then, the interplay between the stability of the native structure, which prevents protein aggregation, and the self-association of sequences from different polypeptide chains, which promotes protein aggregation. Consequently, mutations associated with familial forms of neurodegenerative diseases may promote aggregation by either destabilizing the native state and/or increasing the self-association propensities of exposed sequence fragments under destabilizing conditions. However, the molecular basis underlying protein aggregation and the effect of mutation on aggregation is not well understood. To understand the physical basis of protein aggregation, here we address the following questions: (i) which, if any, sequence fragments in a protein have high amyloidogenicity in isolation, and (ii) how is the association of these fragments modulated by the native structure and stability of the protein during its misfolding?

To address these questions, we develop an *in silico* method to identify sequence fragments and structural regions that have high amyloidogenic propensity. We apply our method for determination of the sequence and structural aggregation propensities to the homodimeric enzyme Cu, Zn superoxide dismutase (SOD1). The mutation-induced aggregation of SOD1 has been implicated in the familial form of the disease amyotrophic lateral sclerosis (FALS) [159]. In its native state, each SOD1 monomer adopts the classic Greek-key fold [173] – a β-barrel composed of two β-sheets, each composed of four β-stands and connected by two cross-over loops (Figure 2.1a). The more than 90 FALS-associated point mutations are scattered throughout the structure of SOD1. A subset of these mutations is known to destabilize SOD1, both *in vitro* and *in vivo* [174-176]. It was previously demonstrated that *in vitro* SOD1 aggregation involves dissociation of the dimer, the loss of

metal ions, and assembly of misfolded apo-monomers into aggregates [140,144,177]. The first step in the SOD1 aggregation possibly occurs via the non-native dimerization of apo-monomers.

The domain swapping mechanism [144,178-180] was suggested as a plausible mechanism for the formation of aberrant dimers. Three-dimensional domain swapping is an event by which a monomer exchanges part of its structure with other identical monomers to form an oligomer where each subunit has a similar structure to the monomer. Domain swapping, initially proposed as a mechanism of functional regulation, has also been proposed to lead to misfolding and aggregation [180-182]. Although there is little direct evidence for domain swapping as a mechanism for aggregation and amyloid formation, several experimental (Ref. [181] and references therein) and computational [183-185] studies support the role of domain swapping in aggregation. For example, a correlation between domain swapping propensity of the protein p13suc1 was found to be correlated with its rate of aggregation [186]. Eisenberg and coworkers have designed both domain-swapped dimers and high-order oligomers from the same three-helix bundle structural motif but with different topologies [180,187,188]. Furthermore, domain-swapped forms of both the human prion protein and the amyloidogenic human cystatin C [183,189] have been crystallized. Computer simulation studies [183-185] using simplified native-structure based Gō-models [190,191] have shown that the monomeric protein topology alone is sufficient for predicting how a protein will form domain-swapped complexes, including higher-order oligomers. In computational domain-swapping studies of the SH3 domain [183,185], two types of topologies have been detected: “closed” domain-swapped dimers which are observed in X-ray crystal structures [192], and more “open” oligomers which can be propagated to form fibrils. Structural features of the

computationally obtained fibrils agree with the X-ray diffraction patterns obtained in experiments [193]. Simulations of domain swapping, therefore, capture the process of misfolding and inter-chain interactions, and provide an avenue to investigate the early events

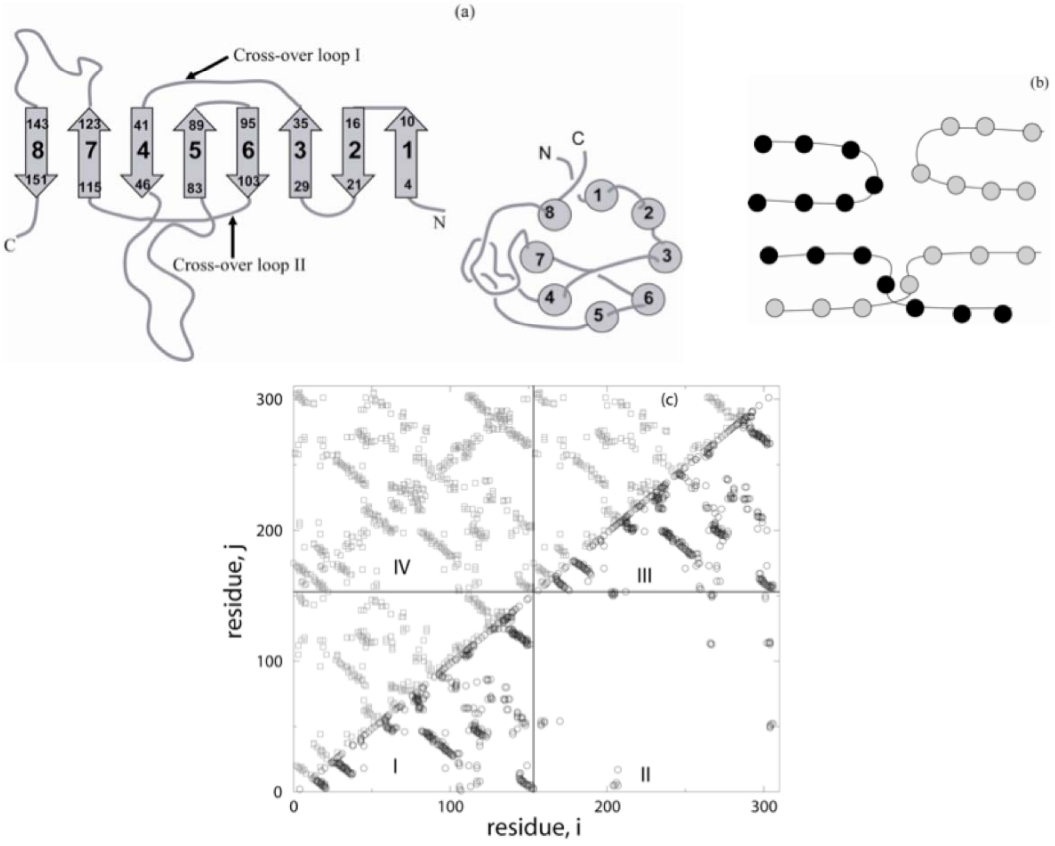


**Figure 2.1. SOD1 topology** (a) A schematic of SOD1. The regions identified as amyloidogenic are the β-strands 1, 4 and 7, and 8 and the two cross-over loops that connect the two β-sheets in the SOD1 barrel. (b) A schematic of domain-swapped interactions and (c) the domain-swapped contact map used for simulations. In the contact map, regions I and III correspond to the intra-monomer contacts of the two monomers, region II corresponds to contacts on the dimer interface, and region IV corresponds to the domain-swapped interactions between the two monomers.

in the amyloidogenesis of proteins. Although little is known experimentally about the structural process of SOD1 aggregation itself, domain swapping has been suggested as a mechanism for the aggregation of β2-microglobulin, a structural homolog of SOD1 [165].

Therefore, domain swapping allows a description of the initial steps in SOD1 fibril formation.

To evaluate the sequence determinants of SOD1 aggregation, we identify sequence fragments that have a high tendency to self-associate into in-register β-strands, based purely on the sequence of SOD1. To determine the structural determinants of SOD1 aggregation, we study the folding and misfolding of the SOD1 dimer, based purely on the geometry of the dimer. Both these complementary approaches identify the same amyloidogenic regions in the protein – corresponding to the two termini, and two β-strands and to the two cross-over loops in SOD1 (Figure 2.1a) – indicating that the high aggregation propensity of SOD1 may be due to both amyloidogenic sequence "hot-spots" and their structural context. Our results suggest that aggregation of proteins may be mediated by the presence of both self-associating sequence fragments and the presence of these fragments in specific aggregation-prone structural elements of the protein.

## Methods

### Preparation of peptide fragment structures

We obtain a total of 147 fragments of seven consecutive residues for the 153 residues in a SOD1 monomer. For each fragment, we construct the following five conformations: monomer, β-strand dimer (parallel and anti-parallel), and β-strand tetramer (parallel and anti-parallel). For constructing the dimer and tetramer, we mount the sequence of each fragment on idealized parallel and anti-parallel β-sheet structures using the package SCWRL. These template structures are constructed using the packages MOE (Schrödinger Inc.) and have ideal parallel or anti-parallel β-sheet geometry. We cap the strands at the N-

and C-termini by acetyl and N-methyl groups respectively, using the package SYBYL (Tripos, St. Louis, MO). For constructing the monomer, the sequence of each fragment is mounted on a random coil conformation generated using SYBYL.

**MD simulations and free energy calculations**

For each fragment, we perform all-atom MD simulations of each conformation and calculate the conformational free energy. For each MD trajectory, the simulation time is 496 picoseconds (ps) in explicit solvent (SPC water model [194]) using the SigmaX2.2 MD program. Conformational free energy is calculated using the ES/IS method [195] for every snapshot. Following the procedure for free energy calculations described in Ref. [196], each MD simulation consists of relaxation of the peptide(s) and water, followed by a production run of 496 picoseconds, where snapshots are collected at intervals of 1 ps. The conformational free energy is

$$G = \langle E \rangle - TS_{conf} + \langle \Delta G_{solv} \rangle, \quad (1)$$

where <…> represents the average over the MD trajectory, $E$ is the internal energy of the peptides in vacuum, $T$ is the absolute temperature (set to 300 K), $S_{conf}$ is the configurational entropy, and $\Delta G_{solv}$ is the solvation free energy, calculated using an implicit solvation model described by Vorobjev and Hermans [197].

For each fragment $i$, the difference between the average conformational free energies of the dimer and two times that of the monomer, $\Delta G_D^i$, represents the free energy of dimerization:

$$\Delta G_D^i = \left( \overline{G_D^i} - 2 \cdot \overline{G_M^i} \right) \pm \sqrt{\sigma^2\left(G_D^i\right) + 4 \cdot \sigma^2\left(G_M^i\right)}, \quad (2)$$

where $\overline{G_D^i}$, $\overline{G_M^i}$, $\sigma^2\left(G_D^i\right)$ and $\sigma^2\left(G_M^i\right)$ are the averages and standard deviations of the conformational free energies of the dimer and the corresponding monomer, respectively. The free energy of tetramerization $\Delta G_T^i$ is similarly the difference between the average conformational free energies of the tetramer and four times that of the monomer. The values $\Delta G_D^i$ and $\Delta G_T^i$ are measures of the amyloidogenicity of a given sequence fragment.

To calculate the per residue amyloidogenicity for the protein sequence, we assume that each residue in a given fragment contributes equally to its calculated amyloidogenicity. The amyloidogenicity of any residue is its average contribution to the amyloidogenicity of all fragments that include this residue. This averaging ensures that the amyloidogenicity of a given residue is modulated by its sequence neighbors. The amyloidogenicity, $\Delta G^j$, of the residue *j* is

$$\Delta G^j = \left( \frac{\sum_{i=1}^{n} \Delta G_D^i}{7n} \right) \pm \frac{\sqrt{\sum_{i=1}^{n} \left( \sigma^2 \left( \Delta G_D^i \right) \right)}}{7n}, \qquad (3)$$

where the sum of $\Delta G_D^i$ is over all dimer fragments, *n* ($1 \leq n \leq 7$), that include a given residue *j*, and the second term in Eq. (3) is the standard deviation. We calculate a similar per-residue amyloidogenicity profile for the tetramer structures.

**Discrete molecular dynamics simulations**

We use a scaled Gō-model, based on the interaction scheme developed by Khare et al. [198], to model the folding and misfolding of the SOD1 dimer. We assign pair-wise, square-well interaction potentials between beads in a simplified polypeptide model according to contacts formed in the native state, i.e. two residues are said to be in contact if any of their atoms

(excluding hydrogen) are within 4.5 Å in the native state crystal structure (Protein Databank accession code 1SPD). This procedure results in a matrix of contacts $\Delta_{ij}$, in which each element is equal to 1 if residues *i* and *j* are in contact, and 0 otherwise (Figure 2.1c). The contact map includes interactions between monomers at the dimer interface. In addition, we allow the formation of both intra- and inter-monomer contacts, for example, Ile 18 from chain A, which forms a native contact with Ala 4 from chain A, can also interact analogously with Ala 4 from chain B. Thus, the effective Gō-like energy of the model protein is

$$E = \sum_{i,j} \varepsilon \cdot \Delta_{ij} + \sum_{i,k} \varepsilon \cdot \Delta_{ik}^{\dim} + \sum_{i,j*} \alpha_{domain-swap} \cdot \varepsilon \cdot \Delta_{ij*}, \quad (4)$$

where ε is the strength of a contact, $\Delta_{ij}$, $\Delta_{ik}^{\dim}$, and $\Delta_{i,j*}$ are the contact maps corresponding to a monomer, the dimer interface, and the domain swapping interactions, respectively. The value $\alpha_{\text{domain-swap}}$ in Eq. (4) is used to regulate the degree of inter-monomer overlap, or the effective concentration of the protein. When $\alpha_{\text{domain-swap}}>1$, interactions between residues from different monomers are stronger than intra-monomer interactions, resulting in a tendency of each chain to penetrate the pervaded volume of the other chain, rather than forming intra-chain contacts. This scenario corresponds to a polypeptide concentration in the semi-dilute regime[199]. There is an additional translational entropic contribution associated with the interactions between amino acids from different protein chains compared to the analogous interactions within the protein chain. Therefore, the magnitude of the inter-protein interactions may differ from the intra-protein interactions between analogous amino acids depending on environmental conditions such as the protein concentration. To capture this effect, we study the dynamics of misfolding at different values of the scaling factor $\alpha_{\text{domain-swap}}$.

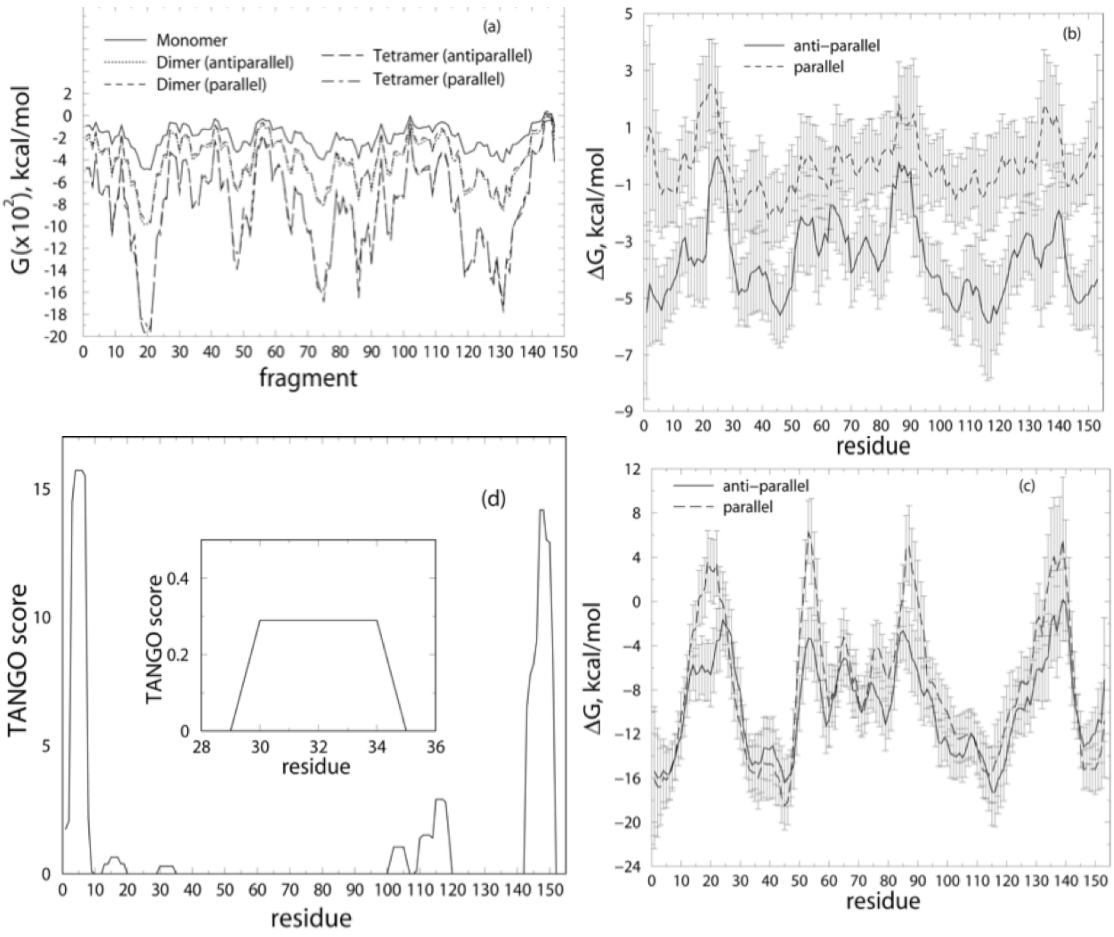


**Figure 2.2. Sequence propensities for aggregation**. (a) The free energy of the 147 overlapping heptamer sequence fragments of SOD1, mounted on various template backbones. We use the average contribution of each residue to the free energy of all fragments containing the residue to evaluate the free energy of oligomerization of the residue. (b) The free energy of dimerization for each residue (c) The free energy of tetramerization for each residue. (d) Sequence profile for aggregation obtained using the TANGO program. The inset shows the region from residue 28-36 at a higher magnification.

# Results

### Sequence determinants of SOD1 amyloidogenesis

Since the formation of β-sheets is a necessary condition for aggregation [157,170], to identify amyloidogenic sequence fragments in SOD1, we use idealized dimer and tetramer β-strand

templates, in both parallel and anti-parallel conformations. We mount overlapping heptapeptide sequences from the SOD1 sequences on each template, and calculate the conformational free energies of the 147 heptapeptide sequence oligomers using explicit solvent 496-ps MD simulations and an implicit solvation energy function (Eq. (1), Figure 2.2 (a)). By subtracting the free energy of two and four monomers from parallel and anti-parallel dimers and tetramers, respectively, we obtain the free energies of dimerization and tetramerization into these parallel and anti-parallel β-structures (Eq. (2)). We use these values to obtain a sequence-profile for amyloidogenicity (Eq. (3), Figures 2.2b and c). The free energy contribution per residue ranges from -5.9 to +2.5 kcal/mol for dimerization (Figure 2.2b), and from -18.3 to +6.1 kcal/mol (Figure 2.2c). Although for a given residue, the magnitude of the amyloidogenicity is larger in the tetramer compared to the dimer, we obtain similar free energy profiles for parallel, anti-parallel, dimer and tetramer (Figures 2.2b and c) structures. Thus, we conclude that the free-energy profiles adequately represent the oligomerization propensity of the SOD1 sequence fragments.

Based on the sequence amyloidogenicity profile, we identify sequence regions with high and low amyloidogenicity. Four regions of the protein have high amyloidogenicity: the N- and the C-termini, and the residues 35-45 and 110-120. The residue sequence 35-45 (IKGLTEGLHGF) is a crossover loop, and connects the two β-strands, β3 and β4, of the sheets in the barrel. The residue sequence 110-120 (HCIGRTLVVH) corresponds to a loop between the strands β6 and β7 (residues 110-114), and the strand β7 (residues 115-120). Residues 113-115 are also part of the dimer interface, and in the native dimer structure are symmetrically placed such that residues 113 and 114 from both subunits form contacts with

each other. Thus, we find that specific regions of the SOD1 sequence have a high propensity to oligomerize into in-register, parallel and anti-parallel β-strands.

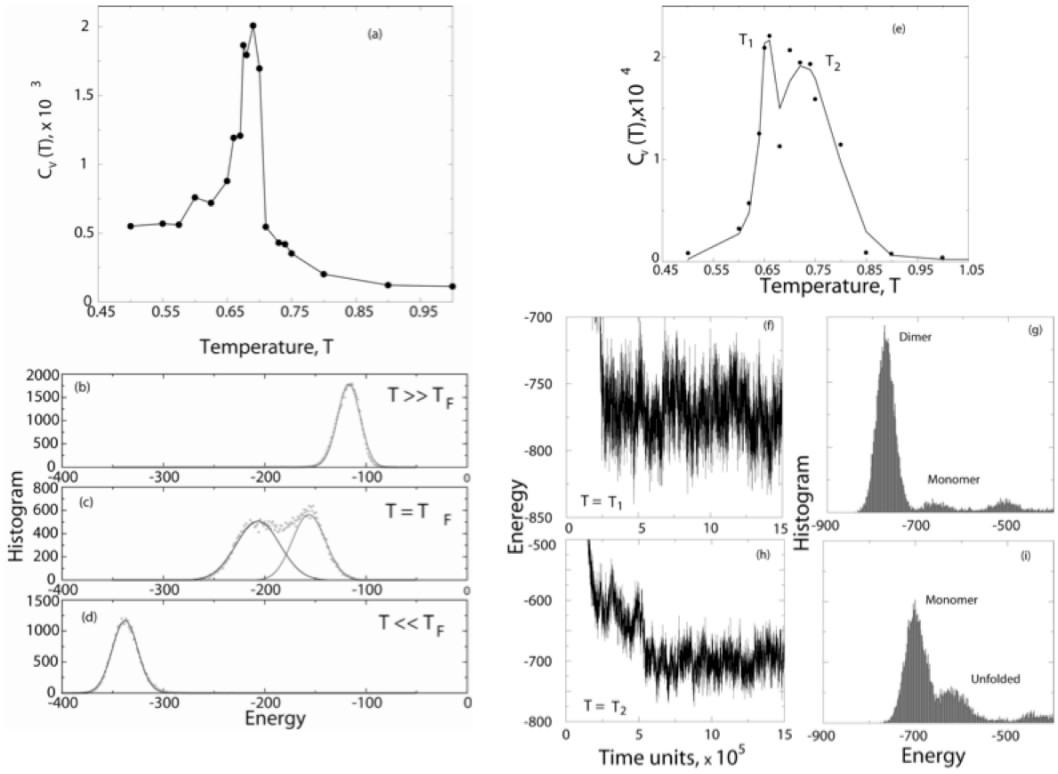


**Figure 2.3. Folding of SOD1 monomer and dimer** (a)-(d) Folding of the SOD1 monomer. (a) The heat capacity as a function of temperature shows a single peak at the folding transition temperature, $T_F$. The histograms of populations at (b) $T<<T_F$ , (c) $T=T_F$ and (d) $T>T_F$ show that the folding transition is two state, as found in experiments. (e)-(i) The folding of the SOD1 dimer. (e) The heat capacity *versus* temperature shows two peaks (at $T_1$=0.66 and $T_2$=0.72) indicating the existence of multiple transitions. Trajectories and population histograms at the two transition temperatures, (f) and (g) at $T_1$, and (h) and (i) at $T_2$ show that the folding/unfolding of the dimer is a three-state process, involving folded dimer, folded monomers and unfolded monomers, as found in experiments.

As a control, we obtain a SOD1 sequence profile for aggregation using the TANGO[200] server developed by Serrano and colleagues. We find that the "β-aggregation propensity" prediction from TANGO (Figure 2.2d) is in good qualitative agreement with the aggregation profile obtained by our free energy method. The prediction from TANGO

identifies the N- and the C-termini, and the residue sequence 100-120 identical to our prediction, and the region 35-45 identified by us is also amyloidogenic (although weakly so) according to the TANGO prediction (Figure 2.2d, inset).

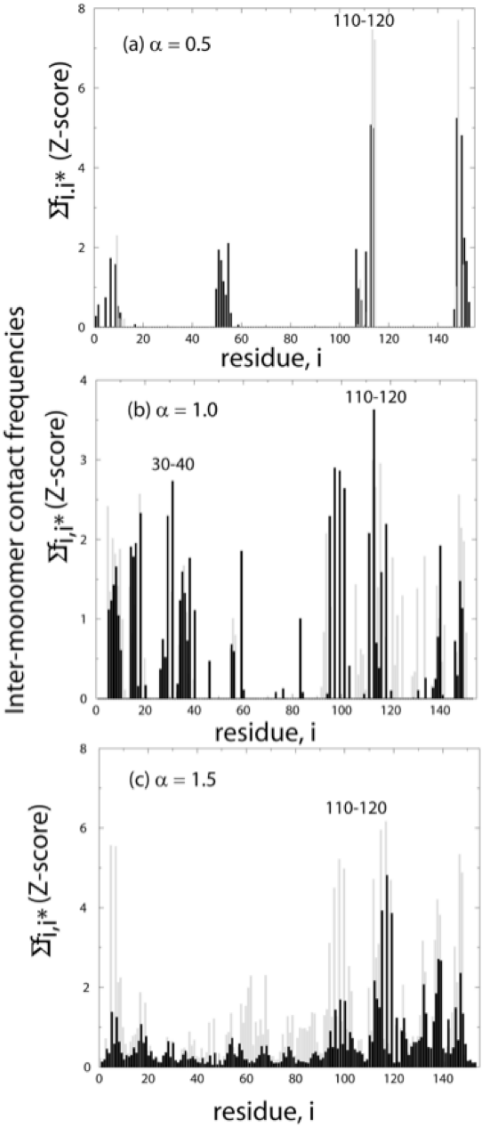


**Figure 2.4. Inter-monomer interactions during misfolding.** (a) The cumulative frequency of inter-monomer contacts at (a) α=0.5, (b) α=1, and (c) α=1.5 at *T*=0.65 (black) and *T*=0.75 (grey). As the strength of domain swapped interactions increases, the native dimer interface is lost and several competing dimeric structures are populated.

**Folding thermodynamics of SOD1 monomer and dimer**

In the context of the entire polypeptide chain, the oligomerization of the identified amyloidogenic "hot-spot" sequences is dependent on the degree to which these sequences are exposed in unfolded or partially folded SOD1. To identify the regulation of amyloidogenic sequences during the misfolding of SOD1, we first model the folding of SOD1 monomer and dimer to reproduce the experimentally observed thermodynamics of folding. Protein folding pathways are largely determined by the topology of the native state [201-206], and, therefore, the native topology of SOD1 determines the specific sub-structures of the protein that are exposed in the aggregation-prone partially folded states (i.e. the structural determinants of SOD1 aggregation). The principal difficulty in studying the folding of proteins *in silico* is the lack of accurate information

about the energetics of interaction between amino acids. Since protein structures have *a posteriori* information about the amino-acid interactions [202], simplified native-structure based models such as the Gō model are used to study folding. In the Gō model [190,191], the energy of the protein is expressed as a sum of pairwise native contact energies. A native contact exists between amino acid residues if they are closer to each other than a cut-off distance in the native state, and folding process is regarded as the acquisition of all native contacts. Typically, in these simplified models of folding, a coarse-grained representation of the protein is used in which each amino acid is represented by one or more beads and the protein chain is represented as beads-on-a-string [207]. For modeling SOD1 folding, we use a coarse-grained representation of the SOD1 polypeptide chain developed by Ding et al. [208] (6-bead model, 4 backbone and 2 side chain beads). We have previously shown that a scaled Gō-model of native-state based inter-residue interactions can reproduce the two-state folding of the SOD1 monomer [198] (see Methods). Starting from a stretched conformation, we perform equilibrium simulations at constant temperatures, $T$, ranging from $T$=0.1 to 1.0 (Figure 2.3a-d). We find that the 6-bead polypeptide model with scaled-Gō interactions reproduces the experimentally observed two-state folding thermodynamics of SOD1. For a two-state protein, the heat capacity is expected to have a single peak (Figure 2.3a) at the folding transition temperature, $T_F$. A MD trajectory at $T=T_F$ consists of two distinct populations – folded and unfolded – at equilibrium with other, characteristic of a two-state protein (Figure 2.3c). At $T>>T_F$ (Figure 2.3b) and $T>T_F$ (Figure 2.3d), on the other hand, only the folded and the unfolded states, respectively, are populated.

Next, we model the folding of the SOD1 dimer (Figures 2.3e-i). In addition to the intra-monomeric contacts of the two monomers, the contact map of the dimer contains

contacts corresponding to the native dimer interface (Square II in Figure 2.1c). Starting from two stretched chains, we perform equilibrium simulations at constant temperature ranging from $T$=0.1 to $T$=1.0. The heat capacity *versus* temperature curve shows the existence of two transitions, corresponding to the temperatures $T_1$=0.66 and $T_2$=0.72 (Figure 2.3e). The MD trajectories at $T_1$ consist of two distinct populations, corresponding to the dimer and two folded monomers respectively (Figures 2.3f and g), whereas at $T_2$, the two populations correspond to the folded monomers and unfolded monomers respectively (Figures 2.3h and i). At low temperatures ($T>>T_2$), the native dimer is formed, where as at high temperatures ($T>T_2$), both chains are unfolded. This is in accord with experimental studies, in which the folding of the dimer has been shown to be a three-step process [140,177,209]:

$$D \rightleftharpoons 2M \rightleftharpoons U, \tag{5}$$

where $D$ is the dimer, $M$ is the monomer and $U$ is the unfolded state Thus, our simulations reproduce the folding thermodynamics of the SOD1 dimer in agreement with the experimentally observed thermodynamics.

**Structural determinants of SOD1 misfolding and aggregation**

After verifying that the SOD1 monomer and dimer models fold to the correct native state with the experimentally observed two-state and three-state thermodynamics respectively (Figure 2. 3), we study the misfolding of the SOD1 dimer. In Eq. (4), when $\alpha_{\text{domain-swap}}>1$, the relatively higher strength of inter-monomer domain-swapped interactions (see Methods) compared to the intra-monomer interactions mimics an increase in the protein concentration. At high concentrations, native structure formation within a monomer competes with the formation of domain-swapped [140,178,179] topologies (Figures 2.1b and c). Further, non-

specific hydrogen bonds can form between the backbones of the two monomers. Under these conditions, we expect to observe non-native topologies. We perform dimer simulations over a range of α-values, $\alpha$ = 0.5, 1, and 1.5, to screen for non-native dimeric forms of SOD. To obtain the aggregation propensity of each residue, we calculate the cumulative frequency of inter-monomer contacts formed by each residue at the temperatures $T$=0.65 and $T$=0.75 (Figure 2.4). For the native dimer, the residues on the dimer interface are 5, 7, 9, 50-53, 113-115, and 150-153, in each monomer. Since aggregation has been shown to occur in a narrow temperature range around the folding transition temperature, first we analyze inter-monomer interactions in simulations with domain-swapped interactions in the range $T$=0.65 to $T$=0.75 (the transition temperatures for the native dimer are $T_1$=0.66 and $T_2$=0.72).

At $\alpha$=0.5, the folding of the dimer is native-like, as evidenced by frequency profile (Figure 2.4a) where residues that are involved in the native dimer interface form inter-monomer contacts with a high frequency at both $T$=0.65 (red bars) and $T$=0.75 (green bars). However, other residues in the vicinity of the dimer interface residues, such as 3, 55, and 107-110 also form inter-monomer contacts with a high probability. Thus, although weak domain-swapping interactions do not significantly alter the folding of the dimer, several residues, especially near the native dimer interface and near residue 110, can induce alternate dimer conformations.

At $\alpha$=1, we observe significant non-native contact formation, especially at $T$=0.65, which is near the transition temperature $T_1$=0.66 for dimer dissociation (Figure 2.4b). The residues that form inter-monomer contacts include the native dimer residues and several other residues, especially at the N- and the C-termini, and the regions 25-40 and 100-120.

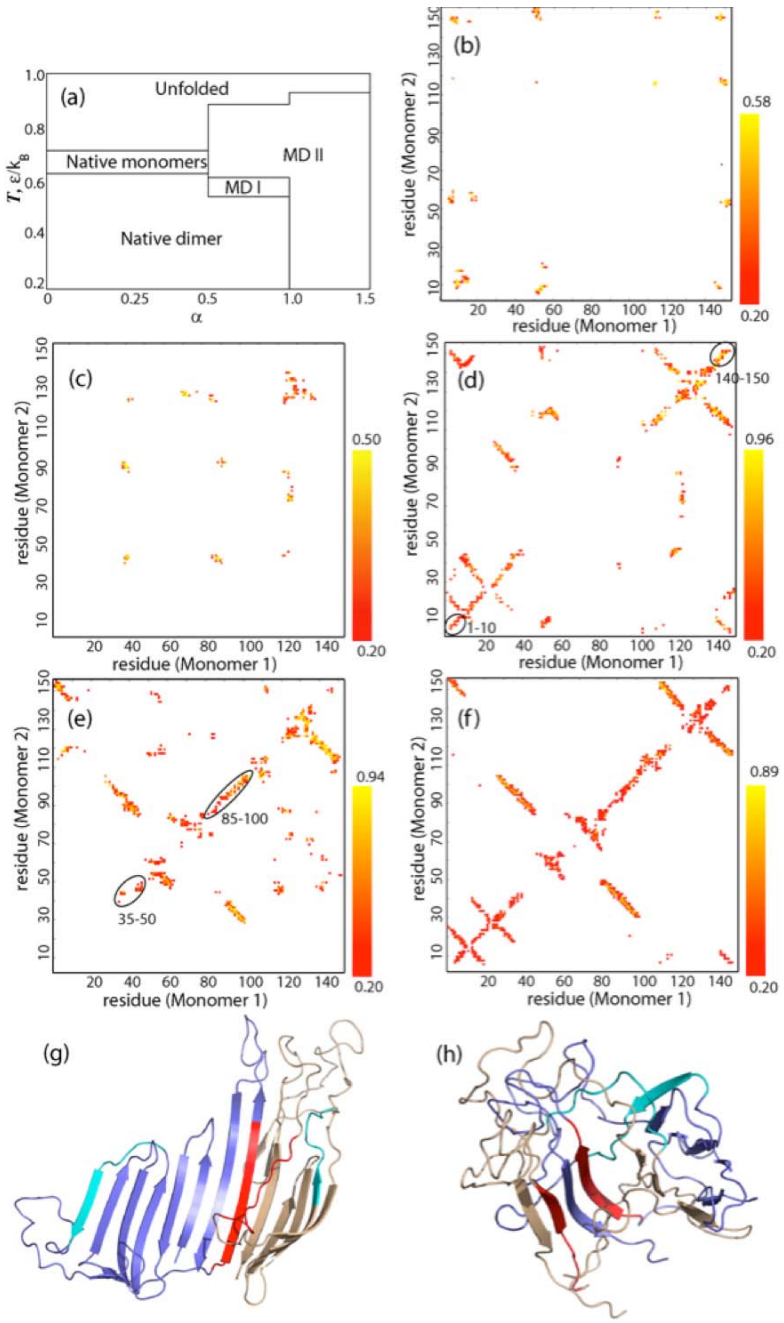


**Figure 2.5. Self-association and domain-swapping.** (a) A "phase diagram" summarizing the dimer topologies observed as a function of α and *T*. At low temperatures and α-values, native topologies (dimer, monomer) are observed, whereas at higher α-values (α=1.0 and 1.5), domain-swapping interactions lead to the appearance of modified dimers (MD I and MD II). Contact frequency maps corresponding to the inter-monomer contacts in (b) native and (c)-(f) modified dimers. Domain-swapping induced by high values of α and *T* is associated with the formation of self-association contacts (between corresponding identical elements of the two chains), which lie on the diagonal of the contact map. (c) MD I, for example at α=1.0 and T=0.5 is characterized by a small number of inter-monomer contacts in isolated elements of the structures, whereas MD II, for example at (d) α=1.5, T=0.4 (e) α=1.5, T=0.5 and (f) α=1.0, T=0.8 is characterized by extensive interactions between β-strands from the two monomers. Topologies observed for both MD I and MD II are diverse. Two representative structures of modified are shown in (g) and (h). These structures are formed by in-register interactions between residues 110-120 (red) or residues 35-45 (blue). We propose that there are multiple mechanisms by which these modified dimers can further propagate the aggregate structures and eventually form fibrils.



The

formation of inter-monomer contacts by both the native dimer interface and specific non-native residues suggests that the formation of an alternate dimer interface competes with the formation of the native dimer interface.

At $\alpha$=1.5 and $T$=0.65, the native dimer interface is not seen as evidenced by a disappearance of inter-monomer contacts by native interface residues (Figure 2.4c). Instead, a new set of residues, 55-65, 90-100, 110-120 is observed to form the most inter-monomer contacts. Thus, at increasing concentrations of the destabilized dimer, simulated by increasing $\alpha$-values, we observe decreased formation of the native dimer interface and an increase in the formation of alternative dimer interfaces.

To investigate the underlying structural interactions responsible for alternative dimer formation in our models, we analyze in detail dimer topology as a function of $\alpha$-values, and $T$. We classify the observed topologies according to the elements of secondary structure forming inter-monomer contacts in a complete phase-diagram (Figure 2.5a). We find that at $\alpha \leq 0.5$, the folding of the dimer is native-like in the temperature range $T$=0.2 to $T$=1.0, and no non-native dimer topologies are formed. The inter-monomer contact frequency map in Figure 2.5b thus resembles the native contact map (Square III in Figure 2.1c). Similarly, at $\alpha$=1 and $T$<0.5, the native-dimer is formed. In the range $0.5 \leq T \leq 0.6$, dimers with a small number of non-native inter-monomer contacts are formed (modified dimer MDI, Figure 2.5c). Interestingly, several of these contacts correspond to the identical sequences from the two monomers interacting with each other, e.g. residue sequences 39-44, 70-74, 85-92 and 123-135 self-associate, and interact with each other (Figure 2.5c). For $\alpha$=1 and $0.6 \leq T \leq 0.8$ (Figure 2.5f), and for $\alpha$=1.5 and $0.2 \leq T \leq 0.9$ (Figure 2.5d and e), extensive self-association of the following fragments occurs during the formation of structures with varying degrees of

domain-swapped interactions (modified dimer MDII): the N-terminal, 21-40, 87-100, 90-115, 120-130 and the C-terminal (Figure 2.5d-f). This finding suggests that for model SOD1 domain swapping, self-association of certain sequences allows the formation of domain-swapping interactions. The self-associated fragments observed in simulations (with no explicit sequence information) overlap with those identified by sequence analysis (N- and C-termini, residues 35-45 and 100-120, Figure 2.2c), indicating a synergy between structural and sequence elements in SOD1 with a high propensity to self-associate.

An examination of the structures with the varying degrees of domain swapping shows a diversity of conformations. This is expected to be the case if dimer formation is under kinetic control and further oligomerization, i.e. the formation of a trimeric or a higher-order species, causes thermodynamic stabilization of some of these topologies. These observations are in agreement with recent computational and experimental studies [210,211] suggesting that kinetic effects play an important role in the early stages of aggregation. Based on the structures of non-native dimers observed in simulation, we propose several plausible, kinetically competing aggregation pathways. For example, two representative structures are shown in Figure 2.5 (g) and 5(h). Each of these two non-native dimeric states persists throughout the entire simulation time of $1.5\times10^5$ time units once it is formed. Figure 2.5g shows a domain swapping interaction to form a native-like beta-barrel using half of the strands from each monomer, while the remainder of each monomer undergoes smaller-scale strand-by-strand pairing between the chains. Interestingly, residues 35-45 from each monomer associate with each other at the interface between the canonical domain-swapped region and the strand-swapped region. Domain swapping of this nature results in the

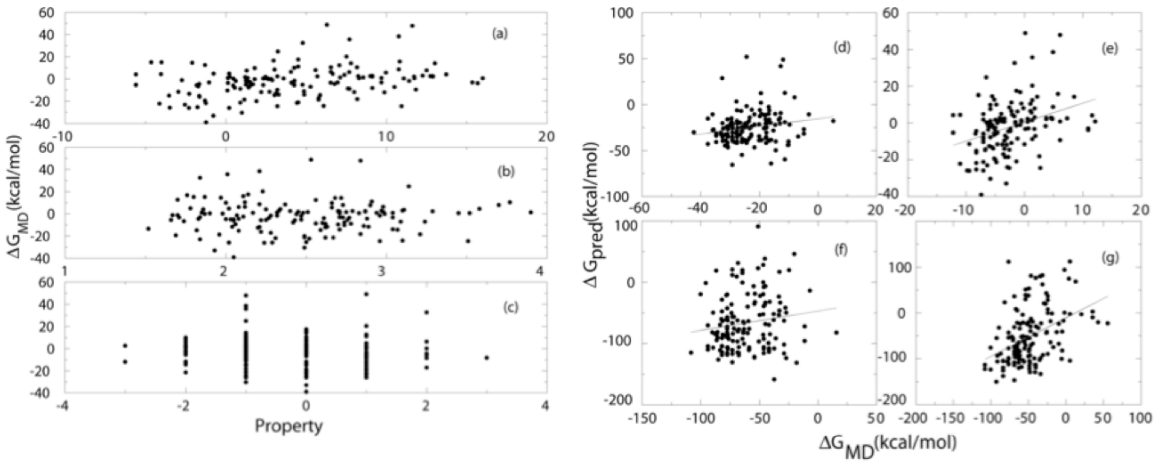


**Figure 2.6. The correlation between the free energies of dimerization into anti-parallel β-strands obtained in MD simulations with physical-chemical properties of the fragment.** Correlations of free-energy of association with (a) the average hydrophobicity (b) β-sheet propensity (c) net charge at pH 7, of the fragment. A linear combination of the three properties also does not correlate well with the free energies calculated from MD simulations of fragments mounted on (d) anti-parallel dimeric (e) parallel dimeric (f) anti-parallel tetrameric (g) parallel tetrameric template structures. We conclude that the free energy of oligomerization calculated in the MD simulation is not sufficiently explained by these physico-chemical properties of the sequence.

apposition of identical, aggregation-prone sequences from each monomer. Figure 2.4h shows a non-native SOD1 dimer in which the native strand pairings form but the monomers do not collapse into the barrel topologies, resulting in the formation of a continuous β-sheet. At the interface between the two flattened sheets, residues 110-120 from the opposite monomers directly interact in a parallel fashion. The residues 35-45 are located on the outside edges of this dimeric β-sheet where they are available for propagating the aggregate further. In this alternative model for multimeric β-sheet association, flattened β-sheets associate via edge-edge interactions mediated by fragment 110-120 and propagate unidirectionally by interactions between the fragments 35-45. Thus, the dimers exhibit a rich variety of structures in which the residues 35-45 and 110-120 form key intermolecular contacts.

## Discussion

### Finding aggregation "hot-spots" in SOD1 using peptide fragments

To obtain the aggregation-propensity of SOD1 sequence fragments, we use the free energy of oligomerization of isolated sequence fragments mounted onto idealized β-sheet templates, composed of two and four β-strands. In a similar approach, de la Paz et al. [170] mounted hexapeptide sequences on each strand of a six-stranded antiparallel β-sheet template to design highly amyloidogenic peptide sequences. Using this simplified design procedure, they found that, for short peptide sequences, the formation of β-structures is necessary, but not sufficient, for the formation of amyloid fibrils.

The β-sheet templates we used included both parallel and anti-parallel conformations. Although protein and peptide aggregation involves conversion to β-sheets, whether the β-sheets are parallel or anti-parallel has not been understood [162]. It has been argued that the early oligomers formed during protein and peptide aggregation can be of either topology, although for small peptides, anti-parallel topologies are preferably formed [212]. In a recent study of the dynamics of peptide dimerization, Hwang et al. [210] found that the β-strand peptide dimers exhibited both parallel and anti-parallel β-sheets, with an overall preference for anti-parallel arrangements. Since both parallel and anti-parallel topologies are likely in the early stages of aggregation, we used both topologies for constructing the templates, and also found that anti-parallel β-sheets have lower free energies for a given sequence (Figures 2.2b and c). We postulate that the lower free energy of the anti-parallel structures is due to less strained hydrogen bonds in the anti-parallel structures compared to the parallel structures.

We find that the thermodynamic contribution of each residue to the aggregation propensity ($\Delta G$) is greater in the tetramer compared to the dimer (Figure 2.2b and c). This finding indicates that the free energy gain upon aggregation increases non-linearly as the size of the aggregate increases, i.e. greater stabilization occurs as higher-order oligomers are formed. Thus, aggregation may be reversible for smaller oligomers, but as the size and the stability of the oligomer of the increases, the disaggregation is less likely. This postulate is in agreement with recent findings of the stability of amyloid β dimers, which suggest that dimers are only marginally stabilized compared to free monomers [213].

The use of overlapping peptide fragments to determine amyloidogenicity of residues ensures that sequence neighbors of a residue modulate its amyloidogenicity. Inclusion of local interactions by use of such peptide models is known to be a successful strategy for modeling protein structure [214]. In protein modeling algorithms, for example the ROSETTA program developed by Baker and co-workers [215,216], the propensity of peptide fragments of a protein to adopt specific secondary structures has been used to successfully predict protein structures. Our approach of predicting aggregation propensities also similarly relies on evaluating the propensities of short peptide fragments to adopt specific structures, and on evaluating the effect of neighboring residues on the amyloidogenicity of a given residue.

**Dependence of amyloidogenicity on the hydrophobicity, β-sheet propensity, and net charge of the sequence**

The residue fragments that we identify as amyloidogenic have a high content of hydrophobic residues, and strategically placed polar (T, H) and charged residues (K, E, R). The charged residues may provide further stabilizing interactions by electrostatic and/or hydrogen bonds. Both hydrophobic and charged interactions are known to be critical to stabilize aggregates

[170,217,218]. The residue sequence 100-109 (EDSVISLSGD) is also amyloidogenic, albeit less than the two highly amyloidogenic fragments 35-45 and 110-120, and shows a similar distribution of charged, polar and hydrophobic residues. Residues fragments that have comparatively low amyloidogenicity are 18-22 (INFEQ), 52-55 (DNTA), 84-88 (LGNVT), and 135-140 (TKTNA). These fragments have a high content of polar, uncharged amino acids (N, Q, T). The fragments containing these residues are stable in tetrameric and dimeric oligomeric states (Figure 2.2 (a)), but the free energy penalty for oligomerization is high (Figure 2.2b and c). We argue that this high penalty is a result of more favorable interactions of the monomers with water compared to the interactions with other peptides in the oligomeric state.

To understand if the per residue amyloidogenicity obtained from our all-atom MD simulations of sequence fragments is simply a reflection of some intrinsic physico-chemical property of the fragments, such as β-strand propensity and hydrophobicity, we compare the amyloidogenicity profile with these physico-chemical properties. Recently, a number of phenomenological approaches have been developed in which these properties and experimental conditions are used as variables to predict aggregation rates of polypeptide chains. We use the model developed by Chiti et al.[219] in which average hydrophobicity, β-sheet propensity, and net charge is calculated for each sequence and a linear regression fit to the aggregation rate is obtained. Following Chiti et al.,[219] we assume that the free energy of multimer formation calculated in our MD simulations is:

$$\Delta G = C_{\beta} \cdot p_{\beta} + C_{hydrophob} \cdot p_{hydrophob} + C_{\pm} \cdot p_{\pm}, \quad (6)$$

where $p_{\beta}$, $p_{hydrophob}$, and $p_{\pm}$ are the β-sheet propensity, hydrophobicity, and net charge of the sequence at pH 7, $C_{\beta}$, $C_{hydrophob}$ and $C_{\pm}$ are scaling coefficients, and $\Delta G$ is free energy of

dimer or tetramer formation determined in MD simulations. First, we find that none of the individual properties correlate with the free energy of multimer formation (Figure 2.6a-c). Second, for each template structure, namely the dimer and the tetramer with parallel and anti-parallel topology, we perform a linear regression analysis using Eq. (6) to determine the set of coefficients $C_{\beta,}$ $C_{hydrophob}$ and $C_{\pm}$. We find that in each case the correlation between the $\Delta G$-values and the sequence properties is poor (Figure 2.6d-g), and conclude that the $\Delta G$ of multimerization is not sufficiently explained by a linear combination of the β-sheet propensity, hydrophobicity, or the net charge of the sequence. Our finding is in agreement with the recent work of Serrano and co-workers in which mean-field aggregation-profiles for protein sequences calculated using their TANGO algorithm did not correlate with the β-strand propensity of the sequence [220].

**The determinants of SOD1 aggregation in FALS**

To determine the sequence and structural determinants of SOD1 aggregation, we evaluate (1) the propensities of oligomerization of all sequence fragments of SOD1, and (2) the structural propensities of different parts of SOD1 to self-associate during misfolding induced by domain swapping. We use no explicit sequence information during the identification of structural regions that are likely to self-associate, and vice versa. Since we find overlapping regions of the SOD1 molecule using these disparate methods, we argue that aggregation of SOD1 is a consequence of both having aggregation-prone sequence fragments, and the topological context of these fragments during misfolding.

We have previously shown [177] that a minimal mechanism for the aggregation of SOD1 is

$$D \rightleftharpoons 2M_{apo} + metals \xrightarrow{k_{agg}} A, \quad (7)$$

where $D$ is the native dimer, $M_{apo}$ is the apo-monomer and $A$ is the aggregate. The mechanism in Eq. (5) is minimal because the second reaction, $M_{apo} \rightarrow A$, is likely to be a multi-step process. The first step in this process is the non-native dimerization of apo-monomers, followed by the further addition of misfolded monomers. A common mechanism for non-native dimerization and aggregation is domain swapping [179,221]. The domain swapping of two monomers leads to the formation of structures that are either "open" and lead to further elongation of the aggregate, or are "closed" and serve as dead-ends that cannot propagate further. It has been shown that domain swapping has a purely topological origin, i.e. it is a consequence of the competition between the formation of native contacts, and the formation of symmetric inter-monomer contacts [184,221]. Therefore, we study the misfolding of SOD1 dimer using domain-swapping, and find that the formation of domain-swapped structures occurs with the self-association of specific elements of the SOD1 structure. These self-associated sequences identified by domain-swapping simulations with no explicit sequence information include all the regions identified by sequence analysis, suggesting that SOD1 domain-swapping-induced misfolding allows, under certain conditions, the self-association of fragments with a propensity to self-associate.

We propose that FALS mutations induce aggregation by affecting the rate and equilibrium constants of dimer dissociation and metal-loss in Eq. (5), and by affecting the degree of domain swapping. To qualitatively model the differential effects of mutations, we introduce the scaling parameter $\alpha_{\text{domain-swap}}$, with which we control the relative of strengths of intra- and inter-chain interactions. Under a range of these destabilizing conditions, we observe the preferential self-association of residues fragments N- and C-termini, 35-45 or

110-120, suggesting that conversion to the aggregate is a specific process governed by the self-association of specific regions of SOD1. We find a number of misfolded dimeric species in which these key interactions formed, but there is considerable conformational diversity in the overall structure of the misfolded dimers. This conformational diversity was absent in the misfolded dimers of the SH3-domain generated using a similar approach, and only two dominant "open" and "closed" topologies were found [221]. Thus, the conformational diversity of the misfolded dimers is an intrinsic property of the SOD1 structure. We expect that once the key interactions for aggregation are formed, different dimer conformations are stabilized, and therefore, initiate aggregation under different experimental conditions. This phenomenon may be responsible for the experimentally observed variety of aggregate morphologies as a function of environmental conditions, such as denaturants, pH and temperature, that have been used to generate the aggregates [113,144,222].

The sequence profile of amyloidogenicity represents an upper bound for the aggregation propensity of SOD1 molecule because it is a measure of the intrinsic property of the SOD1 sequence to self-associate. However, the degree to which these different sequences can self-associate is determined by the structural dynamics during misfolding. The high aggregation-propensity of the destabilized mutant SOD1 may be a result of the synergy between structural dynamics and sequence propensity, such that highly aggregation-prone sequences are also topologically most likely to form inter-chain contacts.

## Acknowledgements.

I would like to thank Sagar D. Khare, Peng Gong, and Nikolay V. Dokholyan for their contribution to the experimental design and execution of the above work. This work was published in Proteins: Structure, Function, and Bioinformatics [156].

I also thank Feng Ding for assistance with DMD simulations and helpful discussions. This work was supported in part by Muscular Dystrophy Association grant MDA3720, Research Grant No. 5-FY03-155 from the March of Dimes Birth Defect Foundation, and the UNC/IBM Junior Investigator Award.

# CHAPTER 3

# MODIFICATIONS OF SUPEROXIDE DISMUTASE IN HUMAN ERYTHROCYTES: A POSSIBLE ROLE IN AMYOTROPHIC LATERAL SCLEROSIS

Over 100 mutations in Cu/Zn superoxide dismutase (SOD1) result in familial amyotrophic lateral sclerosis (FALS). Dimer dissociation is the first step in SOD1 aggregation, and studies suggest nearly every amino acid residue in SOD1 is dynamically connected to the dimer interface. Post-translational modifications of SOD1 residues might be expected to have similar effects to mutations, but few have been identified. Here we show, using SOD1 isolated from human erythrocytes, that human SOD1 is phosphorylated at threonine 2 and glutathionylated at cysteine 111. A second SOD1 phosphorylation was observed and mapped to either Thr-58 or Ser-59. Cysteine-111 glutathionylation promotes SOD1 monomer formation – a necessary initiating step in SOD1 aggregation – by causing a two-fold increase in the $K_d$. This change in the dimer stability is expected to result in a 67 % increase in monomer concentration – 315 nM rather than 212 nM at physiological SOD1 concentrations. Because protein glutathionylation is associated with redox regulation, our finding that glutathionylation promotes SOD1 monomer formation supports a model in which increased oxidative stress promotes SOD1 aggregation.

## Introduction

Familial amyotrophic lateral sclerosis (FALS) is the hereditary form of amyotrophic lateral sclerosis (ALS), a fatal disease characterized by progressive motor neuron loss [159]. A subset of FALS is caused by mutations in the gene encoding homodimeric Cu/Zn superoxide dismutase (SOD1), which forms intraneuronal aggregates [138]. Although SOD1 aggregation is involved in SOD1-mediated FALS, it is generally believed that the functional properties of the enzyme are not related to the toxic gain of function imparted by mutations in SOD1 [223]. However, the discovery of roles for SOD1 in the regulation of the cellular phosphorylation balance [224] and redox state [225] provides additional avenues for connecting the cellular role of SOD1 to FALS. The classical studies of SOD1 were generally performed using bovine erythrocyte SOD1 or recombinant human SOD1. Although recombinant methods are widely used to produce SOD1 mutants, a disadvantage of studying recombinant SOD1 is the absence of potentially important posttranslational modifications present in human tissues. The initial SOD1 crystal structure was solved using bovine erythrocyte SOD1 [226] and no structure of human erythrocyte SOD1 is available. Here we report results using human erythrocyte SOD1 rather than the recombinant enzyme and find that the native enzyme features a consistent pattern of post-translational modifications. Using a combination of “bottom-up” and “top-down” mass spectrometry (MS) approaches, we show that SOD1 isolated from human erythrocytes is posttranslationally phosphorylated and glutathionylated. These modifications occur near the SOD1 dimer interface. Because monomer formation is thought to be the first intermediate leading to SOD1 aggregation [143,144], we tested the dimer stability of modified SOD1 and found, as expected, that glutathionylation promotes the formation of SOD1 monomer.

# EXPERIMENTAL PROCEDURES

## Isolation of hSOD1 from erythrocytes

Expired human erythrocytes were obtained from the UNC-Chapel Hill Hospital blood bank. Human erythrocytes were preserved using one of several anticoagulants: AS-1, AS-3, or AS-5 (stored as long as 42 days before expiration). Bovine erythrocytes preserved with 0.38% sodium citrate were purchased from Pel-Freez Biologicals, Rogers, AR. SOD1 is isolated from human erythrocytes using a modification of the protocol originally used by McCord and Fridovich [227]. Following acetone precipitation of SOD1, we dialyze against 20 mM Tris pH 7.8 and perform hydrophobic interaction chromatography and Anion exchange chromatography using an AKTA-FPLC to remove trace impurities. For hydrophobic interaction chromatography, dry $(NH_4)_2SO_4$ is added to bring the final concentration to 55%. The protein is loaded onto a HiTrap phenyl sepharose column (GE) and eluted with a gradient from 2 M to 0 M $(NH_4)_2SO_4$ in 20 mM Tris pH 7.8. Fractions containing SOD1 are combined and dialyzed against salt-free 20 mM Tris pH 7.8 and anion exchange chromatography is performed using a MonoQ column (GE) with a gradient from 0 M to 1 M NaCl in 20 mM Tris pH 7.8. The fractions containing SOD1 are dialyzed against 20 mM Tris, 150 mM NaCl, pH 7.8 and concentrated.

## Isolation of hSOD1 from *S. cerevisiae*

Human wild type SOD1 is expressed by the plasmid yEP351-hwtSOD1 in the EG118 SOD1-knockout yeast strain (both kindly provided by J.S. Valentine). Growth is carried out at 30 °C for 72 hours in YPD media. We use a modified isolation protocol adapted from Goscin et al. [228] where we replace all steps after stirring the lysate at room temperature with

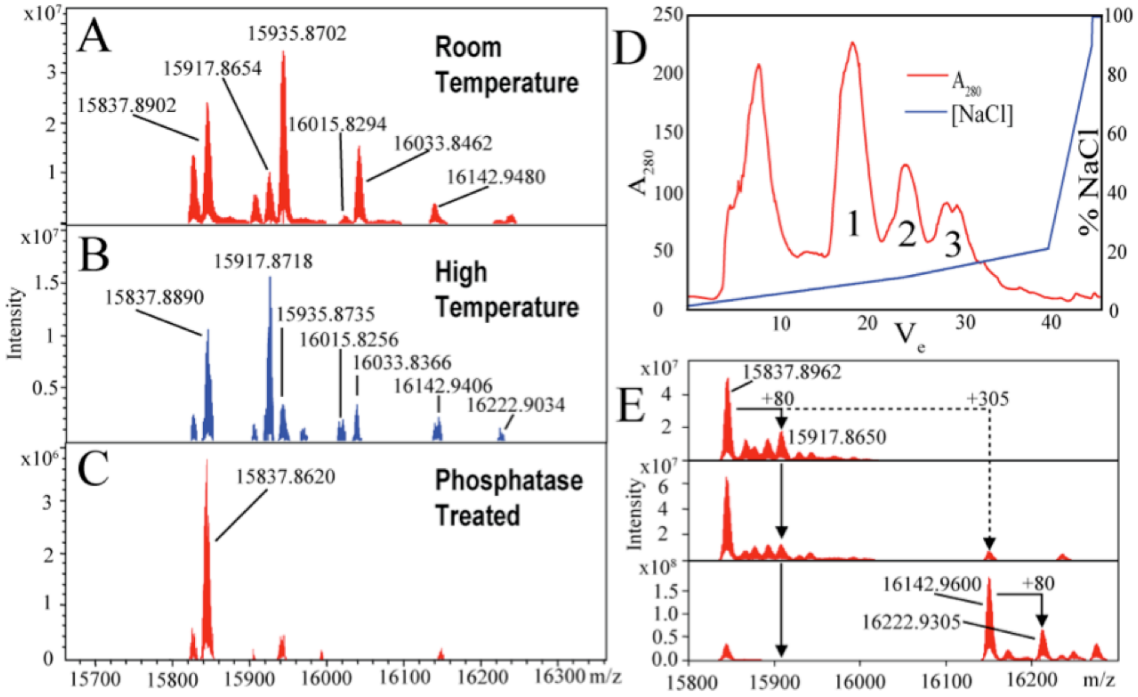


**Figure 3.1 - Post-Translational Modification of SOD1**. μESI-FTICR-MS spectra of A) human SOD1 isolated from erythrocytes, B) high-temperature spectrum of human erythrocyte SOD1 causing phosphorylation peaks to shift from +98 Da to +80 Da, and C) alkaline phosphatase-treated human SOD1 isolated from erythrocytes. (D) A UV trace from anion exchange separation of three populations of human erythrocyte SOD1 – the unlabeled peak is composed of impurities. (E) A comparison of the μESI-FTICR-MS spectra for populations 1-3 from panel D showing SOD1 enrichment of glutathionylation in population 3. Solid vertical arrows indicate phosphorylation. The dashed arrow indicates Glutathionylation.

high speed centrifugation and dialysis of the supernatant against 20 mM Tris pH 7.8 to remove the chloroform and ethanol. Trace impurities are removed by MonoQ and phenyl sepharose chromatography as described above.

Remetallation of hSOD1 from yeast is performed by successive dialysis at 4 °C against: a) 50 mM Acetate pH 3.5, 150 mM NaCl, 10 mM EDTA; b) 50 mM Acetate pH 3.5, 150 mM NaCl; c) 50 mM Acetate pH 3.5, 150 mM NaCl + CuSO4 (5-fold molar excess compared to [SOD1]); d) 20 mM Tris pH 7.8, 150 mM NaCl + $ZnCl_2$ (5-fold molar excess compared to [SOD1]); and e) 20 mM Tris pH 7.8, 150 mM NaCl. Upon concentration with a

YM-10 ultrafiltration membrane (Millipore, Bedford, MA, USA), a blue-green coloration is observed, indicating incorporation of copper into the enzyme.

**Microcapillary (μ) ESI-FT-ICR-MS Analysis (Top-down Approach)**

*MS Conditions*. MS spectra are acquired using a hybrid Qe- Fourier Transform Ion Cyclotron Resonance (FT-ICR) – Mass Spectrometer, equipped with a 12.0 T actively shielded magnet (Apex Qe-FTICR-MS, 12.0 T AS, Bruker Daltonics, Billerica, MA, USA), and an Apollo II microelectrospray source. The voltages on the μESI sprayer, interface plate, heated capillary exit, deflector, ion funnel and skimmer are set at 4.3 kV, 3.9 kV, 300 V, 250 V, 175 V and 80 V, respectively. The temperature of the μESI source is maintained at 180 $^{o}$C. Desolvation is carried out using a nebulization gas flow (2.0 bar) and a countercurrent drying gas flow (4.0 L/second). The Electron Capture Dissociation (ECD) hollow dispenser cathode is heated to increase the temperature inside ICR cell above 180$^{o}$C without application of ECD bias, eliminating non-covalent adducts. SOD1 sample solutions are directly infused using a syringe pump (Harvard Apparatus, Holliston, MA, USA) and a 250-μL syringe (Hamilton, Reno, NV, USA), and electrosprayed at an infusion flow rate of 90 μL/hour. Before transfer, ion packets are accumulated inside the collision cell for a duration of 0.2 s. 50 MS scans per spectrum are acquired in the ICR cell with a resolution of 580,000 at m/z 400.

| Sample No. | Unmodified SOD1 | Phosphorylated SOD1 | Glutathionylated SOD1 | Both |
|---|---|---|---|---|
| 1 | 51.1 % ± 11 % | 8.5 % ± 1.8 %<br>*fP* = 0.30 ± 0.05 | 18.8 % ± 3.9 %<br>*fG* = 0.41 ± 0.06 | 21.7 % ± 4.6 %<br>Expected = 12 % ± 4 % |
| 2 | 36.9 % ± 2.9 % | 6.6 % ± 1.3 %<br>*fP* = 0.29 ± 0.01 | 34.0 % ± 3.6 %<br>*fG* = 0.57 ± 0.05 | 22.6 % ± 0.3 %<br>Expected = 16.5 % ± 1.6 % |
| 3 | 41.1 % ± 5.0 % | 14.4 % ± 4.4 %<br>*fP* = 0.33 ± 0.05 | 25.8 % ± 1.5 %<br>*fG* = 0.45 ± 0.02 | 18.7 % ± 1.6 %<br>Expected = 14.7 % ± 2.3 % |
| 4 | 53.6 % ± 0.7 % | 22.5 % ± 4 %<br>*fP* = 0.35 ± 0.04 | 17.1 % ± 3.6 %<br>*fG* = 0.29 ± 0.04 | 12.2 % ± 1.0 %<br>Expected = 10.2 % ± 1.8 % |
| 5 | 45.2 % ± 3.0 % | 14.6 % ± 0.5 %<br>*fP* = 0.27 ± 0.01 | 31.5 % ± 3.1 %<br>*fG* = 0.44 ± 0.03 | 12.0 % ± 0.3 %<br>Expected = 11.6 % ± 0.9 % |
| 6 | 54.4 % ± 11.4 % | 45.6 % ± 9.6 % | None | None |

**Table 1 – Comparison of modifications in independent erythrocyte samples.** SOD1 isolated from individual samples of human erythrocytes are analyzed by μESI-FTICR-MS without separation of modification states. We calculate the frequencies of phosphorylation (fP), glutathionylation (fG), and both (fPG) from the percentages of each modified SOD1 species in the sample as follows: $fP = \frac{\%P + \%PG}{100}$; $fG = \frac{\%G + \%PG}{100}$; $fPG = \frac{\%PG}{100}$. Assuming that phosphorylation and glutathionylation are independent processes, we expect the frequency of simultaneous phosphorylation and glutathionylation to be $fP \cdot fG = fPG$. Sample blood types are as follows: 1 is AB-, 2 is AB+, 3-5 are O+, and 6 is O-.

**MS/MS fragmentation for sequencing full-length proteins**

FT-MS/MS spectra are obtained from collision-induced dissociation (CID) performed with in-source collision activated dissociation followed by collision cell activated dissociation (C-CAD), or from ECD. In CID experiments, argon is used as the collision gas ($P_{Ar} \approx 1.6 \times 10^{-6}$ Torr). Precursor ions are isolated with Q1 (Mass Selective Quadrupole) and subjected to C-CAD using an isolation window width of 5 Da. 50 MS/MS scans are acquired in the ICR cell with a resolution of 580,000 at m/z 400. In ECD experiments, precursor ions are isolated with Q1 and subjected to ICR cell. Isolation window width is 10 Da. Low energy

| Sample I.D. | Unmodified SOD1 | Phosphorylated SOD1 | Glutathionylated SOD1 | Both |
|---|---|---|---|---|
| A<br>Age: 37 | 38.6 % ± 5.8% | 13.3 % ± 2.0%<br>$fP = 0.23 \pm 0.03$ | 38 % ± 5.7%<br>$fG = 0.48 \pm 0.06$ | 10.1 % ± 1.5%<br>Expected= 11.3 % ± 2.0 % |
| B<br>Age: 73 | 37.4 % ± 5.6% | 8.4 % ± 1.3%<br>$fP = 0.22 \pm 0.02$ | 40.8 % ± 6.1%<br>$fG = 0.54 \pm 0.06$ | 13.4 % ± 2.0%<br>Expected= 11.8 % ± 1.7 % |

**Table 2 – Comparison of modifications in freshly-drawn single erythrocyte samples.** SOD1 isolated immediately after removal from donors and analyzed by μESI-FTICR-MS. Donor age is listed under the sample I.D. All frequencies calculated as in Table 1. The percentage of unmodified SOD1 is calculated using the sum of the intensities of SOD1 peaks that are neither phosphorylated nor glutathionylated (*i.e.* oxidized SOD1 species are considered unmodified).

electrons are generated by a heated hollow dispenser cathode with a bias voltage of -1.5 V. ECD lens voltage is set at 15.0 V. The electrons produced by the hollow cathode are pulsed into the ICR cell with pulse length of 0.0050 second, causing fragmentation of the ions that are already trapped in the ICR cell. To maximize the ion population before irradiation, the cell is filled with 5 iterations of ion accumulation from the external collision cell of the

isolated precursor as suggested [229]. In both CID and ECD experiments, 50 MS/MS scans per spectrum are acquired in the ICR cell with a resolution of 580,000 at m/z 400.

**Tempo LC MALDI Fractionation and MALDI-TOF-TOF Analysis (Bottom-up Approach)**

SOD1 protein samples are digested with trypsin (Promega, Madison, WI, USA) at 37 $^{o}$C overnight in an enzyme-to-substrate ratio of 1:40 by mass. After desalting with ZipTipC18 (Millipore), 0.5 μL of the tryptic digests are directly spotted on a 384 well stainless steel matrix-assisted laser desorption/ionization (MALDI) target plate for pre-scan using a MALDI time-of-flight/time-of-flight (TOF/TOF) tandem mass spectrometer (ABI 4800 Proteomics Analyzer, Applied Biosystems, Foster City, CA). In an analytical run the peptide digests are further separated using a reverse phase liquid chromatography (LC) system (Tempo LC MALDI, Applied Biosystems, Foster City, CA, USA). 10 μL of tryptic peptides are injected and directly loaded on a C18 capillary column (Monolithic silica RP C18 endcapped, 100 μm i.d., 15 cm length, Chromolith® CapRod®, Merck KGaA, Darmstadt, Germany) with a loading buffer ($H_2O$/acetonitrile/trifluoroacetic acid, 98/2/0.1, v/v/v), and separated using a gradient from 100% A ($H_2O$/acetonitrile/trifluoroacetic acid, 98/2/0.1, v/v/v) to 40% B ($H_2O$/acetonitrile/trifluoroacetic acid, 2/98/0.1, v/v/v) over 70 minutes, and 40-80% B in 10 minutes, at a flow rate of 1.0 μL/min. The column eluates are mixed with a matrix solution of ~ 7.0 mg/mL re-crystallized α-cyano-4-hydroxycinnamic acid (Sigma) in $H_2O$/acetonitrile, 30/70, v/v and 5 mM Ammonium Citrate, deposited on a 2000 well stainless steel MALDI target plate at a frequency of 0.15 Hz, and analyzed by ABI 4800 MALDI TOF/TOF (200 Hz Nd:YAG laser, OptiBeam$^{TM}$). Each spot is analyzed in MS mode in the mass range of 800-4000 Da, by accumulating ion signals over 1200 laser shots.

Up to 15 ions with S/N > 30 are selected for MS/MS analysis which is performed with a + 1.0 kV collision energy and $1.0 \times 10^{-6}$ Torr collision gas (air) pressure. Acquisition of an MS/MS spectrum is interrupted when 2000 laser shots (40 sub-spectra from 50 laser shots each) are accumulated. Mass calibration is applied by spotting the standard peptide mixture at six places around the target plate [230]. Acquired MS and MS/MS spectra are searched using Mascot 2.2 (Matrix Science, London, UK) embedded in GPS 3.5 (Applied Biosystems).

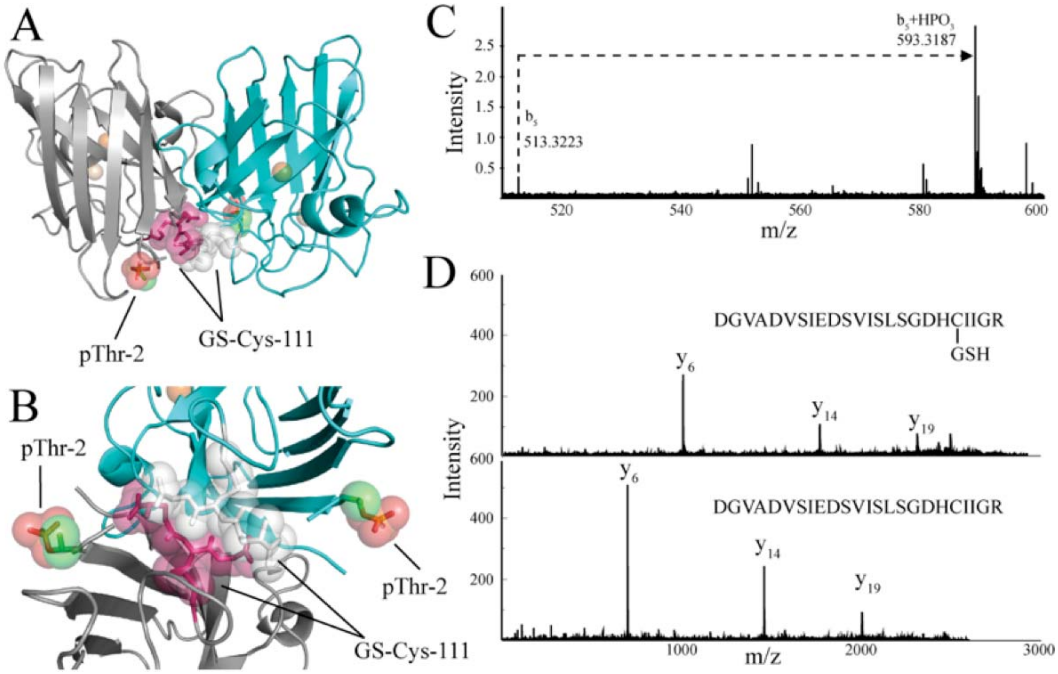


**Figure 3.2 – Location of SOD1 modifications in human erythrocytes.** (A) The SOD1 homodimer (pdb accession code 2V0A) with glutathionylated Cys-111 and phosphorylated Thr-2 modeled using PYMOL (http://pymol.sourceforge.net). (B) The SOD1 dimer interface showing the relative positions of the phosphate and glutathione moieties. (C) A μESI-FTICR-MS-CID MS/MS spectrum with the phosphorylation at Thr-2 for a representative b-ion illustrated. A complete MS/MS spectrum is shown in Figure 3.6. (D) A Tempo LC-MALDI-TOF-TOF MS/MS spectrum with several fragment ions from the parent peptide 92-DGVADVSIEDSVISLSGDHCIIGR-115 highlighted which are shifted by glutathionylation. Complete MS/MS spectra are shown in Figures 3.8 and 3.9.

## Phosphatase Treatment of SOD1

To prepare dephosphorylated. SOD1 we use agarose-linked alkaline phosphatase (Sigma). The beads are washed using 20 mM Tris, 150 mM NaCl, pH 7.8 buffer and added to a solution of SOD1 at a 1:200 v/v ratio. The reaction is performed at 37 °C overnight.

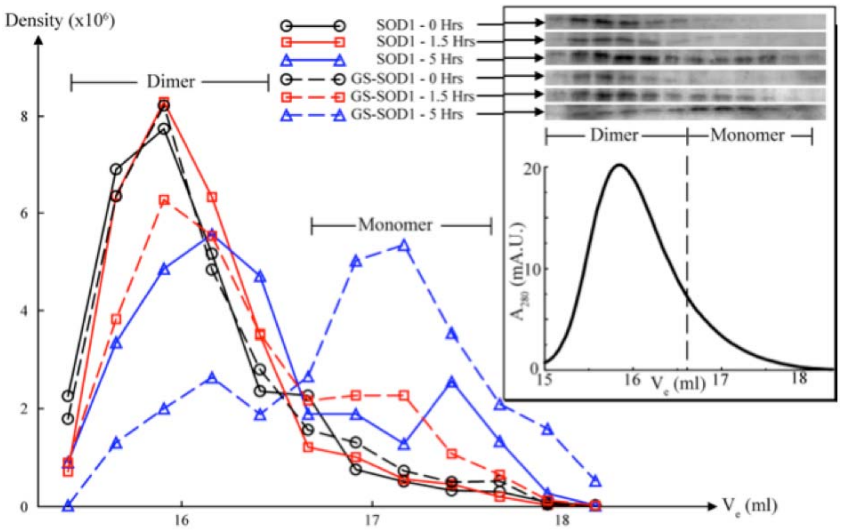


**Figure 3.3 – SOD1 dimer is destabilized by glutathionylation**. Non-glutathionylated (SOD1) and Glutathionylated (GS-SOD1) SOD1 diluted to 1.25 nM is allowed to equilibrate at 37 °C and resolved by size exclusion chromatography to monitor dimer dissociation. Glutathionylated SOD1 dissociates into monomer upon incubation at low concentration whereas non-glutathionylated SOD1 begins to dissociate only slightly after 5 hours at 37 °C. Inset: western blots of 1.25 nM size exclusion chromatography fractions are aligned above a size exclusion chromatograph of 30 μM GS-SOD1 dimer to illustrate the dissociation of GS-SOD at low concentration.

## Size-Exclusion Chromatography

Size exclusion chromatography is carried out using a Superdex 200 10/300 column (GE) and a 200 μL injection loop. The void volume of the column is approximately 8 ml and a flow rate of 0.5 ml/min is used at 4 °C. For measurement of the dimer dissociation constant, $K_d$,

samples of SOD1 at pH 7.8 were diluted to 1.25 nM to facilitate dimer dissociation using the column running buffer (20 mM Tris pH 7.8, 150 mM NaCl, and 10 μg/L bovine serum albumin to prevent SOD1 adherence to the column and the glass collection tubes). Samples are incubated at 37 $^{o}$C for up to 5 hours to ensure proper equilibration. 250 μl fractions are collected throughout the chromatography experiment for use in immunoblotting. Fractions are acetone precipitated by the addition of 4 volumes of cold acetone to sample and a 1-hour incubation at -20 $^{o}$C. The samples are pelleted for 30 minutes at 20,000 rpm. The precipitated SOD1 is resuspended in protein solvent containing sodium dodecyl sulfate and β-mercaptoethanol and resolved by polyacrylamide gel electrophoresis. Following transfer to a polyvinylidene fluoride membrane and blocking with 5% bovine serum albumin, blots were probed with a sheep anti-SOD1 primary antibody (Calbiochem #574597) and a rabbit anti-sheep alkaline phosphatase conjugated secondary antibody (Thermo Scientific #31360). The blots are incubated in ECF reagent (Amersham) and visualized using a Molecular Dynamics STORM 840 phosphorimager. Quantification of band intensities is performed using the ImageQuant software (GE).

**$K_d$ determination using SOD1 Activity**

We test for a reduction in the rate of 6-hydroxydopamine (6-OHDA) autoxidation as previously described [231]. The assay is sufficiently sensitive to allow measurement of SOD1 concentrations as low as 100 pM. The activity of glutathionylated and non-glutathionylated 2.5 nM SOD1 was measured before and after a 3-hour equilibration at 37 °C. Activity assays performed after 3 and 5 hours incubation at 37 ºC show no additional loss in activity, indicating that the monomer-dimer equilibrium has been reached at 3 hours. The percent dimer dissociation at equilibrium was determined using the following equation: % Dimer

dissociation = % Activity loss = 1-, where $v_c$ is the initial rate of the control reaction, $v_E$ is the initial rate of the reaction containing equilibrated SOD1, and $v_i$ is the initial rate of the reaction measured immediately upon dilution of SOD1 from a concentrated stock solution. Assuming a physiological SOD1 concentration of 40 uM [232], we calculated the monomer concentration based on the Kd. For a $K_d$ of 2.25 nM, we expect the monomer concentration to be 212 nM. For a $K_d$ of 5 nM, we expect a monomer concentration of 315 nM, a 67% increase.

## RESULTS

### SOD1 is modified in human erythrocytes

Using a 12 Tesla FT-ICR-MS with ultrahigh mass accuracy and resolution, full-length wild-type SOD1 from human erythrocytes was found to have a monoisotopic mass of 15837.8902 Da (Figure 2.1a), corresponding to the theoretical mass of 15837.8812 Da for N-terminally acetylated wild-type human SOD1. In addition to the acetylated form, two strong peaks with masses of 15935.8702 and 16033.8462 Da corresponding to the respective addition of one (+98 Da) or two (+196 Da) hydrated phosphate groups were observed, as well as a third peak corresponding to the modification of SOD1 by glutathione (+305 Da). The protein was treated with alkaline phosphatase, which resulted in the loss of the +98, and +196 Da peaks (Figure 3.1c), suggesting both sites are related to phosphorylation.

To differentiate between the non-covalent association of $H_3PO_4$ or $H_2SO_4$ and a hydrated phosphate ester – both expected to result in the addition of ~98 Da, we heated the ICR cell to above 180 °C. Heating results in the conversion of +98 Da and +196 Da peaks to +80 Da and +178 Da, respectively, but has no effect on the +305 Da shift (Figure 3.1b). The

CID/ECD spectra of the +80 Da peak (Figure 3.6), which imply phosphorylation at threonine 2 (Thr-2) (Figure 3.2b,), are similar to those of the +98 Da peak (Figure 3.7), indicating that the +98 Da peak belongs to single phosphorylation plus one water molecule. Similarly, the CID/ECD spectra of the +178 Da peak indicates that it possibly arises from double phosphorylation plus one water molecule (Figure 3.9). A +160 Da peak corresponding to double phosphorylation was only observed in SOD1 extracted from freshly drawn human erythrocytes (Figure 3.14). However, the signal intensities of the +160, +178 and +196 Da peaks were insufficient for FT-ECD fragmentation experiments in mapping the second modification site.

We found that human erythrocyte SOD1 is phosphorylated at threonine 2 (Thr-2) (Figures 3.2b, 3.6 and 3.7), but due to difficulty in sequencing doubly-phosphorylated SOD1 – even after the enrichment of phosphorylated protein – we can only report that a second phosphorylation is possibly located at either Thr-58 or Ser-59 (Figure 3.9). Residues 58 and 59 are located in the Zn-loop in SOD1, which both chelates the zinc atom at the active site and accounts for several dimer interface contacts.

The site of glutathionylation in human SOD1 was determined by analyzing tryptic digestions of human erythrocyte SOD1 with a Tempo LC-MALDI Fractionation and MALDI-TOF-TOF. The acquired MS and MS/MS spectra were searched using Mascot 2.2 embedded in GPS 3.5. In 13 unique SOD1 peptides, we found mass shifts of +305 Da from C-terminal ions $y_5$ to $y_{20}$ relative to the MS/MS spectra of the unmodified peptides (Figure 3.8), which indicates that cysteine 111 (Cys-111) is susceptible to glutathionylation. Peptides containing cysteines 6, 57 and 146 were found not to be glutathionylated (Figure 3.10).

Human erythrocyte SOD1 was separated into multiple charge populations by anion exchange chromatography (Figure 3.1d). Each population shows distinct modification patterns in its mass spectrum (Figure 3.1e). The SOD1 that elutes at the highest ionic strength, population 3, (Figure 3.1d, e) has a dominant peak at m/z = 16142.9600 Da, corresponding to the acetylated protein derivatized with glutathione. The extent of phosphorylation varies in SOD1 populations 1 and 2 that elute at low and medium salt concentrations (Figure 3.1d, e). A pool of SOD1 that is simultaneously phosphorylated and glutathionylated was also observed (Figure 3.1e).

**Distribution of modifications in individual erythrocyte samples**

The modifications described above were observed in SOD1 isolated from erythrocytes pooled from multiple donors and as such, any modifications could have arisen due primarily to contributions from a single donor. To investigate the consistency of glutathionylation and phosphorylation levels between individuals, we next compared SOD1 from individual samples of human erythrocytes. Out of six individual samples, five contained both phosphorylation and glutathionylation (Table 1). One sample lacked glutathione but was significantly phosphorylated. Assuming independent probabilities of phosphorylation and glutathionylation of SOD1, we expect the probability of observing both modifications to be the product of the individual frequencies. In erythrocyte samples 1-3, the calculated frequency of combined phosphorylation and glutathionylation is significantly smaller than the measured frequency, suggesting that phosphorylation and glutathionylation are co-dependent in the case of SOD1. However, the observed frequency of combined modification in samples 4 and 5 is only marginally higher than the expected frequency and is within the

experimental error. This behavior may arise from differences in phosphatase activity among individuals, or other variables not controlled for in this study.

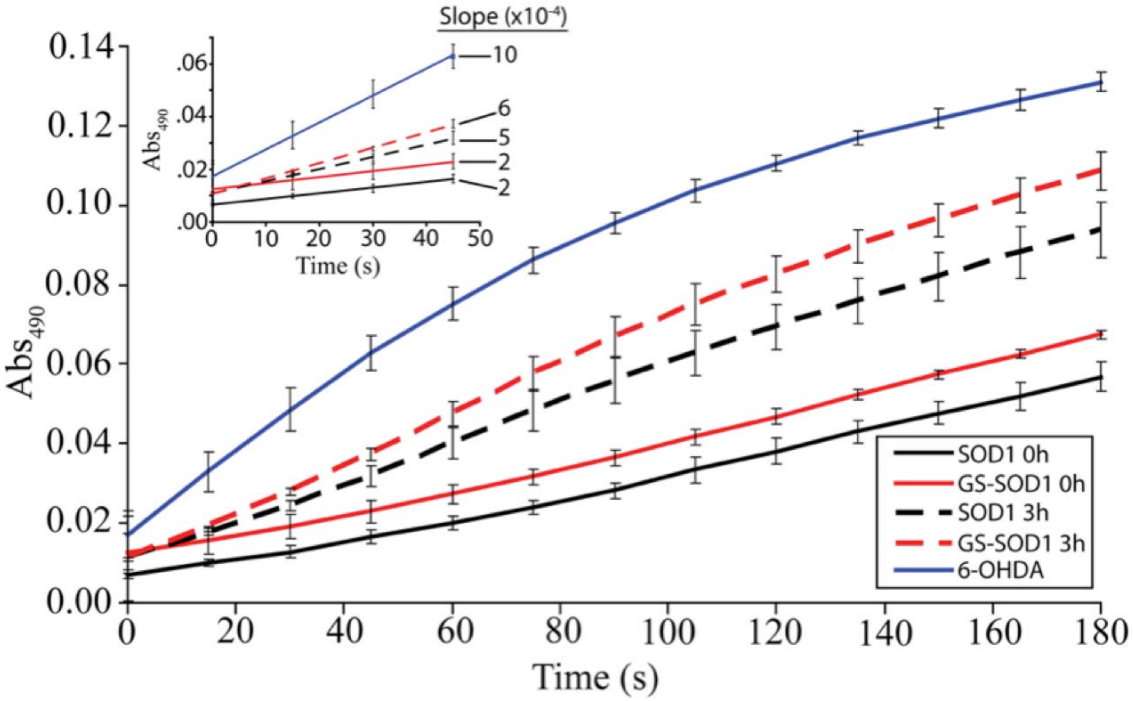


**Figure 3.4 – Measurement of dimer dissociation using an assay for SOD1 activity**. An Activity assay comparing glutathionylated SOD1 (GS-SOD1) to unmodified SOD1 (SOD1) at 2.5 nM. The % activity change due to dimer dissociation was estimated by assaying samples of SOD1 after a 3-hour equilibration at 37 °C (dashed lines) and normalizing against non-equilibrated samples (solid lines). A control reaction containing only 6-OHDA in sample buffer

**Modifications in freshly-drawn human erythrocytes**

The phosphorylation and glutathionylation of human erythrocyte SOD1 does not occur as a result of long-term blood storage. We isolated SOD1 from human erythrocytes immediately following their collection from two donors. The results are summarized in Table 2. Mass spectra from each donor (ages 37 and 73 years) included major peaks related to both SOD1 phosphorylation and glutathionylation. In addition, we observed peaks related to oxidized SOD1. These peaks were shifted +16 and +32 Da from the unmodified mass of SOD1

(Figure 3.14). Because there are no +16 or +32 Da shifted peaks relative to either phosphorylated or glutathionylated SOD1, we postulate that Cys-111 is the site of the oxidation, as has been observed *in vitro* [233]. Alternatively, histidine residues in SOD1 might be oxidized because SOD1 lacks methionine and the oxidation of histidine residues in SOD1 has been observed previously [234]. It is interesting to note the abundance of oxidized SOD1 species in sample B compared to sample A given that the more highly oxidized sample was drawn from a 73-year-old donor while sample A was drawn from a 37-year-old donor. However, a comparison based on only two samples is insufficient to support a hypothesis that the difference is related to age.

**Species/system effects on modifications**

Because *S. cerevisiae* contain a copper chaperone for SOD1, it is widely used for expressing recombinant human SOD1, but do phosphorylation and glutathionylation of human SOD1 occur in yeast or other systems used to isolate SOD1? To answer this question, we purified and analyzed recombinant SOD1 from yeast, as well as endogenous SOD1 from both yeast and bovine erythrocytes. Mass spectra of human SOD1 isolated from *S. cerevisiae* indicate an exact match with the acetylated, unmodified SOD1 found in human erythrocytes (Figure 3.13). We separated a sample of yeast-expressed human SOD1 into sub-populations of high and low negative net charge and found similar mass shifts in the deconvoluted mass spectra indicating SOD1 glutathionylation but not phosphorylation (Figure 3.13). The mass spectrum of SOD1 isolated from bovine erythrocytes using the identical protocol used for human erythrocytes indicates bovine SOD is neither phosphorylated nor glutathionylated, nor is endogenous yeast SOD1 (Figures 3.11 and 3.12, respectively) – an expected result given that neither species has a cysteine at position 111 in SOD1. Cysteine 6 is conserved

between bovine and human SOD1 but we find no glutathionylation of this residue in either species. We hypothesize that SOD1 phosphorylation was not previously observed due to the common use of bovine erythrocyte SOD1 or recombinant human SOD1.

**Effect of Modifications on SOD1 dimer dissociation**

Thr-2 appears to be at a sufficient distance so as not to participate directly in the SOD1 dimer interface. However, phosphorylation can change both the structure and dynamics of proteins [235] and thus, the distance from the interface and the active site does not preclude Thr-2 phosphorylation from altering the stability or activity of SOD1. Cys-111 residues in each SOD1 monomer are directly apposed in a cleft at the dimer interface. We postulated that the addition of the glutathione tripeptide to Cys-111 will result in a measurable decrease in SOD1 dimer stability. Because of the proximity of both Thr-2 phosphorylation and Cys-111 glutathionylation to the dimer interface and evidence that dimer stability is important for preventing SOD1 aggregation [140,147], we measured the effect of glutathionylation and phosphorylation on the *in vitro* stability of dimeric SOD1.

Using size exclusion chromatography, we compared SOD1 species separated by anion exchange as described above (peaks 1 and 3 in Figure 3.1e). Altered dimer stability of SOD1 in peak 3 relative to peak 1 is expected to be the result of Cys-111 glutathionylation because sub-stoichiometric amounts of phosphorylation are present in both SOD1 species. Due to the unusually high stability of the SOD1 dimer (the dissociation constant of human SOD1 isolated from yeast is less than 10 nM [236]), it was necessary to perform the experiment at low concentrations. In order to observe dissociation into monomers, we performed size exclusion chromatography (SEC) using 1.25 nM SOD1. We compared SOD1 with and without glutathionylation and found that glutathionylation has a marked destabilizing effect

on the SOD1 dimer. Progressive SOD1 dimer dissociation was observed upon incubation at 37 °C for up to 5 hours. We observed a 3-fold increase in monomer formation in glutathionylated SOD1 relative to SOD1 unmodified by glutathione (Figure 3.3).

**$K_d$ determination using an assay for SOD1 activity**

Monomeric SOD1 was postulated to have reduced activity based on findings that mutations forcing monomeric SOD1 show an 80% activity loss [237]. We therefore postulated that activity loss can be used as an indicator of dimer dissociation upon dilution from high concentration in measuring the $K_d$ of SOD1. The $K_d$ is important considering that the concentration of the SOD1 species nucleating aggregation depends upon the $N^{th}$ power of the monomer concentration, where N is the number of monomers in the nucleating species. Small increases in the $K_d$, therefore, result in large increases in the number of nuclei, especially as the number of monomers in the nucleus increases. Using a spectrophotometric assay sufficiently sensitive to assay sub-nanomolar concentrations SOD1, we measured the reduction in the reaction rate in the presence of 2.5 nM SOD1 at equilibrium (3 hours), normalized to the activity immediately after dilution (Figure 3.4). We observed a loss in SOD1 activity concomitant with dimer dissociation, evident as a reduction in the initial reaction rate relative to the control reaction. We tested the effect of glutathionylation on dimer stability by comparing SOD1 species separated by anion exchange as described above (peaks 1 and 3 in Figure 3.1e). While the initial reaction rate was similar ($2 \times 10^{-4}$ A.U.·$s^{-1}$), the glutathionylated SOD1 showed a higher rate at equilibrium, indicating less SOD1 activity and therefore, more dimer dissociation. Based on the percent reduction in activity, we estimated the $K_d$ to be 2.25 nM for unmodified SOD1 and 5 nM for modified SOD1.

# DISCUSSION

## Post-translational modifications of native human SOD1

Here we report that SOD1 can be phosphorylated at Thr-2 and at either Thr-58 or Ser-59. We also confirm previous findings of SOD1 glutathionylation and map that modification to Cys-111. Previously in our laboratory, a series of molecular dynamics simulations was carried out which showed that residues in every region of SOD1 show high connectivity to the dimer interface [150] and that residues closely associated with its stability reside on the surface of SOD1 [198]. Other recent findings suggest that loss of Cu and Zn at the metal binding site results in structural fluctuation at the dimer interface [155], providing further rationale for diverse perturbations resulting in SOD1 aggregation via dimer destabilization. In light of these findings, we postulated that post-translational modifications, like point mutations, would have a similar effect on the structure and dynamics of SOD1. To test the effect of post-translational modifications on the enzyme, we separated a sample of SOD1 into a population that contained a low percentage of phosphorylation and a population that was very highly glutathionylated while also phosphorylated to a similar degree as the non-glutathionylated enzyme. We found that these two forms of SOD1 differ in their propensity toward forming monomers – the glutathionylated SOD1 forming monomer more readily. Our previous finding that monomeric SOD1 is the first intermediate formed during SOD1 aggregation suggests that glutathionylation, which has a destabilizing effect on the SOD1 dimer, may affect the initiation of SOD1 aggregation in FALS.

Glutathionylation has been reported several times in erythrocyte SOD1, including erythrocytes collected from FALS patients [238,239], and treatment of apo-SOD1 with GSSG

causes aggregation *in vitro* [240]. We show here that only Cys-111 glutathionylation is present *in vivo*, However, glutathionylation of SOD1 has also been performed *in vitro* and shown to modify each of the four cysteines [240]. The involvement of Cys-111 disulfide bonding during SOD1 aggregation has been suggested [148]. However, bovine SOD1 lacks Cys-111, yet is capable of aggregating at low pH [143]. Therefore, Cys-111 glutathionylation need not interfere with SOD1 aggregation by blocking a specific disulfide bond in the aggregated state.

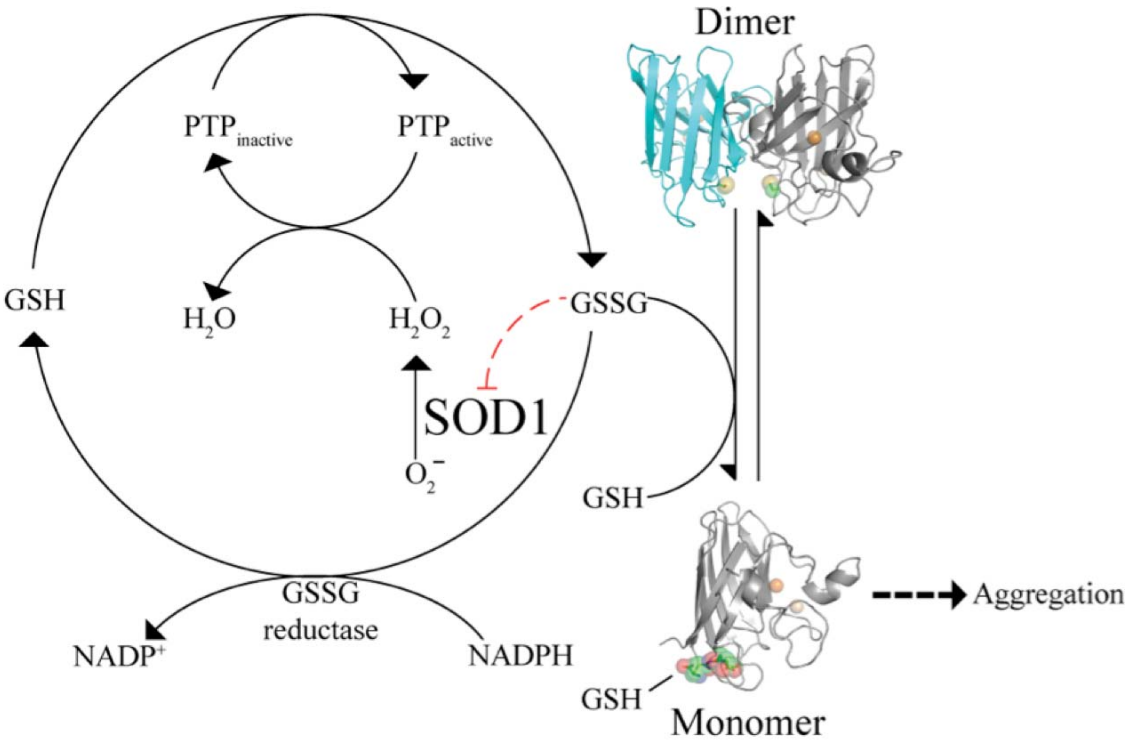


**Figure 3.5 – Model for the participation of SOD1 in protein tyrosine phosphatase (PTP) redox regulation.** SOD1 interacts with redox regulation of phosphatase activity through its conversion of superoxide, $O_2^-$, to hydrogen peroxide, $H_2O_2$. Glutathione reduces the activity of SOD1 (red dashed line) by facilitating monomer formation. SOD1 monomer formation is also associated with aggregation, and ribbon structures are used to show the proposed destabilizing effect on the SOD1 dimer as a result of C111 glutathionylation.

**Oxidation of SOD1 in freshly-drawn human erythrocytes**

We observe SOD1 oxidation, in addition to phosphorylation and glutathionylation, in freshly drawn human erythrocytes. While the sample number is not sufficient to show a relationship between age and the degree of SOD1 oxidation, the two samples show differences in this property. Erythrocytes are short-lived cells and have an average lifespan of 120 days in humans. Therefore, the SOD1 used in our experiments is isolated from both young and old cells. Because virtually all of the unmodified SOD1 in one of the samples was oxidized, we conclude that differences in SOD1 oxidation levels are not the result of a cumulative process wherein a population of SOD1 is slowly modified as each individual erythrocyte "ages," but rather a process in which differences in the individuals that may or may not be age-related, such as oxidizing conditions in erythrocytes or the surrounding plasma are continuously reflected in the modifications to SOD1.

**Modification differences in different systems**

When studying the effects of mutations on SOD1, it is important to have a proper benchmark for SOD1 as it exists inside human tissues. It is clear from our comparison of human SOD1 isolated from both human erythrocytes and yeast that the latter model for native SOD1 lacks at least one feature of native SOD1 – phosphorylation. Because we study wild type SOD1 isolated from a human tissue, we believe that phosphorylation and glutathionylation are features of the SOD1 native state and not a result of a disease-related process. However, analysis of spinal cord tissue from sporadic ALS patients revealed many kinases that are upregulated and found dramatic differences in the phosphorylation of multiple proteins [241], suggesting that changes in SOD1 phosphorylation are possible in FALS.

**Possible regulatory role of SOD1**

Phosphorylation and glutathionylation may impact the function of SOD1 through the mediation of interactions with other proteins. SOD1 is involved in cellular redox regulation through a direct interaction with the Rac1/NOX2 enzyme complex [225]. This example of a physical interaction between SOD1 and a functional enzyme complex illustrates one mechanism through which phosphorylation and/or glutathionylation of SOD1 could play a significant role without altering its traditionally recognized activity as a free radical scavenger.

Glutathione plays a key role in establishing the redox state of the cell [242]. The high ratio of reduced (GSH) to oxidized (GSSG) glutathione is tightly controlled by both glutathione reductase, which uses NADPH to reduce GSSG to GSH, and the active removal of GSSG from the cytosol [243]. During scenarios of oxidative stress, the concentration of GSSG increases dramatically [244] and reversibly glutathionylates free cysteines in what is thought to be a general protective mechanism against permanent oxidation of proteins by reactive oxygen or nitrogen species [245]. In addition to its general role, several examples of specific functional roles for protein glutathionylation are documented [246-249]. Recent evidence also suggests that SOD1 may be involved in growth factor signaling through the production of $H_2O_2$, which acts as a second messenger in modulating the activity of protein tyrosine phosphatases (PTPs) and thus, the balance of phosphorylation in the cell [224]. Predicated on these findings, we present a model for the impact of SOD1 modification on oxidative PTP regulation (Figure 3.5).

SOD1 glutathionylation increases dimer dissociation, facilitating aggregation in the presence of contributing factors such as oxidative damage or destabilizing FALS mutations.

Even a modest effect of glutathionylation on SOD1 dimer dissociation, combined with the effects of mutations, could affect FALS-related aggregation over time. Furthermore, an SOD1 variant engineered to be monomeric retains only 20% activity relative to the wild type dimer [237], and therefore we postulate that glutathionylation, by inducing dimer dissociation, inhibits SOD1 activity (Figure 3.5).

**Decreased dimer stability: Possible implications for FALS**

The link between SOD1 mutations, protein aggregation, and FALS is not fully understood, but there are multiple reports showing that dimer dissociation is an early event during SOD1 aggregation [143,144]. Our finding that modifications can facilitate SOD1 dimer dissociation suggests a possible link between the normal characteristics of SOD1 and its role in FALS. Although relatively modest, a two-fold increase in $K_d$ resulting from SOD1 modification translates to nearly a 70% increase in SOD1 monomer concentration. Because nucleation of SOD1 aggregation is dependent on at least the square of the monomer concentration, we expect a 70% increase in monomer concentration to have a marked effect on the nucleation of SOD1 aggregates. For example, the formation of a hypothetical nucleus made up of 3 glutathionylated SOD1 monomers becomes roughly 5 times more likely and a nucleus of 6 monomers 24 times more likely relative to unmodified SOD1.

## Acknowledgements

I would like to thank Li Zhou, Joshua Jordon, Yi Huang, Yanbao Yu, Rachel L. Redler, Xian Chen, Michael Caplow, and Nikolay V. Dokholyan for their contributions to the experimental design and execution of the above work. This work was published in the Journal of Biological Chemistry [250].

I also thank Dr. Joan S. Valentine for providing the EG118 yeast strain and yEP-351:hwtSOD1 vector and Dr. Matthew P. Torres for helpful discussions. We also thank the UNC Hospitals Blood Bank for providing expired human erythrocytes. This work was funded by The National Institutes of Health grants R01GM080742 (N.V.D.) and 1R01AI064806-01A2 (X.C.), and U.S. Department of Energy grant (BER) DE-FG02-07ER64422 (X.C.).

# Supplemental Figures

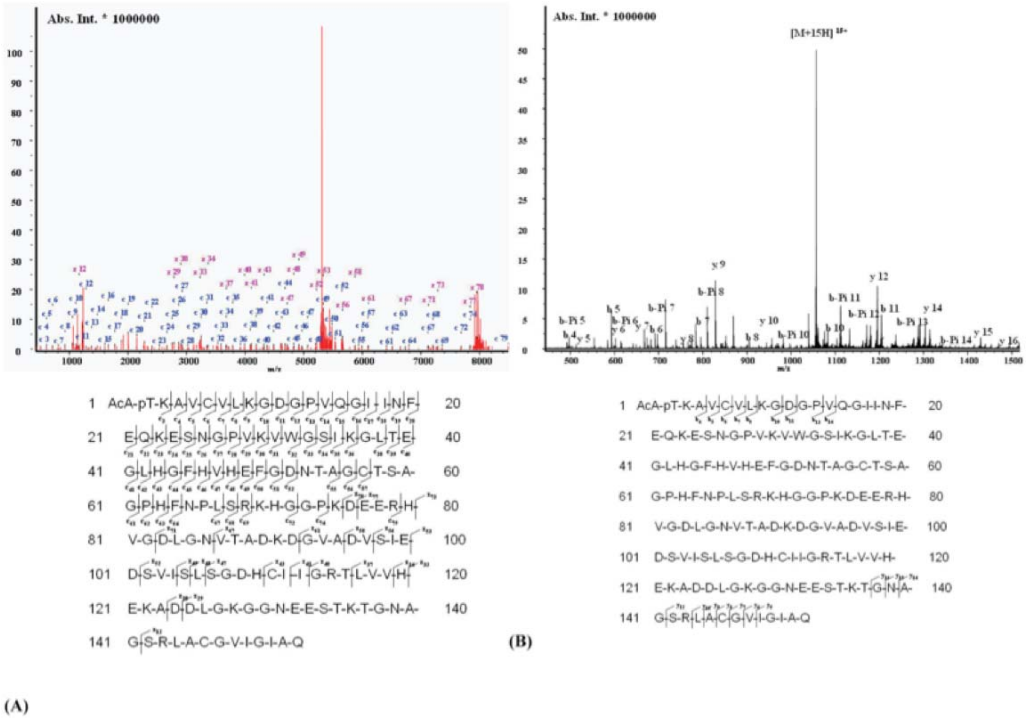


**Figure 3.6 – MS/MS identification of singly-phosphorylated SOD1.**
MS/MS analysis showing ions resulting from the fragmentation of SOD1 containing phosphorylated Thr-2. Ion signals corresponding to singly phosphorylated human SOD1 (precursor: m/z 1063.8 Da, 15+ charge state), are isolated for top-down experiments by µESI-FTICR-MS with (A) electron-capture dissociation (ECD) and (B) collision-induced dissociation (CID) respectively. Inspection of the fragment ions from the CID MS/MS spectrum of singly-phosphorylated human SOD1 (Figure 2 B) reveals the neutral losses of 80 or 98 Da in $b_5$, $b_6$, $b_7$, $b_8$, $b_{10}$ and $b_{11}$. The ECD MS/MS spectrum of singly-phosphorylated SOD1 indicates 100% amino acid sequence coverage. 50 scans.

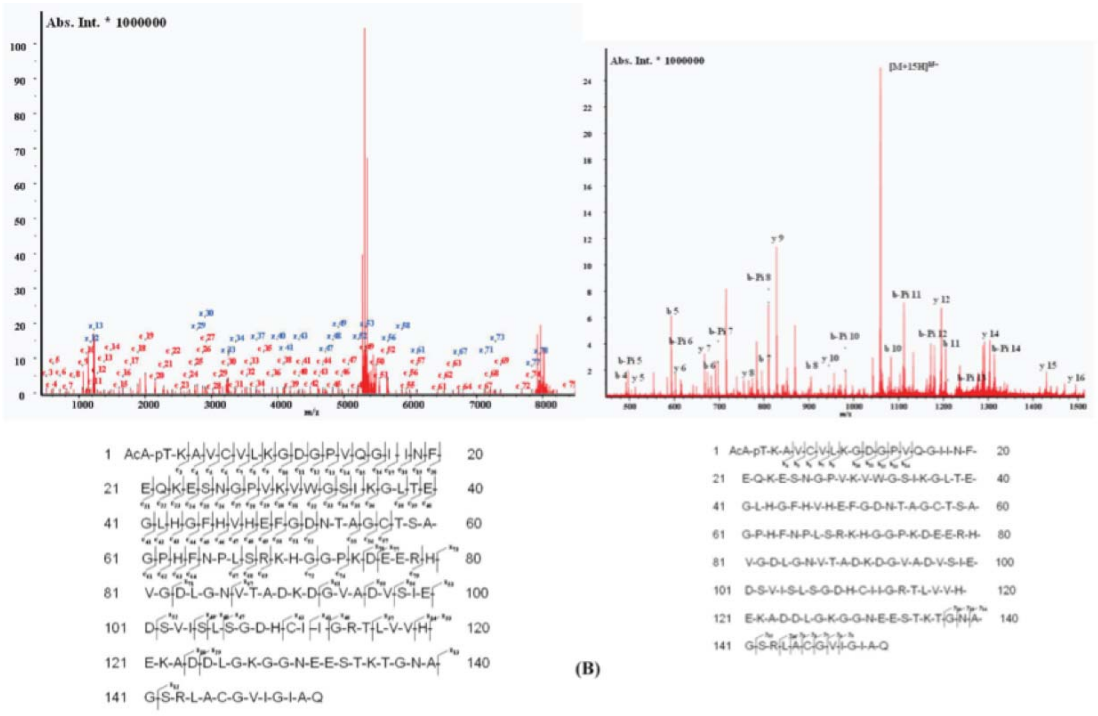


**Figure 3.7 – MS/MS identification of hydrated singly-phosphorylated SOD1.**
MS/MS analysis showing ions resulting from the fragmentation of hydrated SOD1 containing phosphorylated Thr-2. Ion signals corresponding to hydrated singly-phosphorylated human SOD1 (precursor: m/z 1139.6 Da, 14+ charge state), are isolated for top-down experiments by µESI-FTICR-MS with (A) electron-capture dissociation (ECD) and (B) collision-induced dissociation (CID) respectively. Inspection of the fragment ions from the CID MS/MS spectrum of hydrated singly-phosphorylated human SOD1 (Figure 2 B) reveals the neutral loss of 80 or 98 Da in $b_5$, $b_6$, $b_7$, $b_8$, $b_{10}$ and $b_{11}$. The ECD MS/MS spectrum of hydrated singly-phosphorylated SOD1 indicates 100% amino acid sequence coverage. 50 scans.

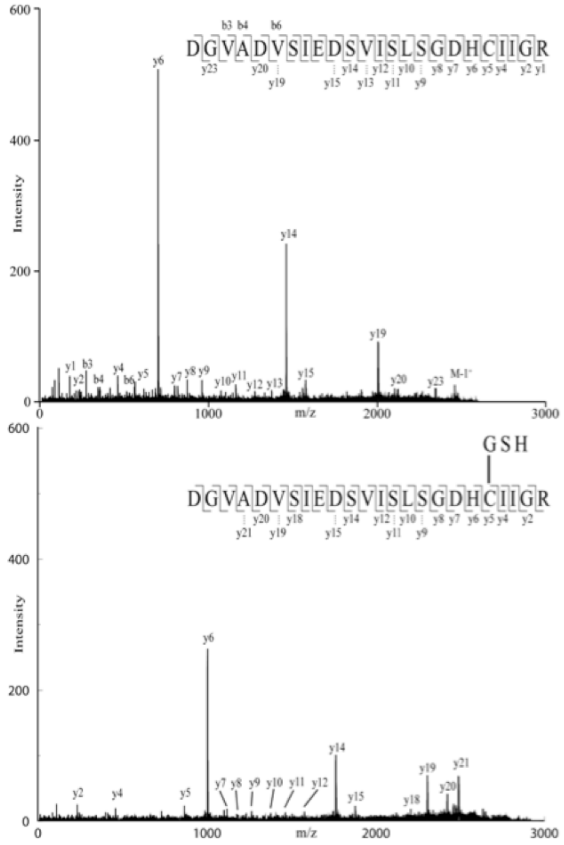


**Figure 3.8 – MS/MS spectrum showing the fragmentation products of the D92-R115 parent peptide ± glutathione.**

**Upper panel:** Observed y- and b-ions are identified in the spectrum and the sequence diagram. The parent peptide, DGVADVSIEDSVISLSGDHCIIGR, has a mass of 2457.24 Da.

**Lower panel:** Observed y- and b-ions are identified in the spectrum and the sequence diagram. The parent peptide DGVADVSIEDSVISLSGDHCIIGR, (glutathionylated at Cys-111), has a mass of 2762.29 Da.

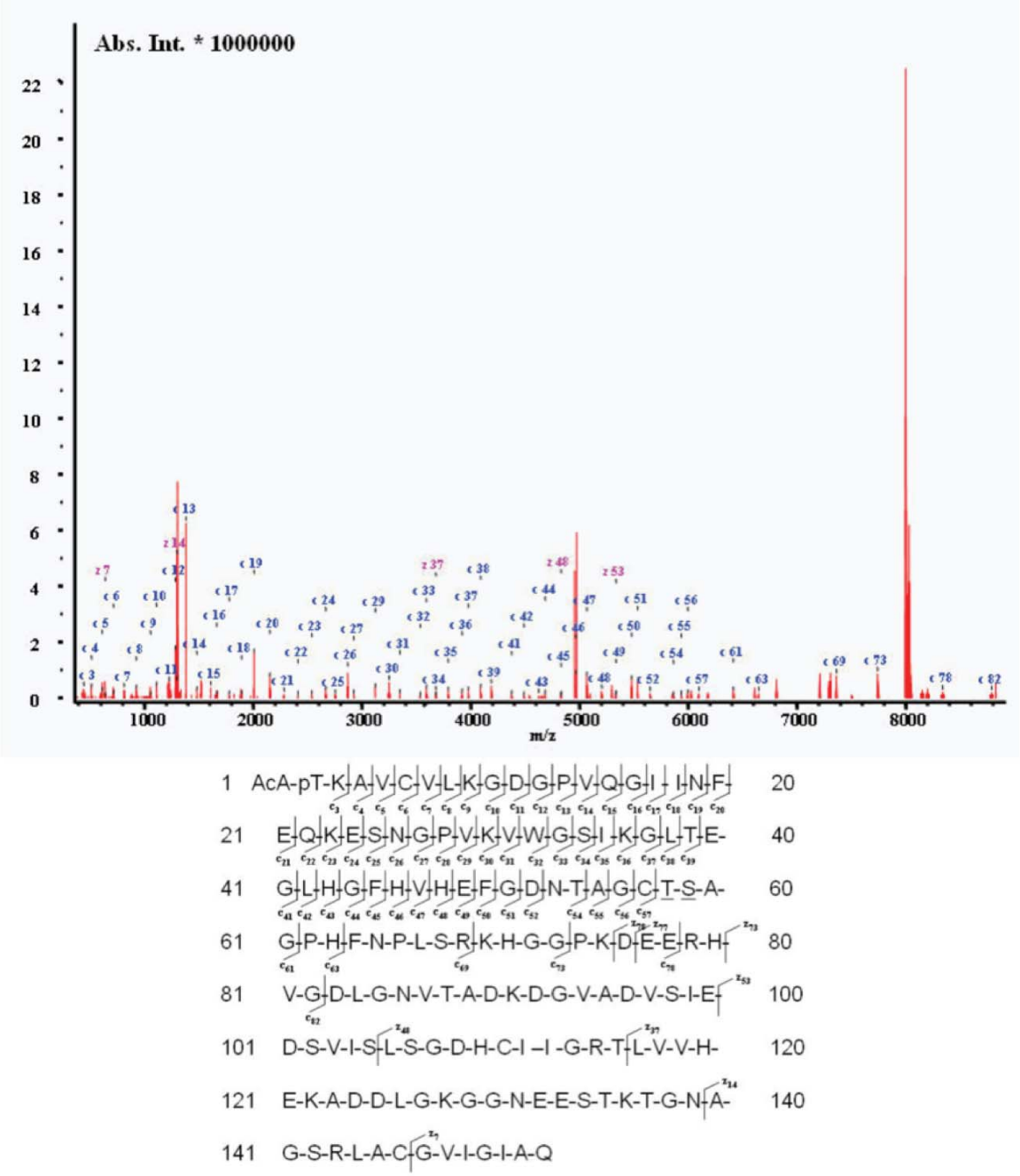


**Figure 3.9 – MS/MS identification of hydrated doubly-phosphorylated SOD1.**
MS/MS analysis showing ions resulting from the fragmentation of hydrated SOD1 containing phosphorylated Thr-2 and Thr-58/Ser-59. Ion signals corresponding to hydrated singly-phosphorylated human SOD1 (Precursor: m/z 1145.6 Da, 14+ charge state.), are isolated for top-down experiments by μESI-FTICR-MS with electron-capture dissociation (ECD). The ECD MS/MS spectrum of hydrated singly-phosphorylated SOD1 indicates 100% amino acid sequence coverage. 50 scans.

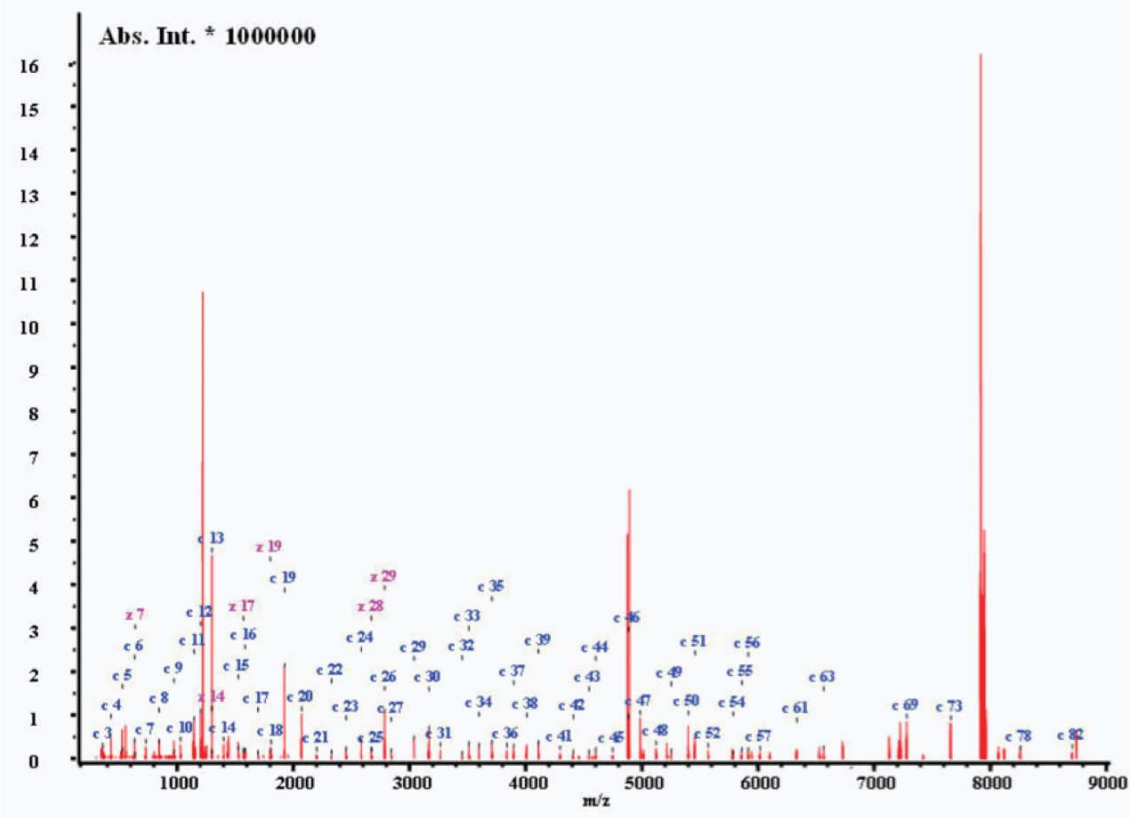


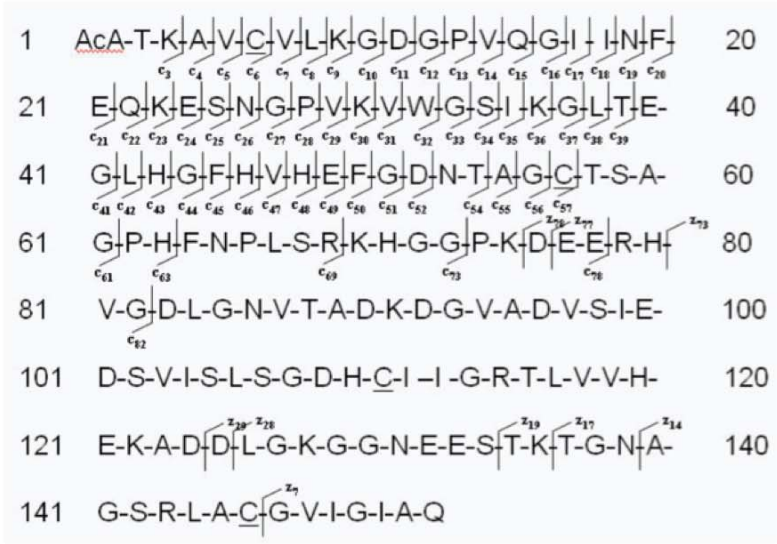


**Figure 3.10 – MS/MS identification of glutathionylated SOD1.**
MS/MS analysis showing ions resulting from the fragmentation of Glutathionylated SOD1. Ion signals corresponding to hydrated singly-phosphorylated human SOD1 (Precursor: m/z 1794.1 Da, 9+ charge state.), are isolated for top-down experiments by μESI-FTICR-MS with electron-capture dissociation (ECD). The ECD MS/MS spectrum of hydrated singly-phosphorylated SOD1 indicates 73% amino acid sequence coverage. 50 scans.

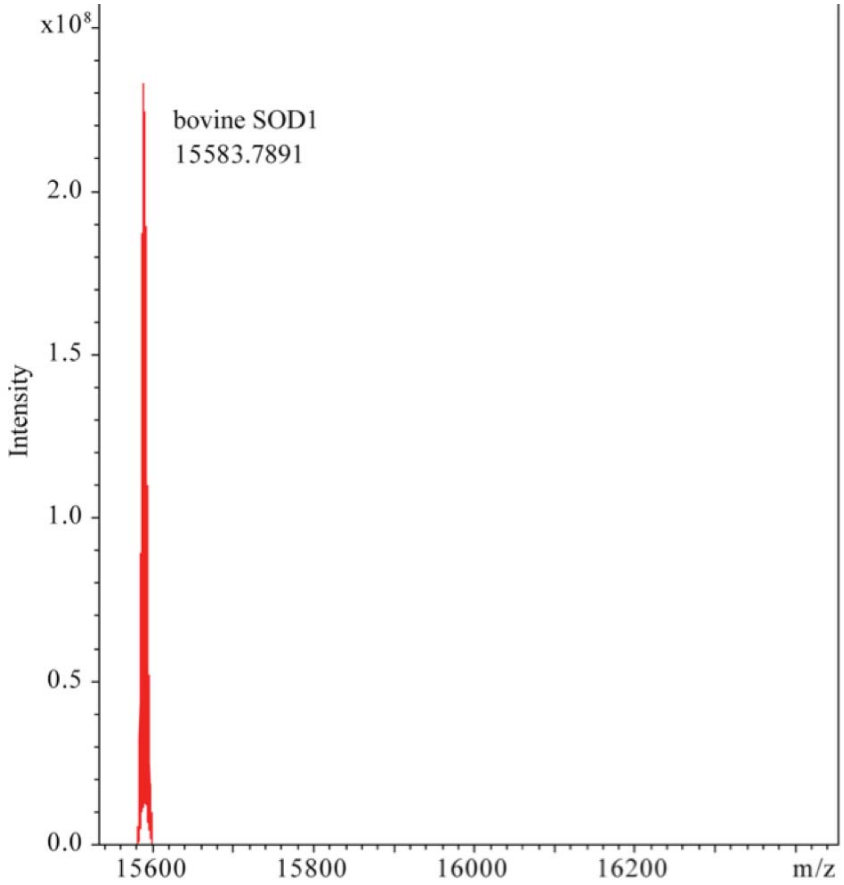


**Figure 3.11 – Mass spectrum of bovine erythrocyte SOD1.** Deconvoluted μESI-FTICR mass spectrum of bovine erythrocyte SOD1. We observe a single peak at a monoisotopic mass of 15583.7891 Da (calculated mass is 15583.7930 Da).

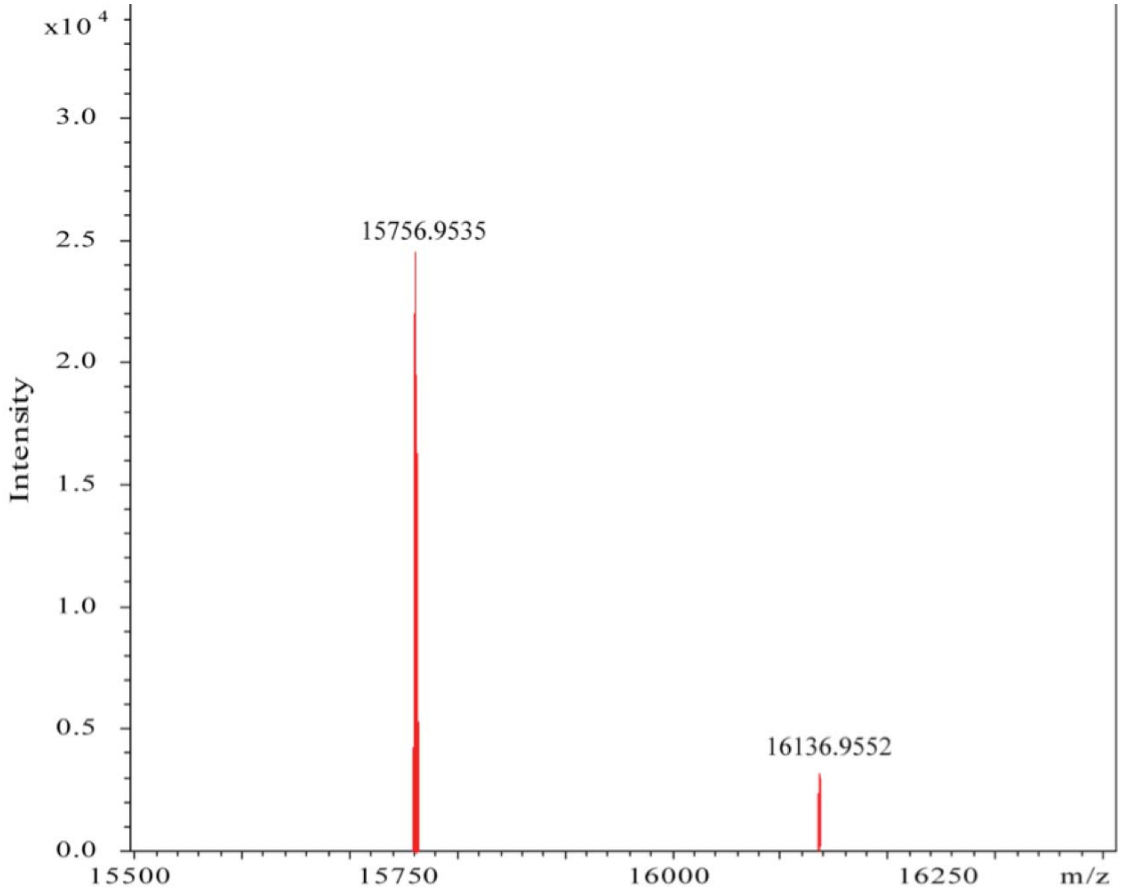


**Figure 3.12 – Mass spectrum of endogenous SOD1 from *S. cerevisiae*.** Deconvoluted μESI-FTICR mass spectrum of endogenous SOD1 isolated from *S. cerevisiae*. We observe monoisotopic mass peaks of 15756.9535 Da (calculated mass is 15756.8339 Da).

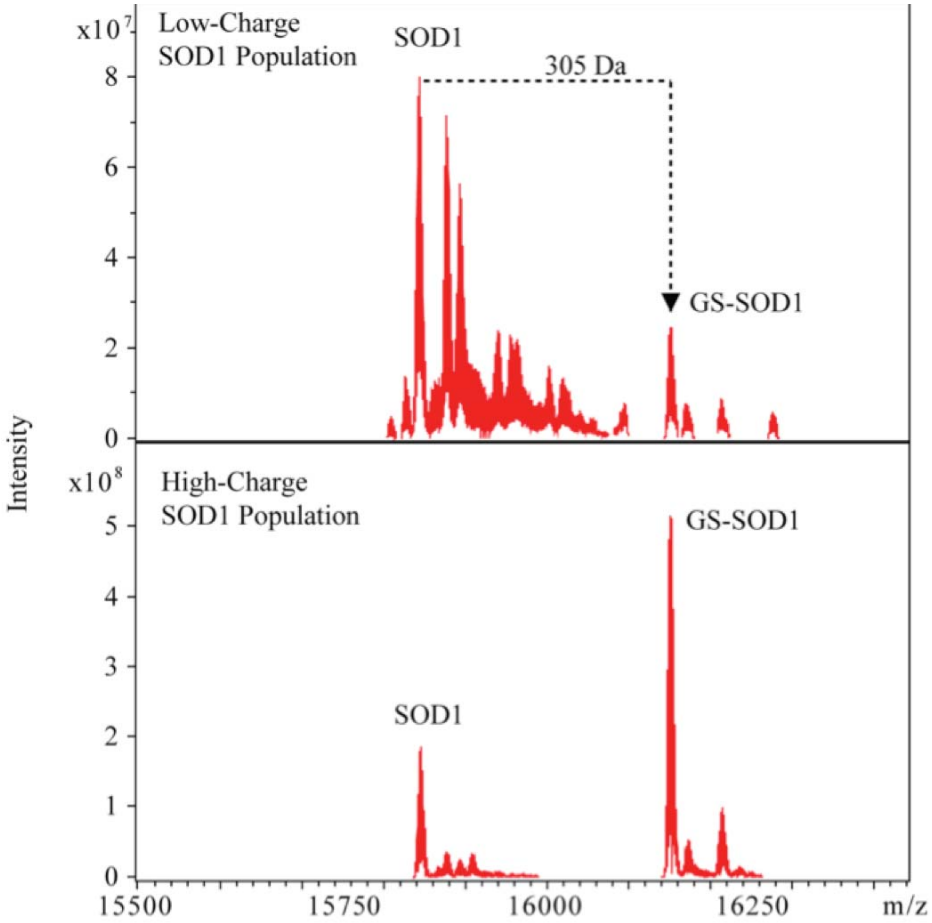


**Figure 3.13 – Mass spectra of high/low charge SOD1 populations in yeast-isolated SOD1.** Deconvoluted μESI-FTICR mass spectra of human SOD1 isolated from *S. cerevisiae* separated into high- and low-charge populations using anion exchange chromatography. We observe a shift due to glutathionylation in the highly-charge SOD1 population relative to the low-charge SOD1 population as in Figure 3.1E. We do not observe phosphorylation.

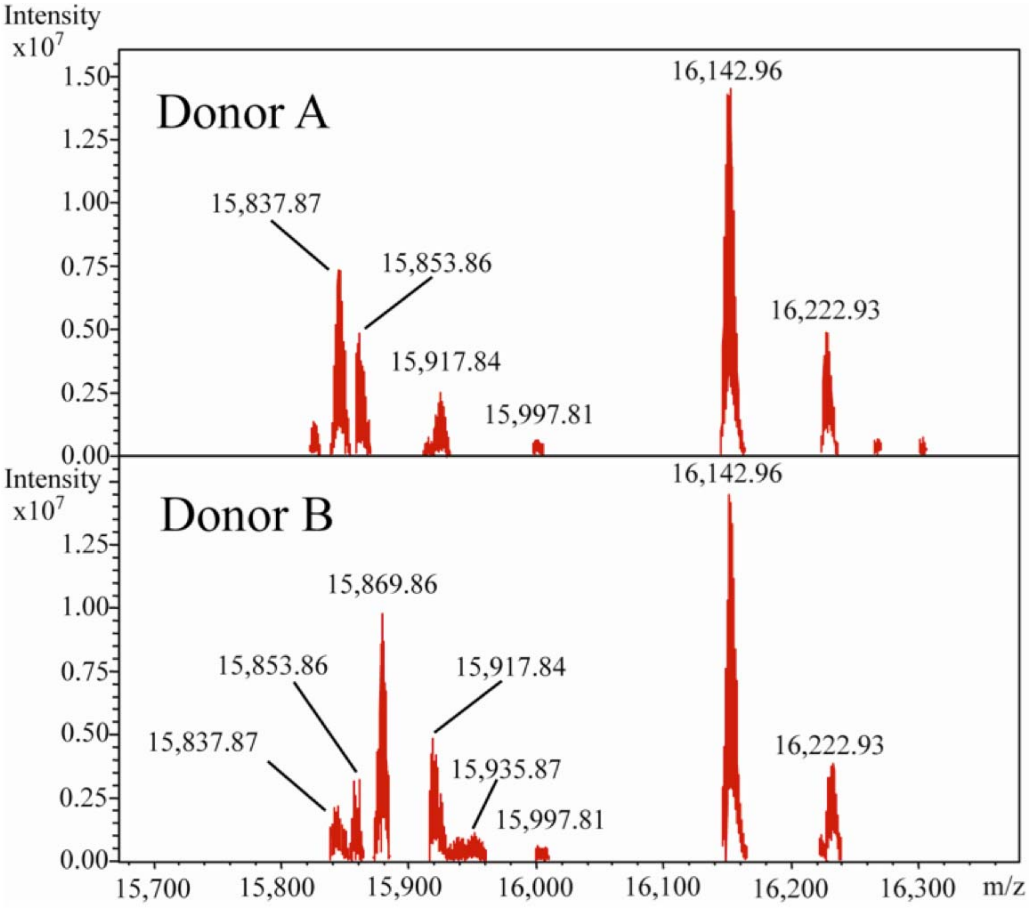


**Figure 3.14 – Mass spectra of SOD1 isolated from freshly-drawn human erythrocytes.** Deconvoluted FTICR-MS spectra of SOD1 isolated from human erythrocytes processed immediately following removal from donors.

# CHAPTER 4

# DDISEASE-RELATED MUTATIONS SHIFT CU,ZN SUPEROXIDE DISMUTASE OLIGOMERIZATION BEHAVIOR


## Abstract

Cytotoxic oligomers are thought to be a common hallmark of protein deposition diseases. The formation of large, soluble oligomers of Cu,Zn superoxide dismutase, which is mutated in a familial form of amyotrophic lateral sclerosis, have been observed in-vitro, but the mechanistic details governing the transition from the native SOD1 dimer to early oligomeric states have not been investigated. Here, we report the consistent formation of small oligomers consisting of 3-4 monomers of wild type SOD1 under conditions promoting the aggregation of bovine SOD1 (pH 3.5, 10 mM EDTA). The oligomers are stable over a timescale of at least one week at pH 3.5 and are not disulfide linked. FALS-associated SOD1 mutations allow oligomer formation under physiological conditions, and we observe a spectrum of oligomerization behavior among the SOD1 mutants sampled, with G93A, A4V, and H46R forming oligomers while I112T and G37R are “wild type like” in this regard and do not form oligomers at physiological pH. The oligomers formed by SOD1 mutants differ in size from those formed by wild type SOD1, forming an apparent hexameric species rather than a trimer or tetramer observed in wild type SOD1 at low pH. The shared

ability to access an alternative early oligomeric state appears to represent a disease-related property available to diverse SOD1 mutations but not wild type SOD1.

## Introduction

### Cu,Zn superoxide dismutase mutations are implicated in FALS

Cu,Zn superoxide dismutase (SOD1) is a homodimeric enzyme with the ubiquitous role of converting harmful superoxide radicals into hydrogen peroxide [227]. A link between SOD1 and a familial form of amyotrophic lateral sclerosis was established in 1993 [251] and, in the intervening years, examination of families suffering hereditary forms of ALS has resulted in the identification of over 100 mis-sense and other mutations in SOD1 – accounting for approximately 2% of the overall incidence [159]. As in the sporadic disease, SOD1-mediated FALS features the progressive loss of motor neurons in the brain stem and spinal cord [252,253]. ALS is similar to other neurodegenerative diseases in that protein aggregation is implicated in its pathogenesis, but the cause of the neuronal toxicity is not known. Recent evidence that the protein TDP-43 forms intraneuronal aggregates in almost all cases of sporadic and familial ALS has focused attention on the involvement of aggregation in ALS, but the single notable exception that shows no TDP-43 pathology is SOD1-mediated FALS. The progression of SOD1-mediated ALS and the TDP-43 associated sporadic disease are nearly identical, which suggests a point of phenotypic convergence between the two disease forms.

### Cytotoxicity: Aggregates versus Oligomers?

Recent evidence in the study of various neurodegenerative disorders has implicated soluble, oligomeric protein species in neurodegeneration rather than the insoluble aggregates

observed in *post mortem* tissue samples [254-256]. Glabe and coworkers generated a single antibody that recognizes an epitope specific to soluble oligomers of a wide variety of aggregating proteins [79,257] and have shown that the epitope exists in oligomers as small as tetramers, in the case of β-amyloid peptides [258]. Therefore, knowledge of early structural transformations leading to oligomer formation may lead both to identifying a mechanism for oligomer toxicity and the design of preventative strategies.

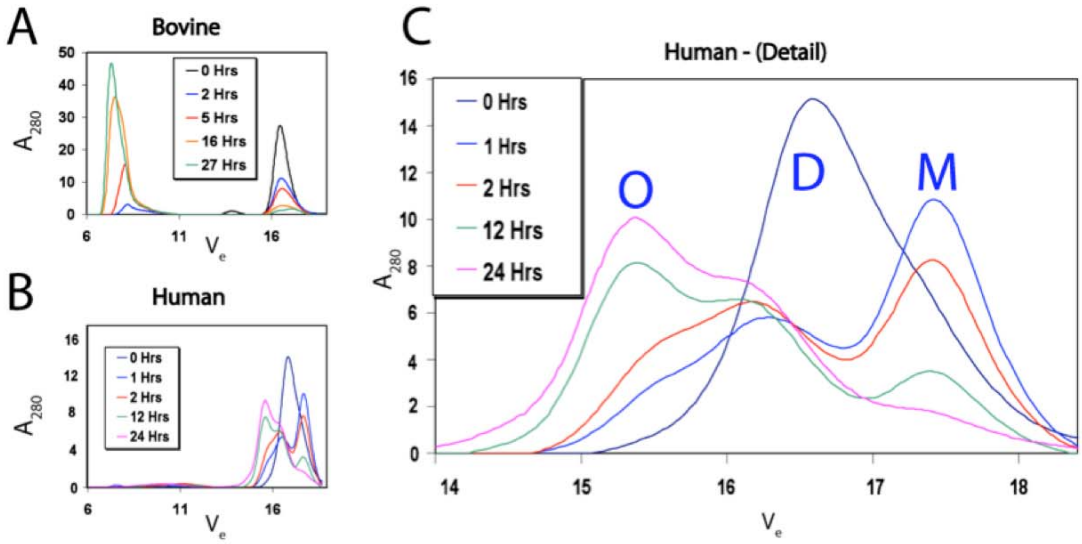


**Figure 4.1. Oligomerization of wild type human SOD1** Human SOD1 forms stable oligomers under conditions in which bovine SOD1 aggregates. (A): Size exclusion chromatograms showing the formation of bovine SOD1 aggregates. (B): Size exclusion chromatograms showing the absence of aggregation in human SOD1 under conditions identical to those in (A). (C): Detail of the experiment in (B) showing the formation of an oligomeric species eluting at 15.5 mL.

## Materials and Methods

### Isolation of SOD1 from erythrocytes and *S. cerevisiae*

SOD1 was isolated from S. cerevisiae and human erythrocytes using published methods [250]. Bovine SOD1 was isolated from bovine erythrocytes using the exact protocol used to isolate

SOD1 from human erythroctyes. Human erythrocytes were obtained from the UNC Hospital blood bank and bovine erythrocytes were purchased from Pel-Freez Biologicals, Rogers, AR. Following purification, samples were stored at -80 °C in 20 mM Tris, 150 mM NaCl, pH 7.8.

**Oligomerization/aggregation of SOD1WT**

SOD1 was thoroughly dialyzed at 4 °C against 50 mM sodium acetate buffer at pH 3.5 with 10 mM EDTA and 150 mM NaCl. Following dialysis, samples were brought to 30 μM (except when examining the concentration dependence of aggregation, where the final concentrations were 40, 60, 80, and 100 μM) by dilution with dialysis buffer, and incubated at 37 °C to initiate oligomerization.

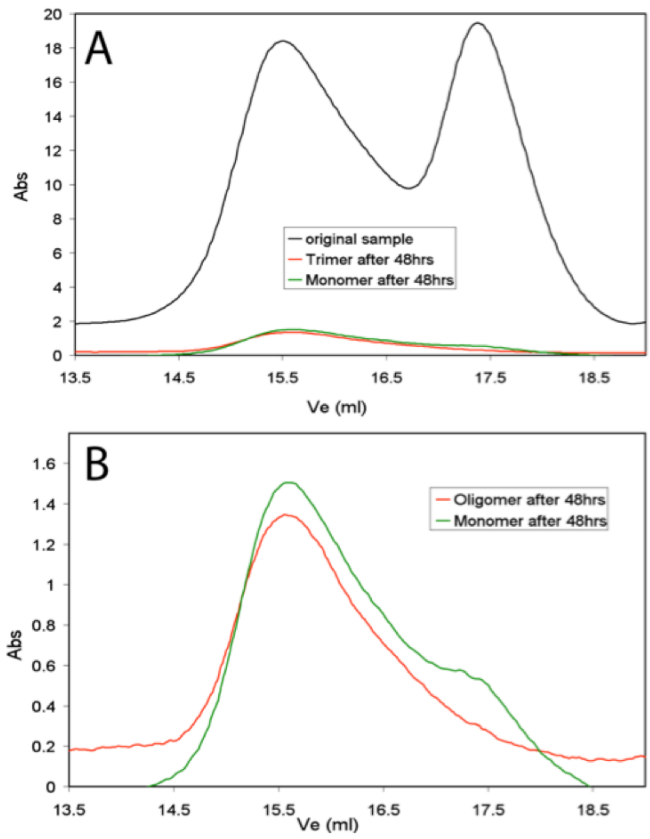


**Figure 4.2. Stability of SOD1 oligomers** (A) A size exclusion chromatography trace showing a mixture of monomeric and oligomeric SOD1 (black curve), re-incubated oligomer (red curve), and re-incubated monomer (green curve). (B) Detail of the re-incubated monomer and oligomer curves

**Oligomerization of mutant SOD1**

SOD1 mutants were diluted to 100 μM using 20 mM Tris pH 7.8 buffer with 150 mM NaCl and incubated at 37 °C in 1.5 mL microcentrifuge tubes.

### Time-resolved size exclusion chromatography

Aliquots of 250 μL were removed from the 37 °C reactions, filtered using 0.22 μm Amicon Ultrafree MC spin filters (Millipore), and applied to a Superdex 200 10/300 column (GE Healthcare) using a 200 μL sample loop. The column was pre-equilibrated in dialysis buffer (for pH 3.5 samples) or Tris buffer (for SOD1 mutants) and was run at 4 °C using an AKTA FPLC (GE Healthcare).

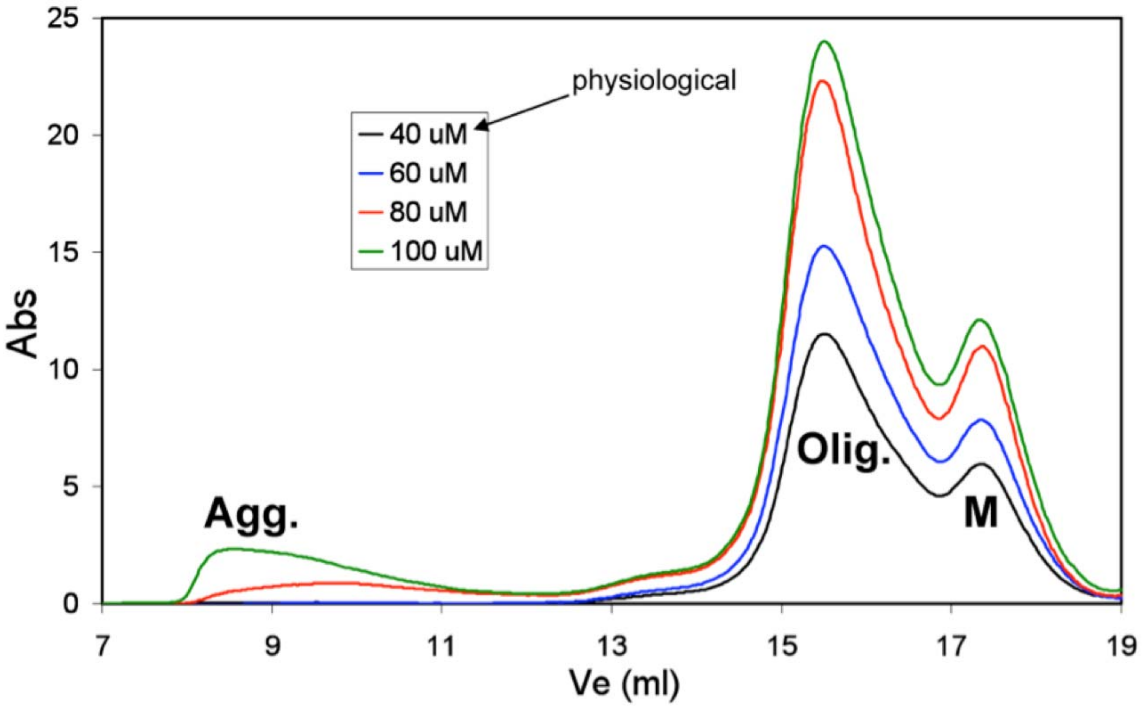


**Figure 4.3. Concentration dependence of SOD1 aggregation** Overlay of size exclusion chromatography traces from 24-hour incubations of SOD1 under destabilizing conditions. Aggregation is evident as concentration exceeds the physiological range.

## Results

### Wild type SOD1 forms small, stable oligomers under destabilizing conditions

Previously, we showed that bovine SOD1 aggregates at 37 °C via a monomeric intermediate in the presence of EDTA at pH 3.5 [74]. In the current study, we isolated SOD1 from both

human and bovine erythrocytes using the same method and monitor their aggregation using size exclusion chromatography.

SOD1 isolated from bovine erythrocytes aggregates to near-completion in 24 hours via a monomeric intermediate (Figure 4.1), as reported previously [74]. Under identical conditions of pH 3.5, 10mM EDTA, and 37 °C, SOD1 isolated from human erythrocytes consistently forms an oligomeric species that elutes with a molecular weight of 45 kDa (Figure 4.1), from a calibration curve calculated at pH 3.5 using proteins of known molecular weights. Performing the above experiments at 4 °C results in the formation of monomeric SOD1 without oligomers formation, indicating that structural fluctuations induced by incubation at high temperature are necessary for the formation of the oligomers from SOD1 monomers (data not shown).

SOD1 oligomers form as quickly as 1 hour after initiating incubation at 37C and are stable for at least 24 hours (Figure 4.1b and c). The population of oligomeric hSOD1 steadily builds and constitutes the major component of the reaction after 12 hours. SOD1 oligomers were returned to pH 7.8 by dialysis, yet they remained oligomeric (Figure 4.2). Recombinant human SOD1 from *E. coli* and *S. cerevisiae* behaves identically to SOD1 isolated from human erythrocytes using the same assay for oligomerization (data not shown).

To further probe the stability of the oligomers, SOD1 was incubated for 12 hours at pH 3.5 with 10 mM EDTA at 37 °C to produce a mixture of SOD1 oligomers and monomers. Fractions comprising the oligomeric and monomeric peaks eluting from the size exclusion experiment were retained and incubated at 37 °C for an additional 48 hours. Upon resolving each reaction over the size exclusion column, the formerly monomeric SOD1

eluted at the same volume as oligomeric SOD1, while the original oligomers remained the same as before the secondary incubation (Figure 4.2).

We performed analytical ultracentrifugation using these stable oligomers, but we could not differentiate between fits to a model including trimer or tetramer formation. Non-reducing SDS-PAGE indicates that the oligomer formed under the above conditions is NOT disulfide linked. This was confirmed by replicating the time-resolved size exclusion experiment in the presence of 1mM DTT at pH 3.5 and 37 °C with the same result as in the absence of DTT (data not shown). However, we do observe disulfide-linked species formed by 100 μM apoSOD1 incubated at neutral pH using both yeast and erythrocyte-derived hSOD1, supporting previous findings in the field [148].

**Concentration-dependent SOD1 aggregation**

The physiological concentration of SOD1 is generally held to be in the range of 40 μM in motor neurons [232]. To assay the concentration dependence of oligomers formation, parallel reactions of 40, 60, 80, and 100 μM SOD1 at pH 3.5 with 10 mM EDTA were incubated at 37C for 24 hours and resolved using size exclusion chromatography. At concentrations up to 60 μM, the oligomers are the terminal state, but at 80 and 100 μM, aggregation occurs in a concentration-dependant fashion (Figure 4.3). Because aggregation behavior is initaited by concentrations above the physiological range, the oligomerization scenario discussed above is more likely to describe the *in vivo* tendencies of SOD1 following the triggering of aggregation. However, high local concentrations of SOD1, such that might be expected to form near mitochondria, may account for the formation of SOD1 aggregates associated with those organelles [34].

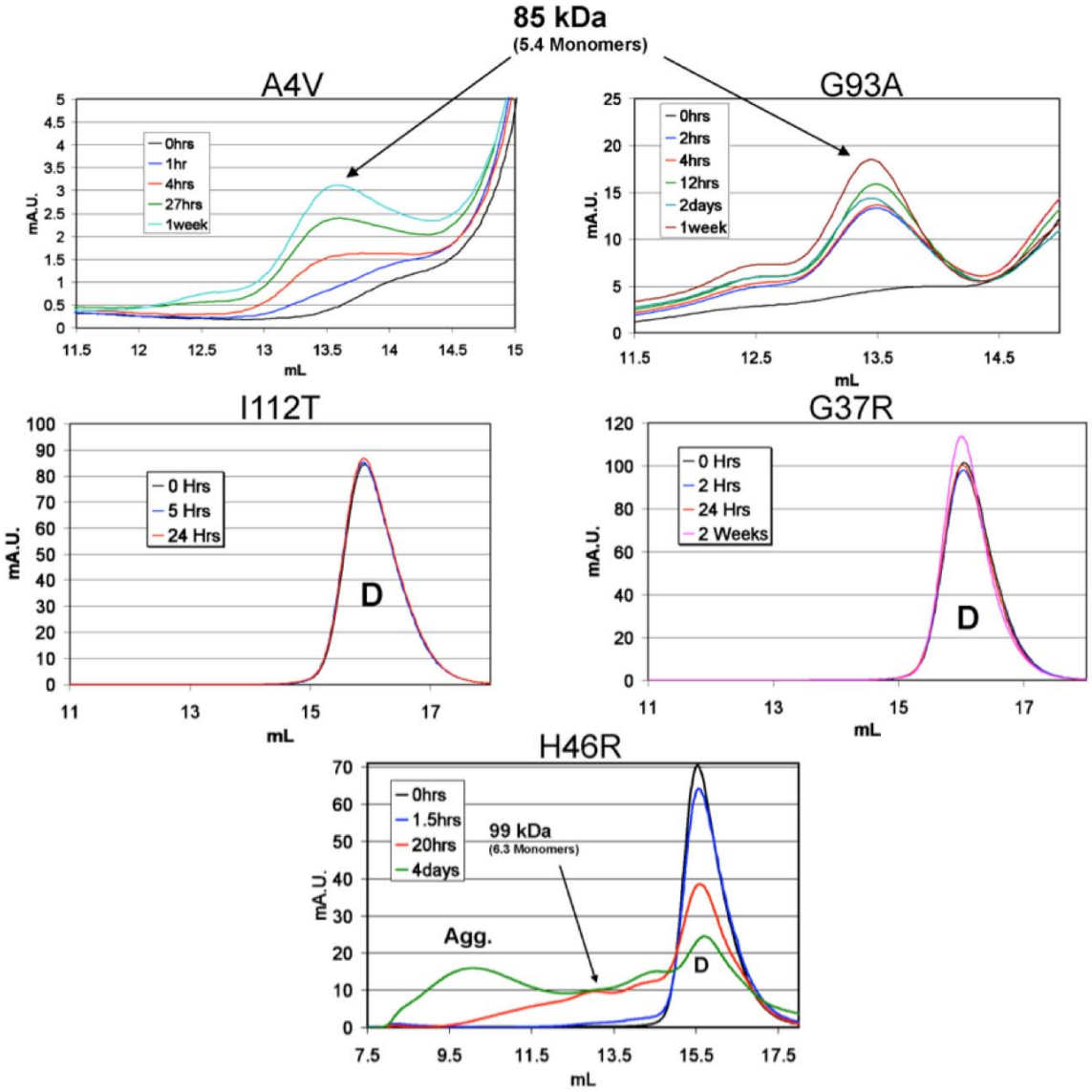


**Figure 4.4. Oligomerization in SOD1 mutants in the physiological range** Size exclusion chromatography experiments illustrating the spectrum of SOD1 mutant oligomerization behavior.

**SOD1 mutants form oligomers at physiological pH**

Using the same size exclusion chromatography techniques as above, we monitored the behavior of a set of SOD1 mutants – A4V, G93A, H46R, G37R, and I112T. All mutants begin in a dimeric state. Upon incubation at 37 °C, a persistent peak is formed centered at 13-13.5 ml (0.54 - 0.56 column volumes), compared to 16 ml (.67 column volumes) for the

dimer. According to a column calibration carried out at pH 7.8, this intermediate corresponds to 85 kDa – roughly, a hexamer of 16 kDa SOD1 monomers. This oligomer was formed by A4V, G93A, and H46R, while G37R and I112T are "wild-type-like" in terms of oligomerization under physiological conditions in that they remain stable dimers with no evidence of dissociation or oligomerization at 37 °C (Figure 4.4). The finding of "wild-type-like" behavior for G37R supports the observation that this particular mutation is associated with a more gradual ALS progression [259]. This oligomer is not active in SOD1 activity assays (data not shown), indicating either the loss of metals from the active site or a structural rearrangement that prohibits SOD1 activity.

## Discussion

### SOD1 aggregation and neuronal toxicity - what is the toxic species?

Mounting evidence suggests that protein aggregates – in ALS and other neurodegenerative diseases featuring protein aggregation – are not, in fact, a toxic species [254-256]. Soluble, oligomeric intermediate species are now held to be toxic, whereas large-scale aggregates have a protective role by acting as a sink for reactive oligomers. While amyloid fibrils and other aggregate structures contain many thousands of monomers and accumulate over long timescales, toxic oligomers can vary widely in size. Like amyloid fibrils, which share common structural features even though they can be assembled from many different proteins, soluble oligomers arising from different precursor proteins exhibit common structural and functional hallmarks [79,81,257]. An antibody against one such structural epitope in disease-associated soluble oligomers was able to recognize Aβ oligomers as small as tetramers and octamers [258].

Oligomer formation in ALS has been studied previously in vivo [260] and in vitro [148,149], but an emphasis was placed on the formation of large soluble oligomers and the chemical nature of the interactions within them – *e.g.* cystein oxidation and disulfide status. Furthermore, the oligomers described in previous studies occur at concentrations at the upper limits of the physiological range. The work described here focuses on the mechanism dimer destabilization and the earliest stages of SOD1 oligomerization at an SOD1 concentration closer to that inside motor neurons. It is during these initial stages that we expect the most relevant structural rearrangements in SOD1 to occur: those early structural rearrangements that are the targets of highest value for preventing the formation of SOD1 oligomers.

Previous studies of the effect of mutations on SOD1 oligomerization found that demetallated mutant and wild type SOD1 form similar high molecular weight oligomers [149]. Instead, we chose to focus on the effect of mutations on the formation of early SOD1 oligomers analogous to those we observed in wild type SOD1. Our findings indicate that mutations in SOD1 allow it not only to access oligomeric states under physiological conditions (pH 7.8, 37 °C), but also allow SOD1 to access different oligomeric states than those formed by wild type SOD1, albeit under different conditions of pH and metal occupancy. We do not observe the formation of high molecular weight oligomers except in H46R – presumably because H46R significantly reduces the ability of SOD1 to bind its metal cofactors. The higher metal occupancy of the other mutants effectively lowers the concentration of apoSOD1 in those reactions, resulting in limited formation of only early oligomers.

It is interesting to note the difference between both the behaviors of bovine and human SOD1 isolated from erythrocytes. Even though the sequence conservation between bovine and human SOD1 is 82 % and the proteins have similar structures and similar stability [261,262], the differences in sequences change the aggregation behavior dramatically.

## Acknowledgements

I would like to thank Joshua Jordon, Rachel L. Redler, Michael Caplow, and Nikolay V. Dokholyan for their contributions to the experimental design and execution of the above work.

# CHAPTER V

# DISCUSSION AND FUTURE DIRECTIONS

## Aggregation in neurodegenerative disease

While all the information needed for proteins to fold is encoded in their amino acid sequence [263], there are many more elements that play a part *in vivo*. In a crowded cellular environment, surrounded by interacting proteins, nascent polypeptides face a formidable challenge in finding the correct interactions that result in a folded and functional protein. Many become "trapped" in meta-stable intermediate structures, which are usually recognized by proteasomal machinery and degraded or refolded by chaperones. Alternatively, they can associate with similar misfolded proteins to form aggregates.

Extant protein sequences are the result of a long history of evolutionary refinement establishing a set of interactions defining the native state. However, the same inherent recognition that occurs between sequences within a protein is the basis for a type of self-association termed 3-dimensional domain swapping ([178], extensively catalogued in 2002 by Liu and Eisenberg [264]). Domain swapping is an important phenomenon, taking part in both normal and disease-related processes, and is intimately tied to protein folding. Domain swapping may be viewed as a natural mechanism for dealing with instability due to evolutionary changes in the amino acid sequence [265]. For example, a mutation that rigidifies a loop connecting two parts of a protein induces strain, which can be relieved without the

loss of function by “swapping” the portion of the protein on one side of the loop with the corresponding part of a similar protein. Dimerization by this mechanism has advantages including a high local concentration of enzymatic activity, since two functional proteins are joined together.

Protein aggregation is now widely viewed as a fundamental property of the polypeptide chain[220], meaning that all of the considerations discussed above must, to some degree, apply to the study of aggregating proteins. Therefore, the study of protein self-association and aggregation really is the study of protein folding in the context of external factors like protein concentration, localization, or evolution. As this field develops and knowledge of protein aggregation as a general phenomenon accumulates, we stand to gain not only vital tools for treating specific diseases, but also insight into the behavior of all proteins with respect to their environment.

## “Triggers” of aggregation

Even proteins having no association with diseases of protein aggregation are capable of accessing multimeric and aggregate states given the proper stimulus [266]. Diverse stimuli, both natural and artificial, are capable of inducing protein aggregation, as described below.

### Mutations

In the case of SOD1, point mutations, deletions, truncations and other mutations can destabilize the native state sufficiently for the protein to misfold and aggregate. Mutations in SOD1 and TDP-43 are associated with familial and sporadic cases of ALS, as discussed in the preceding chapters.

**Modifications**

Post-translational modifications of SOD1 include metal binding at the active site, disulfide bond formation between Cys57 and Cys146, cleavage of methionine from the amino terminus followed by acetylation, and side chain modifications such as oxidation or glutathionylation of Cys111 [233,250] and phosphorylation of Thr2 [250]. It is reasonable to assume that altering SOD1 by either removing or adding chemical groups will impact the stability of SOD1 and its propensity to aggregate. Indeed the formation of the disulfide bond and the metal occupancy at the active site are important determinants of SOD1 stability, the absence of which result in the formation of oligomerization and aggregation of SOD1 [112,148,149]. Though phosphorylation is generally a modification that modulates a protein's function or interactions with binding partners, the addition of a charged group to a side chain of SOD1 is similar to SOD1 mutations associated with ALS that alter the charge (e.g. E21K, E100K). Another consideration is that phosphorylation represents a dramatic chemical change relative to some seemingly inconsequential mutations that result in ALS (e.g. L8V, G114A, L117V).

Another post-translational modification of SOD1 is the oxidation of Cys-111 to cysteine sulfonic acid [233]. Such oxidative modifications to protein side chains represent another mechanism for triggering aggregation. In the case of SOD1, oxidation has been demonstrated to be capable of inducing aggregation in vitro [139,234].

**Artificial triggers**

As discussed above, a number of stimuli can trigger aggregation associated with neurodegenerative and other diseases, inducible aggregation of normally soluble proteins also provides a useful laboratory tool for studying generalizable aspects of protein

misfolding and aggregation. For example, chicken egg white lysozyme aggregates via soluble oligomers and protofibrils when incubated at low pH and an elevated temperature [267], and the PI3-SH3 domain can be induced to form either disordered aggregates or highly-ordered amyloid fibrils depending upon the precise pH used [268,269]. In fact, oligomers of the PI3-SH3 domain and the N-terminal domain of the E. coli HypF protein were shown to have cytotoxic properties similar to oligomers of disease-associated proteins [266], suggesting that the manner in which misfolding and aggregation is induced is of little importance.

Of the methods to induce SOD1 aggregation, the most common is the combination of EDTA, low pH and elevated (physiological) temperature. Other methods include oxidation by H2O2 [139] and, recently, the introduction of mechanical forces using a rotary shaker [270]. Interestingly, the latter method produces fibrillar SOD1 that resembles the amyloid fibrils formed by other disease-related proteins but previously not observed with SOD1.

An altogether different type of artificial aggregation trigger, and one with real implications for human health, is the initiation of $\beta_2$-microglobulin aggregation as a consequence of hemodialysis known as dialysis-related amyloidosis [271]. Prevalent in Japan due to a social stigma against organ transplantation, dialysis-related amyloidosis involves $\beta_2$-microglobulin aggregation triggered by the cleavage of six residues from the N terminus of the protein, inducing structural flexibility in the native state [272].

## Simulations of SOD1 folding and aggregation

Computational studies of protein aggregation have traditionally been inadequate due to the massive complexity of the system in both time and length scale. Several approaches have been used to overcome this complexity (Figure 3.5). Traditional all-atom molecular

dynamics simulations have been carried out to model the aggregation of disease-related peptides such as Aβ and polyglutamine [273-275]. Other techniques seek to identify which parts within larger proteins are responsible for their aggregation behavior, resulting in the identification of sequence stretches in various proteins that are "amyloidogenic," or "hot spots" for aggregation [156,276,277]. Underlying this work is the idea that evolution acts to prevent aggregation by burying aggregation-prone protein sequences or otherwise prohibiting their apposition in protein structures and during folding[2]. To study the nature of subunit assembly and extension during aggregation, which are out of reach for all-atom molecular dynamics in both the size scale and time scale, simplified protein models are being utilized [279]. By accessing aggregation events that are out of the reach of experimentalists, computational studies of aggregation are an essential compliment to the experimental findings regarding aggregate structure and formation mechanisms.

## Future work

### Determine structural effects of modifications

Because phosphorylation and glutathionylation occur near the dimer interface of SOD1, determining whether they have a structural impact on the structure at the interface will offer clues to the mechanism of destabilization. Preliminary work has begun to crystallize modified forms of SOD1 to uncover any structural rearrangements as a result of post-translational modifications. Glutathionylated SOD1 can be efficiently separated from non-glutathionylated SOD1 using anion exchange chromatography, and the possibility to

[2] It is interesting to note here that in the case of Pmel17, which aggregates to form a "functional amyloid" involved in melanin biosynthesis, a protein seems to have evolved to aggregate at an incredible rate, perhaps to minimize the population time in a soluble oligomer form [278].

perform non-enzymatic glutathionylation in-vitro exists if but phosphorylation does not result in altered affinity in similar anion exchange separations. As a means of studying the effect of SOD1 phosphorylation without purifying the modified enzyme, we have engineered a glutamic acid into position 2 to mimic the phosphorylation of the threonine at that position.

**Figure 5.1 Unit cell of modified SOD1** The crystallographic unit cell of modified SOD1 features an atypical 7$^{th}$ SOD1 monomer (upper right – dark blue) compared to published structures.

Preliminary work in crystallizing modified and unmodified forms of wild type SOD1 isolated from human erythrocytes was performed but the resulting structures did not contain the expected modifications. This negative result may be the result of preferential crystallization of trace amounts of unmodified SOD1 in the samples or defects in the crystals that do not allow sufficient refinement to observe modifications. However, crystals of SOD1 containing a high percentage of glutathione formed a unique unit cell containing 7 monomers (Figure 5.1) whereas the unit cell observed in crystals of unmodified SOD1

consists of 6 monomers arranged as a trimer of dimers. This trimer of dimers arrangement is consistent with SOD1 structures published elsewhere [280].

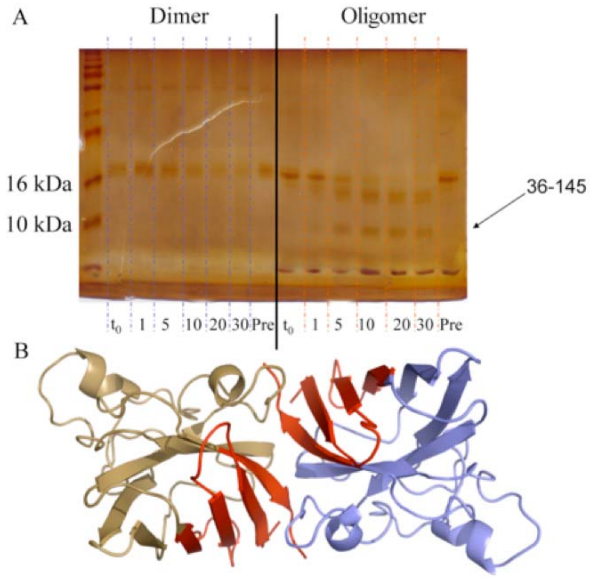


**Figure 5.2 – Limited proteolysis of SOD1 oligomers** A) Pepsin proteolysis of SOD1 dimers and oligomers monitored by SDS-PAGE B) SOD1 structure with cleaved regions in red.

**The structure of SOD1 oligomers**

The ideal treatments for diseases of protein aggregation – in which normally soluble, functional proteins misfold to form some toxic multimeric species – are those that prevent the initial destabilization and misfolding of the disease-associated proteins. Understanding the structural transitions accompanying the initiation of aggregation will hopefully lead to strategies to prevent such events by preventing the formation of interactions unique to key aggregation intermediates. SOD1 is one such protein that can be induced to aggregate by a combination of factors such as mutations, aberrant redox chemistry or possibly post-translational modifications. Chapter IV includes a description of oligomers formed by wild type and mutant SOD1 that may represent valuable targets for disruption by small molecules

or peptides. Furthermore, the consistency with which these early SOD1 oligomers are formed and their remarkable stability makes these species ideal tools for gathering structural information. Even sparse structural constraints will allow the generation of testable hypotheses for oligomer structure and the transitions that occur to allow the native dimers and monomers to adopt aberrant conformations. DMD simulations will likely prove invaluable in this regard, as demonstrated by previous work in this laboratory in which experimental constraints were employed to discover a rare intermediate structure of the FAT domain of focal adhesion kinase [281], which was later supported experimentally [282].

Preliminary work has begun toward characterizing the oligomers formed by SOD1. Using limited proteolysis and mass spectrometry, we aim to generate a list of positions that occur on the outside of SOD1 oligomers. Combining data from the use of a variety of proteases will allow us to collect a diverse array of cut sites on the exterior of the oligomers, which will then be used in combination with DMD simulations to generate candidate structures featuring the exposure of these positions. Initial experiments using pepsin due to its activity in the pH range in which wild type SOD1 forms oligomers have offered very promising results.

As SOD1 parallel reactions of dimers and oligomers are incubated with pepsin, aliquots are collected and analyzed by SDS PAGE. Upon pepsin proteolysis, dimeric SOD1 is uniformly cleaved and the band corresponding to the 16 kDa monomer disappears. In contrast, oligomeric SOD1 yields persistent lower molecular weight species upon pepsin proteolysis (Figure 5.2a). Mass spectrometry was used to match the molecular weight of one such band to a peptide fragment containing residues 36-145 of SOD1. Residues 145 and 146 are buried within the SOD1 dimer interface and must therefore be exposed in order for

pepsin to cleave at that position (Figure 5.2b). More revealing, however, is the resistance of the resulting cleavage products to further proteolysis. We believe this finding implies the formation of SOD1 oligomers via an alternative interface that leaves previously buried residues at the dimer interface exposed and available for pepsin proteolysis. Upon cleavage, the core of the oligomer remains stable and resistant to further proteolysis.

Future studies will focus on expanding the assay to include other proteases and, ultimately, the incorporation of solvent-exposure constraints into simulations of SOD1 oligomerization.

**Examine effects of modifications on regulatory interactions**

Recent evidence that SOD1 may play a role in the regulation oxidative stress through a direct interaction with Rac1 in the NOX complex [225] represents an alternative mechanism of action for SOD1 post-translational modifications – i.e. mediating protein-protein interactions. We are collaborating with Sharon Campbell, an expert in Rho GTPases and Rac1 in particular, to examine the effect of SOD1 modifications on the formation of the SOD1/Rac1 complex and to provide a quantitative analysis of the effect of SOD1 binding on Rac1 GTP hydrolysis.

# REFERENCES


1. Swash M, Desai J. Motor neuron disease: classification and nomenclature. Amyotroph Lateral Scler Other Motor Neuron Disord 2000;1(2):105-112.

2. Lilienfeld DE, Perl DP. Projected neurodegenerative disease mortality in the United States, 1990-2040. Neuroepidemiology 1993;12(4):219-228.

3. Sorenson EJ, Stalker AP, Kurland LT, Windebank AJ. Amyotrophic lateral sclerosis in Olmsted County, Minnesota, 1925 to 1998. Neurology 2002;59(2):280-282.

4. Yoshida S, Mulder DW, Kurland LT, Chu CP, Okazaki H. Follow-up study on amyotrophic lateral sclerosis in Rochester, Minn., 1925 through 1984. Neuroepidemiology 1986;5(2):61-70.

5. Caroscio JT, Mulvihill MN, Sterling R, Abrams B. Amyotrophic lateral sclerosis. Its natural history. Neurol Clin 1987;5(1):1-8.

6. Gubbay SS, Kahana E, Zilber N, Cooper G, Pintov S, Leibowitz Y. Amyotrophic lateral sclerosis. A study of its presentation and prognosis. J Neurol 1985;232(5):295-300.

7. Jokelainen M. Amyotrophic lateral sclerosis in Finland. II: Clinical characteristics. Acta Neurol Scand 1977;56(3):194-204.

8. Li TM, Alberman E, Swash M. Clinical features and associations of 560 cases of motor neuron disease. J Neurol Neurosurg Psychiatry 1990;53(12):1043-1045.

9. Traynor BJ, Codd MB, Corr B, Forde C, Frost E, Hardiman OM. Clinical features of amyotrophic lateral sclerosis according to the El Escorial and Airlie House diagnostic criteria: A population-based study. Arch Neurol 2000;57(8):1171-1176.

10. Brooks BR. Natural history of ALS: symptoms, strength, pulmonary function, and disability. Neurology 1996;47(4 Suppl 2):S71-81; discussion S81-72.

11. Hudson AJ. Amyotrophic lateral sclerosis/parkinsonism/dementia: clinico-pathological correlations relevant to Guamanian ALS/PD. Can J Neurol Sci 1991;18(3 Suppl):387-389.

12. Massman PJ, Sims J, Cooke N, Haverkamp LJ, Appel V, Appel SH. Prevalence and correlates of neuropsychological deficits in amyotrophic lateral sclerosis. J Neurol Neurosurg Psychiatry 1996;61(5):450-455.

13. Portet F, Cadilhac C, Touchon J, Camu W. Cognitive impairment in motor neuron disease with bulbar onset. Amyotroph Lateral Scler Other Motor Neuron Disord 2001;2(1):23-29.

14. Rakowicz WP, Hodges JR. Dementia and aphasia in motor neuron disease: an underrecognised association? J Neurol Neurosurg Psychiatry 1998;65(6):881-889.

15. Lomen-Hoerth C, Murphy J, Langmore S, Kramer JH, Olney RK, Miller B. Are amyotrophic lateral sclerosis patients cognitively normal? Neurology 2003;60(7):1094-1097.

16. Brooks BR, Miller RG, Swash M, Munsat TL. El Escorial revisited: revised criteria for the diagnosis of amyotrophic lateral sclerosis. Amyotroph Lateral Scler Other Motor Neuron Disord 2000;1(5):293-299.

17. Chen KM. [Disappearance of ALS from Guam: implications for exogenous causes]. Rinsho Shinkeigaku 1995;35(12):1549-1553.

18. Galasko D, Salmon DP, Craig UK, Thal LJ, Schellenberg G, Wiederholt W. Clinical features and changing patterns of neurodegenerative disorders on Guam, 1997-2000. Neurology 2002;58(1):90-97.

19. Pringle CE, Hudson AJ, Munoz DG, Kiernan JA, Brown WF, Ebers GC. Primary lateral sclerosis. Clinical features, neuropathology and diagnostic criteria. Brain 1992;115 ( Pt 2):495-520.

20. Zhai P, Pagan F, Statland J, Butman JA, Floeter MK. Primary lateral sclerosis: A heterogeneous disorder composed of different subtypes? Neurology 2003;60(8):1258-1265.

21. Norris F, Shepherd R, Denys E, U K, Mukai E, Elias L, Holden D, Norris H. Onset, natural history and outcome in idiopathic adult motor neuron disease. J Neurol Sci 1993;118(1):48-55.

22. Chio A, Brignolio F, Leone M, Mortara P, Rosso MG, Tribolo A, Schiffer D. A survival analysis of 155 cases of progressive muscular atrophy. Acta Neurol Scand 1985;72(4):407-413.

23. Cervenakova L, Protas, II, Hirano A, Votiakov VI, Nedzved MK, Kolomiets ND, Taller I, Park KY, Sambuughin N, Gajdusek DC, Brown P, Goldfarb LG. Progressive muscular atrophy variant of familial amyotrophic lateral sclerosis (PMA/ALS). J Neurol Sci 2000;177(2):124-130.

24. Tsuchiya K, Sano M, Shiotsu H, Akiyama H, Watabiki S, Taki K, Kondo H, Nakano I, Ikeda K. Sporadic amyotrophic lateral sclerosis of long duration mimicking spinal progressive muscular atrophy exists: additional autopsy case with a clinical course of 19 years. Neuropathology 2004;24(3):228-235.

25. Lomen-Hoerth C. Characterization of amyotrophic lateral sclerosis and frontotemporal dementia. Dement Geriatr Cogn Disord 2004;17(4):337-341.

26. Hodges JR, Davies R, Xuereb J, Kril J, Halliday G. Survival in frontotemporal dementia. Neurology 2003;61(3):349-354.

27. Yoshiyama Y, Yamada T, Asanuma K, Asahi T. Apoptosis related antigen, Le(Y) and nick-end labeling are positive in spinal motor neurons in amyotrophic lateral sclerosis. Acta Neuropathol 1994;88(3):207-211.

28. Troost D, Aten J, Morsink F, de Jong JM. Apoptosis in ALS is not restricted to motoneurons: Bcl-2 expression is increased in post-central cortex, adjacent to the affected motor cortex. J Neurol Sci 1995;129 Suppl:79-80.

29. Ilzecka J, Stelmasiak Z, Dobosz B. Interleukin-1beta converting enzyme/Caspase-1 (ICE/Caspase-1) and soluble APO-1/Fas/CD 95 receptor in amyotrophic lateral sclerosis patients. Acta Neurol Scand 2001;103(4):255-258.

30. Inoue H, Tsukita K, Iwasato T, Suzuki Y, Tomioka M, Tateno M, Nagao M, Kawata A, Saido TC, Miura M, Misawa H, Itohara S, Takahashi R. The crucial role of caspase-9 in the disease progression of a transgenic ALS mouse model. EMBO J 2003;22(24):6665-6674.

31. Mu X, He J, Anderson DW, Trojanowski JQ, Springer JE. Altered expression of bcl-2 and bax mRNA in amyotrophic lateral sclerosis spinal cord motor neurons. Ann Neurol 1996;40(3):379-386.

32. Tews DS, Goebel HH, Meinck HM. DNA-fragmentation and apoptosis-related proteins of muscle cells in motor neuron disorders. Acta Neurol Scand 1997;96(6):380-386.

33. Shinoe T, Wanaka A, Nikaido T, Kanazawa K, Shimizu J, Imaizumi K, Kanazawa I. Upregulation of the pro-apoptotic BH3-only peptide harakiri in spinal neurons of amyotrophic lateral sclerosis patients. Neurosci Lett 2001;313(3):153-157.

34. Pasinelli P, Belford ME, Lennon N, Bacskai BJ, Hyman BT, Trotti D, Brown RH, Jr. Amyotrophic lateral sclerosis-associated SOD1 mutant proteins bind and aggregate with Bcl-2 in spinal cord mitochondria. Neuron 2004;43(1):19-30.

35. Ghadge GD, Lee JP, Bindokas VP, Jordan J, Ma L, Miller RJ, Roos RP. Mutant superoxide dismutase-1-linked familial amyotrophic lateral sclerosis: molecular mechanisms of neuronal death and protection. J Neurosci 1997;17(22):8756-8766.

36. Mattson MP, Kroemer G. Mitochondria in cell death: novel targets for neuroprotection and cardioprotection. Trends Mol Med 2003;9(5):196-205.

37. Chowdhury I, Tharakan B, Bhat GK. Current concepts in apoptosis: the physiological suicide program revisited. Cell Mol Biol Lett 2006;11(4):506-525.

38. Olney JW, Rhee V, Ho OL. Kainic acid: a powerful neurotoxic analogue of glutamate. Brain Res 1974;77(3):507-512.

39. Bensimon G, Lacomblez L, Meininger V. A controlled trial of riluzole in amyotrophic lateral sclerosis. ALS/Riluzole Study Group. N Engl J Med 1994;330(9):585-591.

40. Lacomblez L, Bensimon G, Leigh PN, Guillet P, Meininger V. Dose-ranging study of riluzole in amyotrophic lateral sclerosis. Amyotrophic Lateral Sclerosis/Riluzole Study Group II. Lancet 1996;347(9013):1425-1431.

41. Ryberg H, Askmark H, Persson LI. A double-blind randomized clinical trial in amyotrophic lateral sclerosis using lamotrigine: effects on CSF glutamate, aspartate, branched-chain amino acid levels and clinical parameters. Acta Neurol Scand 2003;108(1):1-8.

42. Cudkowicz ME, Shefner JM, Schoenfeld DA, Brown RH, Jr., Johnson H, Qureshi M, Jacobs M, Rothstein JD, Appel SH, Pascuzzi RM, Heiman-Patterson TD, Donofrio PD, David WS, Russell JA, Tandan R, Pioro EP, Felice KJ, Rosenfeld J, Mandler RN, Sachs GM, Bradley WG, Raynor EM, Baquis GD, Belsh JM, Novella S, Goldstein J, Hulihan J. A randomized, placebo-controlled trial of topiramate in amyotrophic lateral sclerosis. Neurology 2003;61(4):456-464.

43. Miller RG, Moore DH, 2nd, Gelinas DF, Dronsky V, Mendoza M, Barohn RJ, Bryan W, Ravits J, Yuen E, Neville H, Ringel S, Bromberg M, Petajan J, Amato AA, Jackson C, Johnson W, Mandler R, Bosch P, Smith B, Graves M, Ross M, Sorenson EJ, Kelkar P, Parry G, Olney R. Phase III randomized trial of gabapentin in patients with amyotrophic lateral sclerosis. Neurology 2001;56(7):843-848.

44. Plaitakis A, Caroscio JT. Abnormal glutamate metabolism in amyotrophic lateral sclerosis. Ann Neurol 1987;22(5):575-579.

45. Gredal O, Moller SE. Effect of branched-chain amino acids on glutamate metabolism in amyotrophic lateral sclerosis. J Neurol Sci 1995;129(1):40-43.

46. Rothstein JD, Tsai G, Kuncl RW, Clawson L, Cornblath DR, Drachman DB, Pestronk A, Stauch BL, Coyle JT. Abnormal excitatory amino acid metabolism in amyotrophic lateral sclerosis. Ann Neurol 1990;28(1):18-25.

47. Shaw PJ, Forrest V, Ince PG, Richardson JP, Wastell HJ. CSF and plasma amino acid levels in motor neuron disease: elevation of CSF glutamate in a subset of patients. Neurodegeneration 1995;4(2):209-216.

48. Perry TL, Hansen S, Jones K. Brain glutamate deficiency in amyotrophic lateral sclerosis. Neurology 1987;37(12):1845-1848.

49. Tsai GC, Stauch-Slusher B, Sim L, Hedreen JC, Rothstein JD, Kuncl R, Coyle JT. Reductions in acidic amino acids and N-acetylaspartylglutamate in amyotrophic lateral sclerosis CNS. Brain Res 1991;556(1):151-156.

50. Couratier P, Hugon J, Sindou P, Vallat JM, Dumas M. Cell culture evidence for neuronal degeneration in amyotrophic lateral sclerosis being linked to glutamate AMPA/kainate receptors. Lancet 1993;341(8840):265-268.

51. Roisen FJ, Bartfeld H, Donnenfeld H, Baxter J. Neuron specific in vitro cytotoxicity of sera from patients with amyotrophic lateral sclerosis. Muscle Nerve 1982;5(1):48-53.

52. Wolfgram F, Myers L. Amyotrophic lateral sclerosis: effect of serum on anterior horn cells in tissue culture. Science 1973;179(73):579-580.

53. Tikka TM, Vartiainen NE, Goldsteins G, Oja SS, Andersen PM, Marklund SL, Koistinaho J. Minocycline prevents neurotoxicity induced by cerebrospinal fluid from patients with motor neurone disease. Brain 2002;125(Pt 4):722-731.

54. Krieger C, Wagey R, Shaw C. Amyotrophic lateral sclerosis: quantitative autoradiography of [3H]MK-801/NMDA binding sites in spinal cord. Neurosci Lett 1993;159(1-2):191-194.

55. Shaw PJ, Ince PG, Matthews JN, Johnson M, Candy JM. N-methyl-D-aspartate (NMDA) receptors in the spinal cord and motor cortex in motor neuron disease: a quantitative autoradiographic study using [3H]MK-80. Brain Res 1994;637(1-2):297-302.

56. Kawahara Y, Ito K, Sun H, Aizawa H, Kanazawa I, Kwak S. Glutamate receptors: RNA editing and death of motor neurons. Nature 2004;427(6977):801.

57. Shaw PJ, Chinnery RM, Ince PG. Non-NMDA receptors in motor neuron disease (MND): a quantitative autoradiographic study in spinal cord and motor cortex using [3H]CNQX and [3H]kainate. Brain Res 1994;655(1-2):186-194.

58. Takuma H, Kwak S, Yoshizawa T, Kanazawa I. Reduction of GluR2 RNA editing, a molecular change that increases calcium influx through AMPA receptors, selective in the spinal ventral gray of patients with amyotrophic lateral sclerosis. Ann Neurol 1999;46(6):806-815.

59. Aronica E, Catania MV, Geurts J, Yankaya B, Troost D. Immunohistochemical localization of group I and II metabotropic glutamate receptors in control and amyotrophic lateral sclerosis human spinal cord: upregulation in reactive astrocytes. Neuroscience 2001;105(2):509-520.

60. Afifi AK, Aleu FP, Goodgold J, MacKay B. Ultrastructure of atrophic muscle in amyotrophic lateral sclerosis. Neurology 1966;16(5):475-481.

61. Hirano A, Donnenfeld H, Sasaki S, Nakano I. Fine structural observations of neurofilamentous changes in amyotrophic lateral sclerosis. J Neuropathol Exp Neurol 1984;43(5):461-470.

62. Sasaki S, Iwata M. Ultrastructural study of synapses in the anterior horn neurons of patients with amyotrophic lateral sclerosis. Neurosci Lett 1996;204(1-2):53-56.

63. Sasaki S, Iwata M. Ultrastructural change of synapses of Betz cells in patients with amyotrophic lateral sclerosis. Neurosci Lett 1999;268(1):29-32.

64. Wiedemann FR, Manfredi G, Mawrin C, Beal MF, Schon EA. Mitochondrial DNA and respiratory chain function in spinal cords of ALS patients. J Neurochem 2002;80(4):616-625.

65. Carriedo SG, Sensi SL, Yin HZ, Weiss JH. AMPA exposures induce mitochondrial Ca(2+) overload and ROS generation in spinal motor neurons in vitro. J Neurosci 2000;20(1):240-250.

66. Stout AK, Raphael HM, Kanterewicz BI, Klann E, Reynolds IJ. Glutamate-induced neuron death requires mitochondrial calcium uptake. Nat Neurosci 1998;1(5):366-373.

67. Liu D, Wen J, Liu J, Li L. The roles of free radicals in amyotrophic lateral sclerosis: reactive oxygen species and elevated oxidation of protein, DNA, and membrane phospholipids. FASEB J 1999;13(15):2318-2328.

68. Said Ahmed M, Hung WY, Zu JS, Hockberger P, Siddique T. Increased reactive oxygen species in familial amyotrophic lateral sclerosis with mutations in SOD1. J Neurol Sci 2000;176(2):88-94.

69. Blake C, Serpell L. Synchrotron X-ray studies suggest that the core of the transthyretin amyloid fibril is a continuous beta-sheet helix. Structure 1996;4(8):989-998.

70. Eakin CM, Attenello FJ, Morgan CJ, Miranker AD. Oligomeric assembly of native-like precursors precedes amyloid formation by beta-2 microglobulin. Biochemistry 2004;43(24):7808-7815.

71. Knaus KJ, Morillas M, Swietnicki W, Malone M, Surewicz WK, Yee VC. Crystal structure of the human prion protein reveals a mechanism for oligomerization. Nat Struct Biol 2001;8(9):770-774.

72. Sanders A, Jeremy CC, Higgins LD, Giannini S, Conroy MJ, Hounslow AM, Waltho JP, Staniforth RA. Cystatin forms a tetramer through structural rearrangement of domain-swapped dimers prior to amyloidogenesis. J Mol Biol 2004;336(1):165-178.

73. Wiseman RL, Green NS, Kelly JW. Kinetic stabilization of an oligomeric protein under physiological conditions demonstrated by a lack of subunit exchange: implications for transthyretin amyloidosis. Biochemistry 2005;44(25):9265-9274.

74. Khare SD, Caplow M, Dokholyan NV. The rate and equilibrium constants for a multistep reaction sequence for the aggregation of superoxide dismutase in

amyotrophic lateral sclerosis. Proceedings of the National Academy of Sciences of the United States of America 2004;101(42):15094-15099.

75. Johnson SM, Wiseman RL, Sekijima Y, Green NS, mski-Werner SL, Kelly JW. Native state kinetic stabilization as a strategy to ameliorate protein misfolding diseases: a focus on the transthyretin amyloidoses. Acc Chem Res 2005;38(12):911-921.

76. Rao KS, Hegde ML, Anitha S, Musicco M, Zucca FA, Turro NJ, Zecca L. Amyloid beta and neuromelanin--toxic or protective molecules? The cellular context makes the difference. Prog Neurobiol 2006;78(6):364-373.

77. Lue LF, Kuo YM, Roher AE, Brachova L, Shen Y, Sue L, Beach T, Kurth JH, Rydel RE, Rogers J. Soluble amyloid beta peptide concentration as a predictor of synaptic change in Alzheimer's disease. Am J Pathol 1999;155(3):853-862.

78. McLean CA, Cherny RA, Fraser FW, Fuller SJ, Smith MJ, Beyreuther K, Bush AI, Masters CL. Soluble pool of Abeta amyloid as a determinant of severity of neurodegeneration in Alzheimer's disease. Ann Neurol 1999;46(6):860-866.

79. Kayed R, Head E, Thompson JL, McIntire TM, Milton SC, Cotman CW, Glabe CG. Common structure of soluble amyloid oligomers implies common mechanism of pathogenesis. Science 2003;300(5618):486-489.

80. Demuro A, Mina E, Kayed R, Milton SC, Parker I, Glabe CG. Calcium dysregulation and membrane disruption as a ubiquitous neurotoxic mechanism of soluble amyloid oligomers. J Biol Chem 2005;280(17):17294-17300.

81. Kayed R, Sokolov Y, Edmonds B, McIntire TM, Milton SC, Hall JE, Glabe CG. Permeabilization of lipid bilayers is a common conformation-dependent activity of soluble amyloid oligomers in protein misfolding diseases. J Biol Chem 2004;279(45):46363-46366.

82. Baglioni S, Casamenti F, Bucciantini M, Luheshi LM, Taddei N, Chiti F, Dobson CM, Stefani M. Prefibrillar amyloid aggregates could be generic toxins in higher organisms. J Neurosci 2006;26(31):8160-8167.

83. Bukau B, Weissman J, Horwich A. Molecular chaperones and protein quality control. Cell 2006;125(3):443-451.

84. Berke SJ, Paulson HL. Protein aggregation and the ubiquitin proteasome pathway: gaining the UPPer hand on neurodegeneration. Curr Opin Genet Dev 2003;13(3):253-261.

85. Rubinsztein DC. The roles of intracellular protein-degradation pathways in neurodegeneration. Nature 2006;443(7113):780-786.

86. Keller JN, Gee J, Ding Q. The proteasome in brain aging. Ageing Res Rev 2002;1(2):279-293.

87. Lucking CB, Durr A, Bonifati V, Vaughan J, De MG, Gasser T, Harhangi BS, Meco G, Denefle P, Wood NW, Agid Y, Brice A. Association between early-onset Parkinson's disease and mutations in the parkin gene. N Engl J Med 2000;342(21):1560-1567.

88. Neumann M, Sampathu DM, Kwong LK, Truax AC, Micsenyi MC, Chou TT, Bruce J, Schuck T, Grossman M, Clark CM, McCluskey LF, Miller BL, Masliah E, Mackenzie IR, Feldman H, Feiden W, Kretzschmar HA, Trojanowski JQ, Lee VM. Ubiquitinated TDP-43 in frontotemporal lobar degeneration and amyotrophic lateral sclerosis. Science 2006;314(5796):130-133.

89. Buratti E, Baralle FE. Characterization and functional implications of the RNA binding properties of nuclear factor TDP-43, a novel splicing regulator of CFTR exon 92. J Biol Chem 2001;276(39):36337-36343.

90. Gregory RI, Yan KP, Amuthan G, Chendrimada T, Doratotaj B, Cooch N, Shiekhattar R. The Microprocessor complex mediates the genesis of microRNAs. Nature 2004;432(7014):235-240.

91. Van DV, Leverenz JB, Bekris LM, Bird TD, Yuan W, Elman LB, Clay D, Wood EM, Chen-Plotkin AS, Martinez-Lage M, Steinbart E, McCluskey L, Grossman M, Neumann M, Wu IL, Yang WS, Kalb R, Galasko DR, Montine TJ, Trojanowski JQ, Lee VM, Schellenberg GD, Yu CE. TARDBP mutations in amyotrophic lateral sclerosis with TDP-43 neuropathology: a genetic and histopathological analysis. Lancet Neurol 2008;7(5):409-416.

92. Nakashima-Yasuda H, Uryu K, Robinson J, Xie SX, Hurtig H, Duda JE, Arnold SE, Siderowf A, Grossman M, Leverenz JB, Woltjer R, Lopez OL, Hamilton R, Tsuang DW, Galasko D, Masliah E, Kaye J, Clark CM, Montine TJ, Lee VM, Trojanowski JQ. Co-morbidity of TDP-43 proteinopathy in Lewy body related diseases. Acta Neuropathol 2007;114(3):221-229.

93. Amador-Ortiz C, Lin WL, Ahmed Z, Personett D, Davies P, Duara R, Graff-Radford NR, Hutton ML, Dickson DW. TDP-43 immunoreactivity in hippocampal sclerosis and Alzheimer's disease. Ann Neurol 2007;61(5):435-445.

94. Benajiba L, Le BI, Camuzat A, Lacoste M, Thomas-Anterion C, Couratier P, Legallic S, Salachas F, Hannequin D, Decousus M, Lacomblez L, Guedj E, Golfier V, Camu W, Dubois B, Campion D, Meininger V, Brice A. TARDBP mutations in motoneuron disease with frontotemporal lobar degeneration. Ann Neurol 2009;65(4):470-473.

95. Corrado L, Ratti A, Gellera C, Buratti E, Castellotti B, Carlomagno Y, Ticozzi N, Mazzini L, Testa L, Taroni F, Baralle FE, Silani V, D'Alfonso S. High frequency of TARDBP gene mutations in Italian patients with amyotrophic lateral sclerosis. Hum Mutat 2009;30(4):688-694.

96. Gitcho MA, Baloh RH, Chakraverty S, Mayo K, Norton JB, Levitch D, Hatanpaa KJ, White CL, III, Bigio EH, Caselli R, Baker M, Al-Lozi MT, Morris JC, Pestronk A, Rademakers R, Goate AM, Cairns NJ. TDP-43 A315T mutation in familial motor neuron disease. Ann Neurol 2008;63(4):535-538.

97. Kabashi E, Valdmanis PN, Dion P, Spiegelman D, McConkey BJ, Vande VC, Bouchard JP, Lacomblez L, Pochigaeva K, Salachas F, Pradat PF, Camu W, Meininger V, Dupre N, Rouleau GA. TARDBP mutations in individuals with sporadic and familial amyotrophic lateral sclerosis. Nat Genet 2008;40(5):572-574.

98. Kuhnlein P, Sperfeld AD, Vanmassenhove B, Van DV, Lee VM, Trojanowski JQ, Kretzschmar HA, Ludolph AC, Neumann M. Two German kindreds with familial amyotrophic lateral sclerosis due to TARDBP mutations. Arch Neurol 2008;65(9):1185-1189.

99. Lemmens R, Race V, Hersmus N, Matthijs G, Van Den BL, Van DP, Dubois B, Boonen S, Goris A, Robberecht W. TDP-43 M311V mutation in familial amyotrophic lateral sclerosis. J Neurol Neurosurg Psychiatry 2009;80(3):354-355.

100. Rutherford NJ, Zhang YJ, Baker M, Gass JM, Finch NA, Xu YF, Stewart H, Kelley BJ, Kuntz K, Crook RJ, Sreedharan J, Vance C, Sorenson E, Lippa C, Bigio EH, Geschwind DH, Knopman DS, Mitsumoto H, Petersen RC, Cashman NR, Hutton M, Shaw CE, Boylan KB, Boeve B, Graff-Radford NR, Wszolek ZK, Caselli RJ, Dickson DW, Mackenzie IR, Petrucelli L, Rademakers R. Novel mutations in TARDBP (TDP-43) in patients with familial amyotrophic lateral sclerosis. PLoS Genetics 2008;4(9):e1000193.

101. Sreedharan J, Blair IP, Tripathi VB, Hu X, Vance C, Rogelj B, Ackerley S, Durnall JC, Williams KL, Buratti E, Baralle F, de BJ, Mitchell JD, Leigh PN, Al-Chalabi A, Miller CC, Nicholson G, Shaw CE. TDP-43 mutations in familial and sporadic amyotrophic lateral sclerosis. Science 2008;319(5870):1668-1672.

102. Winton MJ, Van DV, Kwong LK, Yuan W, Wood EM, Yu CE, Schellenberg GD, Rademakers R, Caselli R, Karydas A, Trojanowski JQ, Miller BL, Lee VM. A90V TDP-43 variant results in the aberrant localization of TDP-43 in vitro1. FEBS Lett 2008;582(15):2252-2256.

103. Yokoseki A, Shiga A, Tan CF, Tagawa A, Kaneko H, Koyama A, Eguchi H, Tsujino A, Ikeuchi T, Kakita A, Okamoto K, Nishizawa M, Takahashi H, Onodera O. TDP-43 mutation in familial amyotrophic lateral sclerosis. Ann Neurol 2008;63(4):538-542.

104. Banks GT, Kuta A, Isaacs AM, Fisher EM. TDP-43 is a culprit in human neurodegeneration, and not just an innocent bystander. Mamm Genome 2008;19(5):299-305.

105. Mackenzie IR, Bigio EH, Ince PG, Geser F, Neumann M, Cairns NJ, Kwong LK, Forman MS, Ravits J, Stewart H, Eisen A, McClusky L, Kretzschmar HA, Monoranu CM, Highley JR, Kirby J, Siddique T, Shaw PJ, Lee VM, Trojanowski JQ.

Pathological TDP-43 distinguishes sporadic amyotrophic lateral sclerosis from amyotrophic lateral sclerosis with SOD1 mutations. Ann Neurol 2007;61(5):427-434.

106. Maekawa S, Leigh PN, King A, Jones E, Steele JC, Bodi I, Shaw CE, Hortobagyi T, Al-Sarraj S. TDP-43 is consistently co-localized with ubiquitinated inclusions in sporadic and Guam amyotrophic lateral sclerosis but not in familial amyotrophic lateral sclerosis with and without SOD1 mutations. Neuropathology 2009.

107. Tan CF, Eguchi H, Tagawa A, Onodera O, Iwasaki T, Tsujino A, Nishizawa M, Kakita A, Takahashi H. TDP-43 immunoreactivity in neuronal inclusions in familial amyotrophic lateral sclerosis with or without SOD1 gene mutation. Acta Neuropathol 2007;113(5):535-542.

108. Robertson J, Sanelli T, Xiao S, Yang W, Horne P, Hammond R, Pioro EP, Strong MJ. Lack of TDP-43 abnormalities in mutant SOD1 transgenic mice shows disparity with ALS. Neurosci Lett 2007;420(2):128-132.

109. Arnesano F, Banci L, Bertini I, Martinelli M, Furukawa Y, O'Halloran TV. The unusually stable quaternary structure of human Cu,Zn-superoxide dismutase 1 is controlled by both metal occupancy and disulfide status. J Biol Chem 2004;279(46):47998-48003.

110. Cozzolino M, Pesaresi MG, Amori I, Crosio C, Ferri A, Nencini M, Carri MT. Oligomerization of mutant SOD1 in mitochondria of motoneuronal cells drives mitochondrial damage and cell toxicity. Antioxid Redox Signal 2009.

111. Furukawa Y, Fu R, Deng HX, Siddique T, O'Halloran TV. Disulfide cross-linked protein represents a significant fraction of ALS-associated Cu, Zn-superoxide dismutase aggregates in spinal cords of model mice. Proc Natl Acad Sci U S A 2006;103(18):7148-7153.

112. Furukawa Y, Kaneko K, Yamanaka K, O'Halloran TV, Nukina N. Complete loss of post-translational modifications triggers fibrillar aggregation of SOD1 in the familial form of amyotrophic lateral sclerosis. J Biol Chem 2008;283(35):24167-24176.

113. DiDonato M, Craig L, Huff ME, Thayer MM, Cardoso RMF, Kassmann CJ, Lo TP, Bruns CK, Powers ET, Kelly JW, Getzoff ED, Tainer JA. ALS mutants of human superoxide dismutase form fibrous aggregates via framework destabilization. Journal of Molecular Biology 2003;332(3):601-615.

114. Jackson M, Al-Chalabi A, Enayat ZE, Chioza B, Leigh PN, Morrison KE. Copper/zinc superoxide dismutase 1 and sporadic amyotrophic lateral sclerosis: analysis of 155 cases and identification of a novel insertion mutation. Ann Neurol 1997;42(5):803-807.

115. Hosler BA, Nicholson GA, Sapp PC, Chin W, Orrell RW, de Belleroche JS, Esteban J, Hayward LJ, kenna-Yasek D, Yeung L, Cherryson AK, Dench JE, Wilton SD, Laing NG, Horvitz HR, Brown RH, Jr. Three novel mutations and two variants in the

gene for Cu/Zn superoxide dismutase in familial amyotrophic lateral sclerosis. Neuromuscul Disord 1996;6(5):361-366.

116. Andersen PM, Nilsson P, Keranen ML, Forsgren L, Hagglund J, Karlsborg M, Ronnevi LO, Gredal O, Marklund SL. Phenotypic heterogeneity in motor neuron disease patients with CuZn-superoxide dismutase mutations in Scandinavia. Brain 1997;120 ( Pt 10):1723-1737.

117. Khare SD, Caplow M, Dokholyan NV. FALS mutations in Cu, Zn superoxide dismutase destabilize the dimer and increase dimer dissociation propensity: a large-scale thermodynamic analysis. Amyloid 2006;13(4):226-235.

118. Sato T, Nakanishi T, Yamamoto Y, Andersen PM, Ogawa Y, Fukada K, Zhou Z, Aoike F, Sugai F, Nagano S, Hirata S, Ogawa M, Nakano R, Ohi T, Kato T, Nakagawa M, Hamasaki T, Shimizu A, Sakoda S. Rapid disease progression correlates with instability of mutant SOD1 in familial ALS. Neurology 2005;65(12):1954-1957.

119. Nagai M, Re DB, Nagata T, Chalazonitis A, Jessell TM, Wichterle H, Przedborski S. Astrocytes expressing ALS-linked mutated SOD1 release factors selectively toxic to motor neurons. Nat Neurosci 2007;10(5):615-622.

120. Boillee S, Yamanaka K, Lobsiger CS, Copeland NG, Jenkins NA, Kassiotis G, Kollias G, Cleveland DW. Onset and progression in inherited ALS determined by motor neurons and microglia. Science 2006;312(5778):1389-1392.

121. Clement AM, Nguyen MD, Roberts EA, Garcia ML, Boillee S, Rule M, McMahon AP, Doucette W, Siwek D, Ferrante RJ, Brown RH, Jr., Julien JP, Goldstein LS, Cleveland DW. Wild-type nonneuronal cells extend survival of SOD1 mutant motor neurons in ALS mice. Science 2003;302(5642):113-117.

122. Bruijn LI, Houseweart MK, Kato S, Anderson KL, Anderson SD, Ohama E, Reaume AG, Scott RW, Cleveland DW. Aggregation and motor neuron toxicity of an ALS-linked SOD1 mutant independent from wild-type SOD1. Science 1998;281(5384):1851-1854.

123. Howland DS, Liu J, She Y, Goad B, Maragakis NJ, Kim B, Erickson J, Kulik J, DeVito L, Psaltis G, DeGennaro LJ, Cleveland DW, Rothstein JD. Focal loss of the glutamate transporter EAAT2 in a transgenic rat model of SOD1 mutant-mediated amyotrophic lateral sclerosis (ALS). Proceedings of the National Academy of Sciences of the United States of America 2002;99(3):1604-1609.

124. Rothstein JD, Van Kammen M, Levey AI, Martin LJ, Kuncl RW. Selective loss of glial glutamate transporter GLT-1 in amyotrophic lateral sclerosis. Ann Neurol 1995;38(1):73-84.

125. Aggarwal A, Nicholson G. Detection of preclinical motor neurone loss in SOD1 mutation carriers using motor unit number estimation. J Neurol Neurosurg Psychiatry 2002;73(2):199-201.

126. Kong J, Xu Z. Massive mitochondrial degeneration in motor neurons triggers the onset of amyotrophic lateral sclerosis in mice expressing a mutant SOD1. J Neurosci 1998;18(9):3241-3250.

127. Bendotti C, Calvaresi N, Chiveri L, Prelle A, Moggio M, Braga M, Silani V, De Biasi S. Early vacuolization and mitochondrial damage in motor neurons of FALS mice are not associated with apoptosis or with changes in cytochrome oxidase histochemical reactivity. J Neurol Sci 2001;191(1-2):25-33.

128. Jaarsma D, Rognoni F, van Duijn W, Verspaget HW, Haasdijk ED, Holstege JC. CuZn superoxide dismutase (SOD1) accumulates in vacuolated mitochondria in transgenic mice expressing amyotrophic lateral sclerosis-linked SOD1 mutations. Acta Neuropathol 2001;102(4):293-305.

129. Higgins CM, Jung C, Xu Z. ALS-associated mutant SOD1G93A causes mitochondrial vacuolation by expansion of the intermembrane space and by involvement of SOD1 aggregation and peroxisomes. BMC Neurosci 2003;4:16.

130. Xu Z, Jung C, Higgins C, Levine J, Kong J. Mitochondrial degeneration in amyotrophic lateral sclerosis. J Bioenerg Biomembr 2004;36(4):395-399.

131. Okado-Matsumoto A, Fridovich I. Amyotrophic lateral sclerosis: a proposed mechanism. Proceedings of the National Academy of Sciences of the United States of America 2002;99(13):9010-9014.

132. Liu J, Lillo C, Jonsson PA, Vande Velde C, Ward CM, Miller TM, Subramaniam JR, Rothstein JD, Marklund S, Andersen PM, Brannstrom T, Gredal O, Wong PC, Williams DS, Cleveland DW. Toxicity of familial ALS-linked SOD1 mutants from selective recruitment to spinal mitochondria. Neuron 2004;43(1):5-17.

133. Chou SM, Wang HS, Komai K. Colocalization of NOS and SOD1 in neurofilament accumulation within motor neurons of amyotrophic lateral sclerosis: an immunohistochemical study. J Chem Neuroanat 1996;10(3-4):249-258.

134. Chou SM, Wang HS, Taniguchi A. Role of SOD-1 and nitric oxide/cyclic GMP cascade on neurofilament aggregation in ALS/MND. J Neurol Sci 1996;139 Suppl:16-26.

135. Shibata N, Asayama K, Hirano A, Kobayashi M. Immunohistochemical study on superoxide dismutases in spinal cords from autopsied patients with amyotrophic lateral sclerosis. Dev Neurosci 1996;18(5-6):492-498.

136. Shibata N, Hirano A, Kobayashi M, Sasaki S, Kato T, Matsumoto S, Shiozawa Z, Komori T, Ikemoto A, Umahara T, et al. Cu/Zn superoxide dismutase-like

immunoreactivity in Lewy body-like inclusions of sporadic amyotrophic lateral sclerosis. Neurosci Lett 1994;179(1-2):149-152.

137. Shibata N, Hirano A, Kobayashi M, Siddique T, Deng HX, Hung WY, Kato T, Asayama K. Intense superoxide dismutase-1 immunoreactivity in intracytoplasmic hyaline inclusions of familial amyotrophic lateral sclerosis with posterior column involvement. J Neuropathol Exp Neurol 1996;55(4):481-490.

138. Bruijn LI, Houseweart MK, Kato S, Anderson KL, Anderson SD, Ohama E, Reaume AG, Scott RW, Cleveland DW. Aggregation and motor neuron toxicity of an ALS-linked SOD1 mutant independent from wild-type SOD1. Science 1998;281(5384):1851-1854.

139. Chung J, Yang H, de Beus MD, Ryu CY, Cho K, Colon W. Cu/Zn superoxide dismutase can form pore-like structures. Biochem Biophys Res Commun 2003;312(4):873-876.

140. Ray SS, Nowak RJ, Strokovich K, Brown RH, Jr., Walz T, Lansbury PT, Jr. An intersubunit disulfide bond prevents in vitro aggregation of a superoxide dismutase-1 mutant linked to familial amytrophic lateral sclerosis. Biochemistry 2004;43(17):4899-4905.

141. Lashuel HA, Hartley D, Petre BM, Walz T, Lansbury PT, Jr. Neurodegenerative disease: amyloid pores from pathogenic mutations. Nature 2002;418(6895):291.

142. Lashuel HA, Petre BM, Wall J, Simon M, Nowak RJ, Walz T, Lansbury PT, Jr. Alpha-synuclein, especially the Parkinson's disease-associated mutants, forms pore-like annular and tubular protofibrils. J Mol Biol 2002;322(5):1089-1102.

143. Khare SD, Caplow M, Dokholyan NV. The rate and equilibrium constants for a multistep reaction sequence for the aggregation of superoxide dismutase in amyotrophic lateral sclerosis2. ProcNatlAcadSciUSA 2004;101(42):15094-15099.

144. Rakhit R, Crow JP, Lepock JR, Kondejewski LH, Cashman NR, Chakrabartty A. Monomeric Cu,Zn-superoxide dismutase is a common misfolding intermediate in the oxidation models of sporadic and familial amyotrophic lateral sclerosis. J Biol Chem 2004;279(15):15499-15504.

145. Lindberg MJ, Normark J, Holmgren A, Oliveberg M. Folding of human superoxide dismutase: disulfide reduction prevents dimerization and produces marginally stable monomers. Proceedings of the National Academy of Sciences of the United States of America 2004;101(45):15893-15898.

146. Ray SS, Lansbury PT, Jr. A possible therapeutic target for Lou Gehrig's disease. Proceedings of the National Academy of Sciences of the United States of America 2004;101(16):5701-5702.

147. Ray SS, Nowak RJ, Brown RH, Jr., Lansbury PT, Jr. Small-molecule-mediated stabilization of familial amyotrophic lateral sclerosis-linked superoxide dismutase mutants against unfolding and aggregation. Proceedings of the National Academy of Sciences of the United States of America 2005;102(10):3639-3644.

148. Banci L, Bertini I, Durazo A, Girotto S, Gralla EB, Martinelli M, Valentine JS, Vieru M, Whitelegge JP. Metal-free superoxide dismutase forms soluble oligomers under physiological conditions: a possible general mechanism for familial ALS. Proceedings of the National Academy of Sciences of the United States of America 2007;104(27):11263-11267.

149. Banci L, Bertini I, Boca M, Girotto S, Martinelli M, Valentine JS, Vieru M. SOD1 and amyotrophic lateral sclerosis: mutations and oligomerization. PLoS One 2008;3(2):e1677.

150. Khare SD, Dokholyan NV. Common dynamical signatures of familial amyotrophic lateral sclerosis-associated structurally diverse Cu, Zn superoxide dismutase mutants. Proceedings of the National Academy of Sciences of the United States of America 2006;103(9):3147-3152.

151. Strange RW, Yong CW, Smith W, Hasnain SS. Molecular dynamics using atomic-resolution structure reveal structural fluctuations that may lead to polymerization of human Cu-Zn superoxide dismutase. Proceedings of the National Academy of Sciences of the United States of America 2007;104(24):10040-10044.

152. Falconi M, Stroppolo ME, Cioni P, Strambini G, Sergi A, Ferrario M, Desideri A. Dynamics-function correlation in Cu, Zn superoxide dismutase: a spectroscopic and molecular dynamics simulation study. Biophys J 2001;80(6):2556-2567.

153. Shen J, Subramaniam S, Wong CF, McCammon JA. Superoxide dismutase: fluctuations in the structure and solvation of the active site channel studied by molecular dynamics simulation. Biopolymers 1989;28(12):2085-2096.

154. Wade RC, Gabdoulline RR, Ludemann SK, Lounnas V. Electrostatic steering and ionic tethering in enzyme-ligand binding: insights from simulations. Proceedings of the National Academy of Sciences of the United States of America 1998;95(11):5942-5949.

155. Ding F, Dokholyan NV. Dynamical roles of metal ions and the disulfide bond in Cu,Zn superoxide dismutase folding and aggregation. Proceedings of the National Academy of Sciences of the United States of America 2008;105:19696-19701.

156. Khare SD, Wilcox KC, Gong P, Dokholyan NV. Sequence and structural determinants of Cu, Zn superoxide dismutase aggregation. Proteins 2005;61(3):617-632.

157. Dobson CM. Protein folding and misfolding. Nature 2003;426(6968):884-890.

158. Dobson CM. In the footsteps of alchemists. Science 2004;304(5675):1259-+.

159. Cleveland DW, Rothstein JD. From Charcot to Lou Gehrig: Deciphering selective motor neuron death in ALS. Nature Reviews Neuroscience 2001;2(11):806-819.

160. Reches M, Porat Y, Gazit E. Amyloid fibril formation by pentapeptide and tetrapeptide fragments of human calcitonin. J Biol Chem 2002;277(38):35475-35480.

161. Tenidis K, Waldner M, Bernhagen J, Fischle W, Bergmann M, Weber M, Merkle ML, Voelter W, Brunner H, Kapurniotu A. Identification of a penta- and hexapeptide of islet amyloid polypeptide (IAPP) with amyloidogenic and cytotoxic properties. Journal of Molecular Biology 2000;295(4):1055-1071.

162. Thirumalai D, Klimov DK, Dima RI. Emerging ideas on the molecular basis of protein and peptide aggregation. Current Opinion in Structural Biology 2003;13(2):146-159.

163. Villegas V, Zurdo J, Filimonov VV, Aviles FX, Dobson CM, Serrano L. Protein engineering as a strategy to avoid formation of amyloid fibrils. Protein Sci 2000;9(9):1700-1708.

164. Ventura S, Zurdo J, Narayanan S, Parreno M, Mangues R, Reif B, Chiti F, Giannoni E, Dobson CM, Aviles FX, Serrano L. Short amino acid stretches can mediate amyloid formation in globular proteins: The Src homology 3 (SH3) case. Proceedings of the National Academy of Sciences of the United States of America 2004;101(19):7258-7263.

165. Ivanova MI, Sawaya MR, Gingery M, Attinger A, Eisenberg D. An amyloid-forming segment of beta 2-microglobulin suggests a molecular model for the fibril. Proceedings of the National Academy of Sciences of the United States of America 2004;101(29):10584-10589.

166. Tycko R. Progress towards a molecular-level structural understanding of amyloid fibrils. Current Opinion in Structural Biology 2004;14(1):96-103.

167. Benzinger TLS, Gregory DM, Burkoth TS, Miller-Auer H, Lynn DG, Botto RE, Meredith SC. Propagating structure of Alzheimer's beta-amyloid((10-35)) is parallel beta-sheet with residues in exact register. Proceedings of the National Academy of Sciences of the United States of America 1998;95(23):13407-13412.

168. Makin OS, Atkins E, Sikorski P, Johansson J, Serpell LC. Molecular basis for amyloid fibril formation and stability. Proceedings of the National Academy of Sciences of the United States of America 2005;102(2):315-320.

169. Gordon DJ, Balbach JJ, Tycko R, Meredith SC. Increasing the amphiphilicity of an amyloidogenic peptide changes the beta-sheet structure in the fibrils from antiparallel to parallel. Biophys J 2004;86(1):428-434.

170. de la Paz ML, Serrano L. Sequence determinants of amyloid fibril formation. Proceedings of the National Academy of Sciences of the United States of America 2004;101(1):87-92.

171. Rochet JC, Lansbury PT. Amyloid fibrillogenesis: themes and variations. Current Opinion in Structural Biology 2000;10(1):60-68.

172. Richardson JS, Richardson DC. Natural beta-sheet proteins use negative design to avoid edge-to-edge aggregation. Proceedings of the National Academy of Sciences of the United States of America 2002;99(5):2754-2759.

173. Tainer JA, Getzoff ED, Beem KM, Richardson JS, Richardson DC. Determination and Analysis of the 2A Structure of Copper, Zinc Superoxide-Dismutase. Journal of Molecular Biology 1982;160(2):181-217.

174. Rodriguez JA, Valentine OS, Eggers DK, Roe JA, Tiwari A, Brown RH, Hayward LJ. Familial amyotrophic lateral sclerosis-associated mutations decrease the thermal stability of distinctly metallated species of human copper/zinc superoxide dismutase. J Biol Chem 2002;277(18):15932-15937.

175. Lindberg MJ, Tibell L, Oliveberg M. Common denominator of Cu/Zn superoxide dismutase mutants associated with amyotrophic lateral sclerosis: Decreased stability of the apo state. Proceedings of the National Academy of Sciences of the United States of America 2002:262527099.

176. Johnston JA, Dalton MJ, Gurney ME, Kopito RR. Formation of high molecular weight complexes of mutant Cu,Zn-superoxide dismutase in a mouse model for familial amyotrophic lateral sclerosis. Proceedings of the National Academy of Sciences of the United States of America 2000;97(23):12571-12576.

177. Khare SD, Caplow M, Dokholyan NV. Determination of the rate and equilibrium constants for a multi-step reaction for aggregation of superoxide dismutase in ALS. PNAS 2004;101:15094-15099.

178. Bennett MJ, Choe S, Eisenberg D. Domain Swapping - Entangling Alliances Between Proteins. Proceedings of the National Academy of Sciences of the United States of America 1994;91(8):3127-3131.

179. Schlunegger MP, Bennett MJ, Eisenberg D. Oligomer formation by 3D domain swapping: A model for protein assembly and misassembly. Advances in Protein Chemistry, Vol 50 1997;50:61-122.

180. Liu YS, Gotte G, Libonati M, Eisenberg D. A domain-swapped RNase A dimer with implications for amyloid formation. Nature Structural Biology 2001;8(3):211-214.

181. Rousseau F, Schymkowitz JWH, Itzhaki LS. The unfolding story of three-dimensional domain swapping. Structure 2003;11(3):243-251.

182. Liu Y, Eisenberg D. 3D domain swapping: As domains continue to swap. Protein Sci 2002;11(6):1285-1299.

183. Ding F, Dokholyan NV, Buldyrev SV, Stanley HE, Shakhnovich EI. Molecular dynamic simulations of the SH3 domain aggregation suggests a generic amyloidogenesis mechanism. Journal of Molecular Biology 2002;324:851-857.

184. Yang SC, Cheung MS, Onuchic JN, Levine H. Molecular dynamics simulations on domain swapping. Biophys J 2004;86(1):267A-268A.

185. Yang SC, Cho SS, Levy Y, Cheung MS, Levine H, Wolynes PG, Onuchic JN. Domain swapping is a consequence of minimal frustration. Proceedings of the National Academy of Sciences of the United States of America 2004;101(38):13786-13791.

186. Rousseau F, Schymkowitz JWH, Wilkinson HR, Itzhaki LS. Three-dimensional domain swapping in p13suc1 occurs in the unfolded state and is controlled by conserved proline residues. Proceedings of the National Academy of Sciences of the United States of America 2001;98(10):5596-5601.

187. Liu YS, Hart PJ, Schlunegger MP, Eisenberg D. The crystal structure of a 3D domain-swapped dimer of RNase A at a 2.1-angstrom resolution. Proceedings of the National Academy of Sciences of the United States of America 1998;95(7):3437-3442.

188. Liu YS, Gotte G, Libonati M, Eisenberg D. Structures of the two 3D domain-swapped RNase A trimers. Protein Sci 2002;11(2):371-380.

189. Janowski R, Kozak M, Jankowska E, Grzonka Z, Grubb A, Abrahamson M, Jaskolski M. Human cystatin C, an amyloidogenic protein, dimerizes through three-dimensional domain swapping. Nature Structural Biology 2001;8(4):316-320.

190. Go N, Abe H. Noninteracting local-structure model of folding and unfolding transition in globular proteins. I. Formulation. Biopolymers 1981;20:991-1011.

191. Abe H, Go N. Noninteracting local-structure model of folding and unfolding transition in globular proteins. II. Application to two-dimensional lattice proteins. Biopolymers 1981;20:1013-1031.

192. Kishan KVR, Scita G, Wong WT, DiFiore PP, Newcomer ME. The SH3 domain of Eps8 exists as a novel intertwined dimer. Nature Structural Biology 1997;4(9):739-743.

193. Sunde M, Serpell LC, Bartlam M, Fraser PE, Pepys MB, Blake CCF. Common core structure of amyloid fibrils by synchrotron X-ray diffraction. Journal of Molecular Biology 1997;273(3):729-739.

194. Hermans J, Berendsen HJC, Vangunsteren WF, Postma JPM. A Consistent Empirical Potential for Water-Protein Interactions. Biopolymers 1984;23(8):1513-1518.

195. Vorobjev YN, Almagro JC, Hermans J. Discrimination between native and intentionally misfolded conformations of proteins: ES/IS, a new method for calculating conformational free energy that uses both dynamics simulations with an explicit solvent and an implicit solvent continuum model. Proteins-Structure Function and Genetics 1998;32(4):399-413.

196. Urbanc B, Cruz L, Ding F, Sammond D, Khare S, Buldyrev S, Stanley HE, Dokholyan NV. Molecular dynamics simulations of Amyloid beta dimer formation. Biophys J 2004.

197. Vorobjev YN, Hermans J. Free energies of protein decoys provide insight into determinants of protein stability. Protein Sci 2001;10(12):2498-2506.

198. Khare SD, Ding F, Dokholyan NV. Folding of Cu, Zn superoxide dismutase and familial amyotrophic lateral sclerosis. Journal of Molecular Biology 2003;334(3):515-525.

199. Rubinstein M, Colby RH. Polymer Physics. New York: Oxford University Press; 2003. 12-14 p.

200. Fernandez-Escamilla AM, Rousseau F, Schymkowitz J, Serrano L. Prediction of sequence-dependent and mutational effects on the aggregation of peptides and proteins. Nature Biotechnology 2004;22(10):1302-1306.

201. Dokholyan NV, Li L, Ding F, Shakhnovich EI. Topological determinants of protein folding. Proceedings of the National Academy of Sciences of the United States of America 2002;99(13):8637-8641.

202. Dokholyan NV, Borreguero JM, Buldyrev SV, Ding F, Stanley HE, Shakhnovich EI. Identifying importance of amino acids for protein folding from crystal structures. Macromolecular Crystallography, Pt D 2003;374:616-+.

203. Pande VS, Grosberg AY, Tanaka T. Heteropolymer freezing and design: Towards physical models of protein folding. Reviews of Modern Physics 2000;72(1):259-314.

204. Bryngelson JD, Onuchic JN, Socci ND, Wolynes PG. Funnels, Pathways, and the Energy Landscape of Protein-Folding - A Synthesis. Proteins-Structure Function and Genetics 1995;21(3):167-195.

205. Shea JE, Onuchic JN, Brooks CL. Molecular dynamics study of the mechanism and thermodynamics of folding of the src-SH3 protein. Abstracts of Papers of the American Chemical Society 2001;221:U406-U407.

206. Plotkin SS, Onuchic JN. Understanding protein folding with energy landscape theory - Part I: Basic concepts. Quarterly Reviews of Biophysics 2002;35(2):111-167.

207. Dokholyan NV, Buldyrev SV, Stanley HE, Shakhnovich EI. Discrete molecular dynamics studies of the folding of a protein-like model. Folding & Design 1998;3(6):577-587.

208. Ding F, Borreguero JM, Buldyrey SV, Stanley HE, Dokholyan NV. Mechanism for the alpha-helix to beta-hairpin transition. Proteins-Structure Function and Genetics 2003;53(2):220-228.

209. Mei G, Rosato N, Silva N, Rusch R, Gratton E, Savini I, FinazziAgro A. Denaturation of Human Cu/Zn Superoxide-Dismutase by Guanidine-Hydrochloride - A Dynamic Fluorescence Study. Biochemistry 1992;31(32):7224-7230.

210. Hwang W, Zhang SG, Kamm RD, Karplus M. Kinetic control of dimer structure formation in amyloid fibrillogenesis. Proceedings of the National Academy of Sciences of the United States of America 2004;101(35):12916-12921.

211. Tcherkasskaya O, Sanders W, Chynwat V, Davidson EA, Orser CS. The role of hydrophobic interactions in amyloidogenesis: Example of prion-related polypeptides. Journal of Biomolecular Structure & Dynamics 2003;21(3):353-365.

212. Tycko R, Petkova A, Oyler N, Chan CC, Balbach J. Probing the molecular structure of amyloid fibrils with solid state NMR. Biophys J 2002;82(1):187A-187A.

213. Urbanc B, Cruz L, Ding F, Sammond D, Khare S, Buldyrev SV, Stanley HE, Dokholyan NV. Molecular dynamics simulation of amyloid beta dimer formation. Biophys J 2004;87(4):2310-2321.

214. Doyle R, Simons K, Qian H, Baker D. Local interactions and the optimization of protein folding. Proteins-Structure Function and Genetics 1997;29(3):282-291.

215. Simons KT, Ruczinski I, Kooperberg C, Fox BA, Bystroff C, Baker D. Improved recognition of native-like protein structures using a combination of sequence-dependent and sequence-independent features of proteins. Proteins-Structure Function and Genetics 1999;34(1):82-95.

216. Bystroff C, Baker D. Prediction of local structure in proteins using a library of sequence-structure motifs. Journal of Molecular Biology 1998;281(3):565-577.

217. Chiti F, Stefani M, Taddei N, Ramponi G, Dobson CM. Rationalization of the effects of mutations on peptide and protein aggregation rates. Nature 2003;424(6950):805-808.

218. Gazit E. A possible role for pi-stacking in the self-assembly of amyloid fibrils. Faseb Journal 2002;16(1):77-83.

219. Chiti F, Calamai M, Taddei N, Stefani M, Ramponi G, Dobson CM. Studies of the aggregation of mutant proteins in vitro provide insights into the genetics of amyloid

diseases. Proceedings of the National Academy of Sciences of the United States of America 2002;99(90004):16419-16426.

220. Linding R, Schymkowitz J, Rousseau F, Diella F, Serrano L. A comparative study of the relationship between protein structure and beta-aggregation in globular and intrinsically disordered proteins. Journal of Molecular Biology 2004;342(1):345-353.

221. Ding F, Dokholyan NV, Buldyrev SV, Stanley HE, Shakhnovich EI. Molecular dynamics simulation of the SH3 domain aggregation suggests a generic amyloidogenesis mechanism. Journal of Molecular Biology 2002;324(4):851-857.

222. Stathopulos PB, Rumfeldt JAO, Scholz GA, Irani RA, Frey HE, Hallewell RA, Lepock JR, Meiering EM. Cu/Zn superoxide dismutase mutants associated with amyotrophic lateral sclerosis show enhanced formation of aggregates in vitro. Proceedings of the National Academy of Sciences of the United States of America 2003;100(12):7021.

223. Reaume AG, Elliott JL, Hoffman EK, Kowall NW, Ferrante RJ, Siwek DF, Wilcox HM, Flood DG, Beal MF, Brown RH, Jr., Scott RW, Snider WD. Motor neurons in Cu/Zn superoxide dismutase-deficient mice develop normally but exhibit enhanced cell death after axonal injury. Nat Genet 1996;13(1):43-47.

224. Juarez JC, Manuia M, Burnett ME, Betancourt O, Boivin B, Shaw DE, Tonks NK, Mazar AP, Donate F. Superoxide dismutase 1 (SOD1) is essential for H2O2-mediated oxidation and inactivation of phosphatases in growth factor signaling1. Proceedings of the National Academy of Sciences of the United States of America 2008.

225. Harraz MM, Marden JJ, Zhou W, Zhang Y, Williams A, Sharov VS, Nelson K, Luo M, Paulson H, Schoneich C, Engelhardt JF. SOD1 mutations disrupt redox-sensitive Rac regulation of NADPH oxidase in a familial ALS model. J Clin Invest 2008;118(2):659-670.

226. Richardson J, Thomas KA, Rubin BH, Richardson DC. Crystal structure of bovine Cu,Zn superoxide dismutase at 3 A resolution: chain tracing and metal ligands. Proceedings of the National Academy of Sciences of the United States of America 1975;72(4):1349-1353.

227. McCord JM, Fridovich I. Superoxide dismutase. An enzymic function for erythrocuprein (hemocuprein). J Biol Chem 1969;244(22):6049-6055.

228. Goscin SA, Fridovich I. The purification and properties of superoxide dismutase from Saccharomyces cerevisiae. Biochim Biophys Acta 1972;289(2):276-283.

229. Borchers CH, Thapar R, Petrotchenko EV, Torres MP, Speir JP, Easterling M, Dominski Z, Marzluff WF. Combined top-down and bottom-up proteomics identifies a phosphorylation site in stem-loop-binding proteins that contributes to high-affinity RNA binding. Proceedings of the National Academy of Sciences of the United States of America 2006;103(9):3094-3099.

230. Pflieger D, Junger MA, Muller M, Rinner O, Lee H, Gehrig PM, Gstaiger M, Aebersold R. Quantitative proteomic analysis of protein complexes: concurrent identification of interactors and their state of phosphorylation. Mol Cell Proteomics 2008;7(2):326-346.

231. Heikkila RE, Cabbat F. A sensitive assay for superoxide dismutase based on the autoxidation of 6-hydroxydopamine. Anal Biochem 1976;75(2):356-362.

232. Kurobe N, Suzuki F, Okajima K, Kato K. Sensitive enzyme immunoassay for human Cu/Zn superoxide dismutase. Clin Chim Acta 1990;187(1):11-20.

233. Fujiwara N, Nakano M, Kato S, Yoshihara D, Ookawara T, Eguchi H, Taniguchi N, Suzuki K. Oxidative modification to cysteine sulfonic acid of Cys111 in human copper-zinc superoxide dismutase. J Biol Chem 2007;282(49):35933-35944.

234. Rakhit R, Cunningham P, Furtos-Matei A, Dahan S, Qi XF, Crow JP, Cashman NR, Kondejewski LH, Chakrabartty A. Oxidation-induced misfolding and agagaregation of superoxide dismutase and its implications for amyotrophic lateral sclerosis. J Biol Chem 2002;277(49):47551-47556.

235. Baker JM, Hudson RP, Kanelis V, Choy WY, Thibodeau PH, Thomas PJ, Forman-Kay JD. CFTR regulatory region interacts with NBD1 predominantly via multiple transient helices. Nat Struct Mol Biol 2007;14(8):738-745.

236. Doucette PA, Whitson LJ, Cao X, Schirf V, Demeler B, Valentine JS, Hansen JC, Hart PJ. Dissociation of human copper-zinc superoxide dismutase dimers using chaotrope and reductant. Insights into the molecular basis for dimer stability. J Biol Chem 2004;279(52):54558-54566.

237. Ferraroni M, Rypniewski W, Wilson KS, Viezzoli MS, Banci L, Bertini I, Mangani S. The crystal structure of the monomeric human SOD mutant F50E/G51E/E133Q at atomic resolution. The enzyme mechanism revisited. J Mol Biol 1999;288(3):413-426.

238. Nakanishi T, Kishikawa M, Miyazaki A, Shimizu A, Ogawa Y, Sakoda S, Ohi T, Shoji H. Simple and defined method to detect the SOD-1 mutants from patients with familial amyotrophic lateral sclerosis by mass spectrometry. J Neurosci Methods 1998;81(1-2):41-44.

239. Marklund SL, Andersen PM, Forsgren L, Nilsson P, Ohlsson PI, Wikander G, Oberg A. Normal binding and reactivity of copper in mutant superoxide dismutase isolated from amyotrophic lateral sclerosis patients. J Neurochem 1997;69(2):675-681.

240. Furukawa Y, O'Halloran TV. Amyotrophic lateral sclerosis mutations have the greatest destabilizing effect on the apo- and reduced form of SOD1, leading to unfolding and oxidative aggregation. J Biol Chem 2005;280(17):17266-17274.

241. Hu JH, Zhang H, Wagey R, Krieger C, Pelech SL. Protein kinase and protein phosphatase expression in amyotrophic lateral sclerosis spinal cord. J Neurochem 2003;85(2):432-442.

242. Maher P. Redox control of neural function: background, mechanisms, and significance. Antioxid Redox Signal 2006;8(11-12):1941-1970.

243. Leier I, Jedlitschky G, Buchholz U, Center M, Cole SP, Deeley RG, Keppler D. ATP-dependent glutathione disulphide transport mediated by the MRP gene-encoded conjugate export pump. Biochem J 1996;314 ( Pt 2):433-437.

244. Schafer FQ, Buettner GR. Redox environment of the cell as viewed through the redox state of the glutathione disulfide/glutathione couple. Free Radic Biol Med 2001;30(11):1191-1212.

245. Ghezzi P. Regulation of protein function by glutathionylation. Free Radic Res 2005;39(6):573-580.

246. Adachi T, Pimentel DR, Heibeck T, Hou X, Lee YJ, Jiang B, Ido Y, Cohen RA. S-glutathiolation of Ras mediates redox-sensitive signaling by angiotensin II in vascular smooth muscle cells. J Biol Chem 2004;279(28):29857-29862.

247. Cross JV, Templeton DJ. Oxidative stress inhibits MEKK1 by site-specific glutathionylation in the ATP-binding domain. Biochem J 2004;381(Pt 3):675-683.

248. Klatt P, Molina EP, De Lacoba MG, Padilla CA, Martinez-Galesteo E, Barcena JA, Lamas S. Redox regulation of c-Jun DNA binding by reversible S-glutathiolation. FASEB J 1999;13(12):1481-1490.

249. Wang J, Boja ES, Tan W, Tekle E, Fales HM, English S, Mieyal JJ, Chock PB. Reversible glutathionylation regulates actin polymerization in A431 cells. J Biol Chem 2001;276(51):47763-47766.

250. Wilcox KC, Zhou L, Jordon JK, Huang Y, Yu Y, Redler RL, Chen X, Caplow M, Dokholyan NV. Modifications of superoxide dismutase (SOD1) in human erythrocytes: a possible role in amyotrophic lateral sclerosis. J Biol Chem 2009;284(20):13940-13947.

251. Rosen DR, Siddique T, Patterson D, Figlewicz DA, Sapp P, Hentati A, Donaldson D, Goto J, O'Regan JP, Deng HX, et al. Mutations in Cu/Zn superoxide dismutase gene are associated with familial amyotrophic lateral sclerosis. Nature 1993;362(6415):59-62.

252. Lawyer T, Jr., Netsky MG. Amyotrophic lateral sclerosis. AMA Arch Neurol Psychiatry 1953;69(2):171-192.

253. Hughes JT. Pathology of amyotrophic lateral sclerosis. Adv Neurol 1982;36:61-74.

254. Caughey B, Lansbury PT. Protofibrils, pores, fibrils, and neurodegeneration: separating the responsible protein aggregates from the innocent bystanders. Annu Rev Neurosci 2003;26:267-298.

255. Glabe CG. Common mechanisms of amyloid oligomer pathogenesis in degenerative disease. Neurobiol Aging 2006;27(4):570-575.

256. Haataja L, Gurlo T, Huang CJ, Butler PC. Islet amyloid in type 2 diabetes, and the toxic oligomer hypothesis. Endocr Rev 2008;29(3):303-316.

257. Glabe CG, Kayed R. Common structure and toxic function of amyloid oligomers implies a common mechanism of pathogenesis. Neurology 2006;66(2 Suppl 1):S74-78.

258. Necula M, Kayed R, Milton S, Glabe CG. Small molecule inhibitors of aggregation indicate that amyloid beta oligomerization and fibrillization pathways are independent and distinct. J Biol Chem 2007;282(14):10311-10324.

259. Juneja T, Pericak-Vance MA, Laing NG, Dave S, Siddique T. Prognosis in familial amyotrophic lateral sclerosis: progression and survival in patients with glu100gly and ala4val mutations in Cu,Zn superoxide dismutase. Neurology 1997;48(1):55-57.

260. Wang J, Farr GW, Zeiss CJ, Rodriguez-Gil DJ, Wilson JH, Furtak K, Rutkowski DT, Kaufman RJ, Ruse CI, Yates JR, 3rd, Perrin S, Feany MB, Horwich AL. Progressive aggregation despite chaperone associations of a mutant SOD1-YFP in transgenic mice that develop ALS. Proceedings of the National Academy of Sciences of the United States of America 2009;106(5):1392-1397.

261. Abernethy JL, Steinman HM, Hill RL. Bovine erythrocyte superoxide dismutase. Subunit structure and sequence location of the intrasubunit disulfide bond. J Biol Chem 1974;249(22):7339-7347.

262. Hartz JW, Deutsch HF. Subunit structure of human superoxide dismutase. J Biol Chem 1972;247(21):7043-7050.

263. Anfinsen CB, Haber E, Sela M, White FH, Jr. The kinetics of formation of native ribonuclease during oxidation of the reduced polypeptide chain. Proceedings of the National Academy of Sciences of the United States of America 1961;47:1309-1314.

264. Liu Y, Eisenberg D. 3D domain swapping: as domains continue to swap. Protein Sci 2002;11(6):1285-1299.

265. Schymkowitz JW, Rousseau F, Wilkinson HR, Friedler A, Itzhaki LS. Observation of signal transduction in three-dimensional domain swapping. Nat Struct Biol 2001;8(10):888-892.

266. Bucciantini M, Giannoni E, Chiti F, Baroni F, Formigli L, Zurdo J, Taddei N, Ramponi G, Dobson CM, Stefani M. Inherent toxicity of aggregates implies a

common mechanism for protein misfolding diseases. Nature 2002;416(6880):507-511.

267. Hill SE, Robinson J, Matthews G, Muschol M. Amyloid protofibrils of lysozyme nucleate and grow via oligomer fusion. Biophys J 2009;96(9):3781-3790.

268. Guijarro JI, Sunde M, Jones JA, Campbell ID, Dobson CM. Amyloid fibril formation by an SH3 domain. Proceedings of the National Academy of Sciences of the United States of America 1998;95(8):4224-4228.

269. Zurdo J, Guijarro JI, Jimenez JL, Saibil HR, Dobson CM. Dependence on solution conditions of aggregation and amyloid formation by an SH3 domain. J Mol Biol 2001;311(2):325-340.

270. Chattopadhyay M, Durazo A, Sohn SH, Strong CD, Gralla EB, Whitelegge JP, Valentine JS. Initiation and elongation in fibrillation of ALS-linked superoxide dismutase. Proceedings of the National Academy of Sciences of the United States of America 2008;105(48):18663-18668.

271. Gejyo F, Yamada T, Odani S, Nakagawa Y, Arakawa M, Kunitomo T, Kataoka H, Suzuki M, Hirasawa Y, Shirahama T, et al. A new form of amyloid protein associated with chronic hemodialysis was identified as beta 2-microglobulin. Biochem Biophys Res Commun 1985;129(3):701-706.

272. Esposito G, Michelutti R, Verdone G, Viglino P, Hernandez H, Robinson CV, Amoresano A, Dal Piaz F, Monti M, Pucci P, Mangione P, Stoppini M, Merlini G, Ferri G, Bellotti V. Removal of the N-terminal hexapeptide from human beta2-microglobulin facilitates protein aggregation and fibril formation. Protein Sci 2000;9(5):831-845.

273. Han W, Wu YD. A strand-loop-strand structure is a possible intermediate in fibril elongation: long time simulations of amyloid-beta peptide (10-35). J Am Chem Soc 2005;127(44):15408-15416.

274. Khare SD, Ding F, Gwanmesia KN, Dokholyan NV. Molecular origin of polyglutamine aggregation in neurodegenerative diseases. PLoS Computational Biology 2005;1(3):230-235.

275. Marchut AJ, Hall CK. Spontaneous formation of annular structures observed in molecular dynamics simulations of polyglutamine peptides. Comput Biol Chem 2006;30(3):215-218.

276. Fernandez-Escamilla AM, Rousseau F, Schymkowitz J, Serrano L. Prediction of sequence-dependent and mutational effects on the aggregation of peptides and proteins. Nat Biotechnol 2004;22(10):1302-1306.

277. Thompson MJ, Sievers SA, Karanicolas J, Ivanova MI, Baker D, Eisenberg D. The 3D profile method for identifying fibril-forming segments of proteins. Proceedings of

the National Academy of Sciences of the United States of America 2006;103(11):4074-4078.

278. Fowler DM, Koulov AV, ory-Jost C, Marks MS, Balch WE, Kelly JW. Functional amyloid formation within mammalian tissue. PLoS Biology 2006;4(1):e6.

279. Peng S, Ding F, Urbanc B, Buldyrev SV, Cruz L, Stanley HE, Dokholyan NV. Discrete molecular dynamics simulations of peptide aggregation. Phys Rev E Stat Nonlin Soft Matter Phys 2004;69(4 Pt 1):041908.

280. Strange RW, Antonyuk S, Hough MA, Doucette PA, Rodriguez JA, Hart PJ, Hayward LJ, Valentine JS, Hasnain SS. The structure of holo and metal-deficient wild-type human Cu, Zn superoxide dismutase and its relevance to familial amyotrophic lateral sclerosis. J Mol Biol 2003;328(4):877-891.

281. Dixon RD, Chen Y, Ding F, Khare SD, Prutzman KC, Schaller MD, Campbell SL, Dokholyan NV. New insights into FAK signaling and localization based on detection of a FAT domain folding intermediate. Structure 2004;12(12):2161-2171.

282. Zhou Z, Feng H, Bai Y. Detection of a hidden folding intermediate in the focal adhesion target domain: Implications for its function and folding. Proteins 2006;65(2):259-265.